

**EXPERIMENTAL AND NUMERICAL
STABILITY INVESTIGATIONS ON
NATURAL CIRCULATION
BOILING WATER REACTORS**

EXPERIMENTAL AND NUMERICAL STABILITY INVESTIGATIONS ON NATURAL CIRCULATION BOILING WATER REACTORS

Proefschrift

ter verkrijging van de graad van doctor
aan de Technische Universiteit Delft,
op gezag van de Rector Magnificus prof. dr. ir. J.T. Fokkema,
voorzitter van het College voor Promoties,
in het openbaar te verdedigen op maandag 29 oktober 2007 om 15:00 uur

door

Christian Pablo MARCEL

Ingeniero Nuclear
Instituto Balseiro, Universidad Nacional de Cuyo, Argentinië

geboren te Buenos Aires, Argentinië

Dit proefschrift is goedgekeurd door de promotor:

Prof. dr. ir. T.H.J.J. van der Hagen

Samenstelling promotiecommissie:

Rector Magnificus,	voorzitter
Prof. dr. ir. T.H.J.J. van der Hagen,	Technische Universiteit Delft, promotor
Prof. dr. R.F. Mudde,	Technische Universiteit Delft
Prof. dr. ir. A.E. Larreteguy,	Universidad Argentina de la Empresa
Prof. dr. ir. G. Guido-Lavalle,	Esc. Superior de Economía y Adm. de Empresas
Dr. ir. M. Rohde (Gast),	Technische Universiteit Delft
Dr. B.S. Shiralkar (Gast),	General Electric Co.

Copyright © 2007 by Christian Pablo Marcel and IOS Press

All rights reserved. No part of this book may be reproduced, stored in a retrieval system, or transmitted, in any form or by any means, without prior permission from the publisher.

ISBN 978-1-58603-803-8

Keywords:

Natural circulation Boiling Water Reactors, stability performance, fluid-to-fluid modeling, density wave oscillations, flashing phenomenon, neutronic-thermal-hydraulic coupling

Published and distributed by IOS Press under the imprint Delft University Press

Publisher

IOS Press

Nieuwe Hemweg 6b

1013 BG Amsterdam

The Netherlands

tel: +31-20-688 3355

fax: +31-20-687 0019

email: info@iospress.nl

www.iospress.nl

www.dupress.nl

LEGAL NOTICE

The publisher is not responsible for the use which might be made of the following information.

PRINTED IN THE NETHERLANDS

Dedicated to Flavia and Kolya

Table of Contents

Summary	xi
Samenvatting	xv
Chapter 1. Introduction.....	1
1.1 Introduction.....	1
1.2 Natural circulation BWRs basic principle	2
1.3 Classification of BWR instabilities.....	3
1.4 High Pressure vs. Low Pressure stability	5
1.5 Coupled Neutronics – Thermal-hydraulics	6
1.6 Motivation behind the present work	7
1.7 Outline of this thesis.....	9
1.8 References	11
Chapter 2. Downscaling the thermal – hydraulics of natural circulation BWRs: The GENESIS facility	13
2.1 Introduction.....	13
2.2 Design philosophy – The scaling.....	15
2.2.1 Defining the operational conditions	17
2.2.2 Geometrical scaling	18
2.2.3 Scaling of the dynamics	24
2.2.4 Treatment of the distortions.....	28
2.2.5 Scaling sensitivity to the operational pressure.....	32
2.3 Application of the proposed scaling design approach.....	33
2.4 Conclusions	39
2.5 References	40
Chapter 3. Experimental investigations on the stability of natural circulation BWRs.....	41
3.1 Introduction.....	41
3.2 The VRF system	43
3.2.1 The VRF system design.....	43
3.2.2 The VRF system implementation	44
3.3 Stability performance of natural circulation BWRs	50
3.3.1 Experiments on thermal-hydraulic stability	50
3.3.2 Experiments on reactor-kinetic stability.....	51
3.3.3 The ATHLET numerical results	54
3.4 Conclusions	56
3.5 References	57

Chapter 4. An experimental parametric study of natural circulation BWRs stability	59
4.1 Introduction.....	59
4.2 GENESIS improvements.....	60
4.3 Parametric study.....	63
4.3.1 Effect of the improved VRF system	64
4.3.2 Effect of the modeling of the ESBWR fuel rods.....	64
4.3.3 Effect of changing the rod diameter.....	65
4.3.4 Effect of using a MOX fuel	66
4.3.5 Effect of the pressure.....	67
4.3.6 Effect of the feedwater sparger position	68
4.3.7 Effect of the void reactivity feedback coefficient	69
4.4 Conclusions	73
4.5 References	74
Chapter 5. Experimental and analytical investigations on flashing-induced instabilities in a single channel	75
5.1 Introduction.....	75
5.2 The CIRCUS facility in the single chimney configuration	76
5.3 Experimental results.....	77
5.3.1 The stability maps	78
5.3.2 Dynamical characterization of the instabilities	79
5.3.3 From single-phase to stable two-phase flow	80
5.3.3.a High subcooling stable flow circulation	81
5.3.3.b Intermittent oscillations	82
5.3.3.c Sinusoidal oscillations	83
5.3.3.d Low subcooling stable flow circulation.....	85
5.3.4 Analysis of the dynamics of the flashing front.....	86
5.3.5 Analysis of the inertia of the loop	87
5.4 A lumped parameter model.....	88
5.5 Experimental results vs. numerical results	90
5.6 A numerical parametric study	91
5.7 Conclusions	93
5.8 References	94
Chapter 6. Flashing – induced oscillations in parallel channels	95
6.1 Introduction.....	95
6.2 Description of the CIRCUS facility with two chimneys	96
6.3 Experimental results.....	97
6.3.1 The stability behavior.....	98
6.3.2 Phenomenological description – From region I to IV.....	99
6.3.2.a Region I – High subcooling stable flow circulation	99
6.3.2.b Region II – Unstable <i>in-phase</i> flow circulation	100
6.3.2.c Region III – Unstable a-periodical oscillations.....	102
6.3.2.d Region IV – Unstable out-of-phase oscillations.....	103
6.3.3 Analysis of the instability mechanism.....	104

Table of contents

6.3.4 Single channel stability vs. two-parallel channels stability	106
6.3.5 Non-linear analysis of the oscillations.....	109
6.3.5.a Experimental evidence of bifurcations	109
6.3.5.b Investigations on the nature of the a-periodical oscillations	110
6.4 Conclusions	115
6.5 References	116
 7. Conclusions and recommendations	 117
 APPENDICES	 123
APPENDIX A: GENESIS techical details	123
APPENDIX B: Noise analysis basic principles and DR estimation	125
APPENDIX C: MOX fuel reference neutronic data	128
APPENDIX D: Analysis of the fluctuations of the primary flow signal	129
APPENDIX E: The nodal Model.....	130
APPENDIX F: The Geysering phenomenon	131
APPENDIX G: The Lyapunov exponents and the Kolmogorov entropy	132
 Nomenclature	 135
 Curriculum Vitae	 139

Summary

In the design of novel nuclear reactors active systems are replaced by passive ones in order to reduce the risk of failure. For that reason natural circulation is being considered as the primary cooling mechanism in next generation reactor designs such as the natural circulation boiling water reactor (BWR). In such a reactor, however, the flow is not a controlled parameter but is dependent on the power. As a result, the dynamical behavior significantly differs from that in conventional forced circulation BWRs. For that reason, predicting the stability characteristics of these reactors has to be carefully studied. In this work, a number of open issues are investigated regarding the stability of natural circulation BWRs (e.g. margins to instabilities at rated conditions, interaction between the thermal-hydraulics and the neutronics, and the occurrence of flashing induced instabilities) *with a strong emphasis on experimental evidence*. The prototypical Economical Simplified BWR (ESBWR) design from the General Electric Company was thereby taken as the reference natural circulation BWR. Two experimental facilities located at the Delft University of Technology were used for that purpose: the GENESIS facility which uses Freon as working fluid and the water-based CIRCUS facility.

Nominal conditions

First of all, the stability of the ESBWR *under nominal conditions* was studied. The purpose was to experimentally determine the ESBWR stability characteristics *as accurately as possible* and to compare the results with numerical results of different origin. In order to study the ESBWR stability under less severe conditions than the nominal ones, a downscaled facility, called GENESIS, was designed and constructed based on a fluid-to-fluid scaling approach. Since the rods in the facility are electrically heated, an artificial void reactivity feedback mechanism was implemented.

Both the thermal-hydraulic and the neutronic-thermal-hydraulic stability performance of the ESBWR for a wide range of conditions were investigated. From the analysis of the results it was found that the GENESIS facility (representing the ESBWR at nominal conditions) is very stable and exhibits a large margin to instability. From the comparison between numerical simulations performed by using the system codes TRACG and ATHLET, a

significant discrepancy was observed in the predicted decay ratio at nominal conditions. This finding indicates that limitations still exist in the numerical estimation of the stability performance of nuclear reactors involving complex two-phase flows. For this reason both numerical and experimental tools should be used for such a task.

The GENESIS facility was also used to perform a study in which a number of parameters such as the steam separator friction (the steam separator is a typical ESBWR part located at the top of the chimney section), the void-reactivity feedback and the axial position of the feedwater sparger inlet were varied. As a result, it was observed that the characteristic resonance frequency of the thermal-hydraulic mode is found to be much lower (~ 0.11 Hz) than in forced-circulation BWRs (~ 1 Hz), indicating a static head dominated phenomenon since it corresponds well with typical frequencies of density wave oscillations traveling through the core-plus-chimney sections. In addition, it was experimentally found that the position of the feedwater sparger inlet influences the stability of the thermal-hydraulic oscillatory mode.

Start-up conditions

Some experiments and analyses indicated that thermal-hydraulic oscillations may occur under certain low pressure and power conditions during the startup of a natural circulation BWR. For that reason the stability of the ESBWR *at start-up conditions* was investigated by using both numerical and experimental tools.

In the ESBWR, the chimney is split up into many parallel channels; hence, coupling effects between the channels are of relevance. Two different cases were therefore studied with the help of the CIRCUS facility: the single channel configuration and the two parallel channels configuration for which study CIRCUS was especially modified.

For the *single channel* configuration, detailed experiments were performed on flashing-induced oscillations occurring in the CIRCUS facility. Both the axial temperature and axial void fraction temporal evolution were used to investigate the mechanisms causing the flashing-induced oscillations. A novel way of plotting the axial temperatures in the channel was thereby used. The experimental results were also used to validate a proposed lumped parameter model. Then the code was used to further investigate the influence of the core inlet friction and chimney exit restriction on the stability. It was found that increasing the core inlet restriction stabilizes the system at high subcooling values and destabilizes the system at low subcooling values. In addition, the model predicted a destabilizing effect of the chimney exit restriction coefficient at low subcooling values and no changes in the high subcooling range.

From experiments performed with the *two parallel channel* configuration, it was found that reverse flow plays an important role in the spatial and temporal evolution of the temperature and vapor production in both parallel channels. Four different behaviors were found, depending on the operational conditions: (i) high subcooling, stable flow, (ii) in-phase oscillations, (iii) a-periodical oscillations which are attributed to multi-fractal deterministic chaos, and (iv) out-of-phase oscillations.

The results from the one and two parallel channel configurations also showed that vapor can be produced while the reactor remains stable. In this way, the reactor can be pressurized without encountering instabilities.

The work presented in this thesis shows that a natural circulation BWR can be safely operated from start-up to nominal conditions. Despite the discrepancies between the experimental and numerical results, it was shown that the ESBWR has large margins to instability at rated conditions. These discrepancies also emphasize the importance of using *both* (validated) numerical and experimental tools during the design phase of future nuclear reactors. This work indeed shows that the results from these complementary tools facilitate the comprehension of the system dynamics.

Samenvatting

Nieuwe kernreactoren worden zoveel mogelijk voorzien van 'passieve systemen' in plaats van 'actieve systemen' om de veiligheid van dergelijke systemen te vergroten. Er wordt daarom overwogen om in toekomstige kerncentrales het koelmiddel rond te pompen door middel van natuurlijke circulatie. In een dergelijke reactor is de stroming echter afhankelijk van het afgegeven vermogen en is dus niet meer een vrij in te stellen parameter. Het dynamische gedrag van deze reactorsystemen verschilt daarom sterk van het dynamische gedrag van systemen waar het koelmiddel geforceerd rondgepompt wordt. Gedegen onderzoek naar de stabiliteit van reactoren met natuurlijke systemen is daarom noodzakelijk. In dit onderzoek wordt een aantal aspecten bestudeerd met betrekking tot de stabiliteit van Kokend Water Reactoren (BWR's) met natuurlijke circulatie, zoals de marge tot instabiliteit bij nominale condities, het samenspel tussen thermohydraulica en neutronica en het optreden van instabiel gedrag door flashing. De Economic Simplified Boiling Water Reactor (ESBWR, General Electric Company) wordt hierbij als uitgangspunt gebruikt. In dit onderzoek ligt de nadruk op experimenteel werk, waarbij twee opstellingen worden gebruikt: de GENESIS opstelling (gevuld is met Freon-134a als schalingsvloeistof) en de met water gevulde CIRCUS opstelling.

Nominale condities

Allereerst werd de stabiliteit van de ESBWR bij nominale condities bestudeerd. Het doel was om de stabiliteit experimenteel, en zo *nauwkeurig* mogelijk te bepalen en de resultaten te vergelijken met numerieke resultaten van verschillende herkomst. Hiervoor werd een geschaalde versie van de ESBWR ontworpen en gebouwd (de GENESIS opstelling), zodat bij lagere drukken en temperaturen gewerkt kon worden. Bovendien werd in de opstelling het elektrische vermogen van de verwarmingsstaven aangepast aan de aanwezige damp in de kern om zo de koppeling tussen de dichtheid en de reactiviteit te kunnen simuleren (het 'Void Reactivity Feedback' (VRF) systeem).

De stabiliteit van de ESBWR werd onder een groot scala van condities bestudeerd, waarbij zowel het puur thermohydraulische systeem (vermogen verandert niet met de dichtheid van het koelmiddel) als het reactorsysteem

(reactiviteit afhankelijk van de dichtheid van het koelmiddel) werden beschouwd. Uit de experimenten bleek dat de GENESIS opstelling (die de ESBWR representeert bij nominale condities) zeer stabiel is en een grote marge tot instabiliteit vertoont. De experimentele resultaten werden vervolgens vergeleken met numerieke resultaten die verkregen werden uit simulaties uitgevoerd met de TRACG en ATHLET systeemcodes. Er bleken grote onderlinge verschillen te bestaan tussen de numeriek verkregen decay ratios (DRs) en de experimenteel verkregen waardes. De laatste bevinding toont aan dat het bepalen van de stabiliteit van complexe twee-fasen systemen met behulp van numerieke codes nog steeds geen sine cure is. Het bestuderen van dergelijke systemen moet daarom zowel met behulp van numerieke als experimentele hulpmiddelen gebeuren.

De GENESIS opstelling werd ook gebruikt om een parameterstudie uit te voeren. Hierbij werden parameters zoals de frictie van de stoomscheiders (in de ESBWR geplaatst bovenop de schoorsteen), de dichtheidscoëfficiënt en de plaats van de feedwaterinlaat gevarieerd. Hieruit kon worden geconcludeerd dat de resonantiefrequentie van het thermohydraulische systeem een stuk lager is (~ 0.11 Hz) dan de frequentie van BWR's met geforceerde stroming (~ 1 Hz). Deze bevinding toont aan dat de frequenties voor het thermohydraulische systeem voornamelijk bepaald worden door de tijd die het kost voor een dampgolf om door de kern én de schoorsteen te bewegen. Ook werd aangetoond dat de positie van de feedwaterinlaat de stabiliteit van het thermohydraulische systeem beïnvloedt.

Opstartcondities

Eerdere experimenten en analyses hebben aangetoond dat oscillaties kunnen optreden tijdens het opstarten (d.i. lage druk, laag vermogen) van een BWR met natuurlijke circulatie. In dit onderzoek werd daarom de stabiliteit van de ESBWR onder opstartcondities bestudeerd met behulp van zowel numerieke codes als twee experimentele opstellingen.

In de ESBWR is de schoorsteen opgedeeld in vele parallelle kanalen. De koppeling van deze kanalen kan daarom een belangrijke invloed hebben op de stabiliteit van de ESBWR tijdens het opstartproces. Om deze invloed te kunnen bestuderen werd gebruik gemaakt van twee verschillende opstellingen: de CIRCUS opstelling met één kanaal en de CIRCUS opstelling met twee parallelle kanalen.

Met de opstelling voorzien van één kanaal werden de oscillaties, geïnduceerd door flashing, onderzocht door de axiale temperatuurs- en dampprofielen te meten in de tijd. Daarna werden de experimenteel verkregen resultaten gebruikt om een lumped-parameter model te valideren. Vervolgens

werd de code (waarin het model verwerkt is) gebruikt om de invloed van de frictie van de kerninlaat en de uitlaat van de schoorsteen op de stabiliteit te bestuderen. Uit de berekeningen werd geconcludeerd dat een vergrootte inlaatfrictie het systeem stabiliseert bij hoge subcooling getallen en destabiliseert bij lage subcooling getallen. Bovendien werd gevonden dat een vergrootte uitlaatfrictie het systeem destabiliseert bij lage subcooling getallen en dat de frictie geen invloed heeft op de stabiliteit bij hoge subcooling getallen.

Uit de experimenten met twee parallelle kanalen werd geconcludeerd dat neerwaartse stroming veel invloed heeft op het temperatuursprofiel en het ontstaan en verdwijnen van damp in beide kanalen. Vier verschillende stabiliteitszones konden worden geïdentificeerd, te weten (i) hoge subcooling, stabiele stroming, (ii) in-fase oscillaties, (iii) multi-fractaal, deterministisch chaotisch gedrag en (iv) uit-fase oscillaties.

De resultaten, voortkomend uit de opstellingen met één en twee kanalen lieten ook zien dat damp gemaakt kan worden zonder de reactor instabiel te maken. Op deze manier zou de reactor op een veilige manier op druk gebracht kunnen worden.

Dit onderzoek toont dat een BWR met natuurlijke circulatie veilig kan opereren onder zowel opstart- als de nominale condities. De marge tot instabiliteit is groot, ondanks het feit dat de numerieke resultaten verschillen van de experimentele bevindingen. Deze verschillen laten duidelijk zien dat experimenteel en numeriek onderzoek complementair zijn en dat *beiden* nodig zijn om de stabiliteit van toekomstige nucleaire reactoren op gedegen wijze te kunnen onderzoeken.

Chapter 1

Introduction

1.1 Introduction

One of the most challenging tasks the future generations will face is to produce enough electricity to satisfy the expected energy demand of all the population worldwide. This goal has to be achieved in a sustainable way while minimizing any adverse environmental effects. From all the options being considered for large scale electricity generation, one of the most advantageous energy sources is nuclear fission since it does not contribute to the global warming effect and it can be applied at large scale while the amount of waste produced is very little compared to others¹. Nowadays, around 435 nuclear power reactors are in operation in 33 countries². From these reactors, most of them are of the so-called Pressurized Water Reactor (PWR) and Boiling Water Reactor (BWR) type, which use light water (H_2O) as coolant and moderator. In PWRs, water is heated at a pressure level at which the boiling phenomenon is suppressed. The hot water is used to produce

steam in a secondary loop which drives the turbines producing electricity. In contrast, BWRs directly produce steam in the reactor core which simplifies the system by avoiding the use of large steam generators. The presence of steam in BWRs, however, increases the complexity of the physical processes taking place in the reactor (e.g. by reinforcing the coupling of thermal-hydraulics and neutronics) making the stability performance more difficult to predict³.

For the development of new generation BWRs, economics and reliability are being carefully studied and optimized in order to improve their possibilities as a main source of electricity generation⁴. From all possible designs the natural-circulation BWR is the most important one. This reactor is characterized by the absence of pumps in the main circuit. This characteristic induces new instability mechanisms that need to be thoroughly investigated in order to assure a safe reactor operation in all conditions. The only BWR of this type is the Dodewaard prototype reactor with an electric power of 57 MWe which was operated in The Netherlands between 1968-1997.

1.2 Natural circulation BWRs basic principle

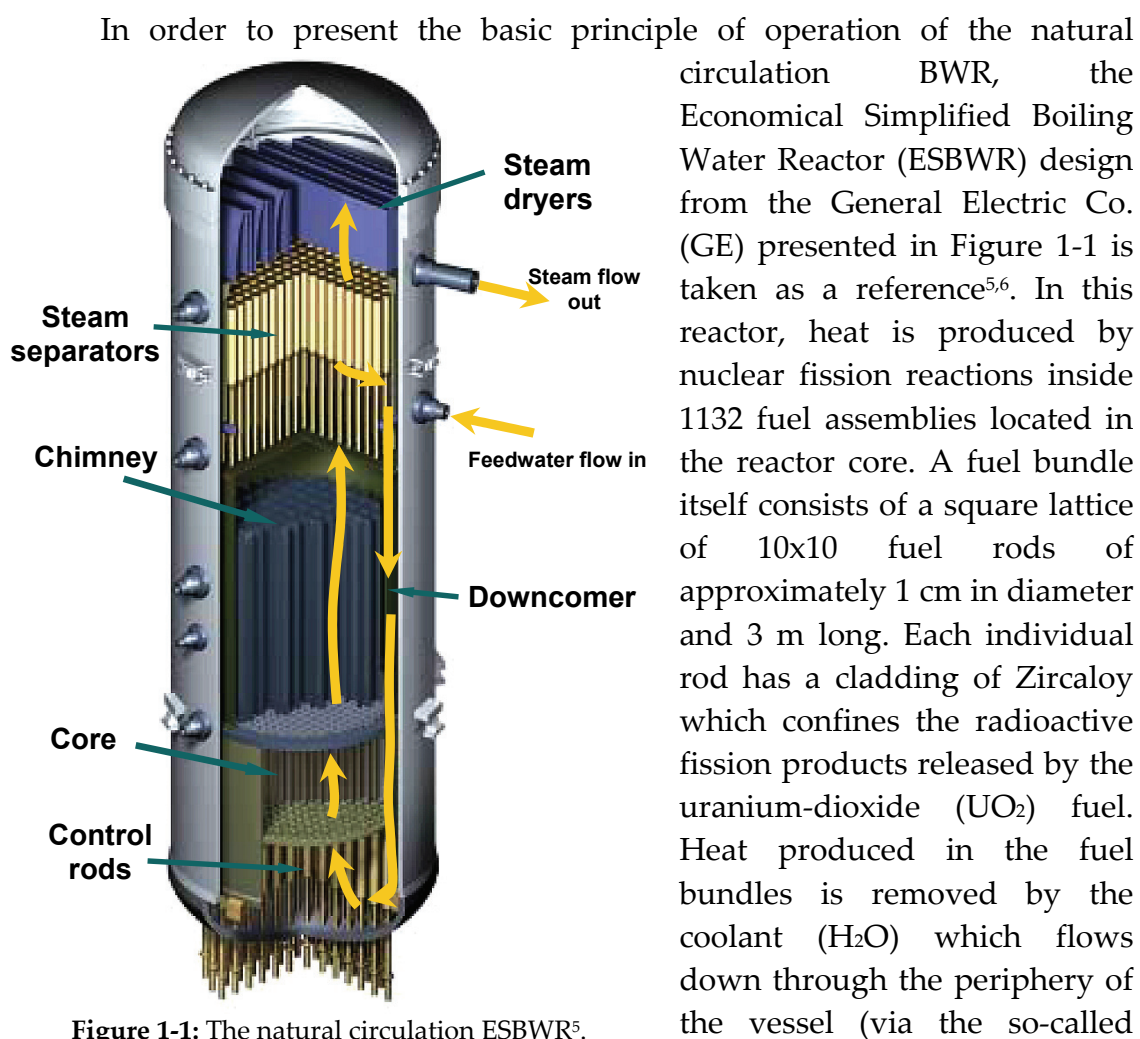


Figure 1-1: The natural circulation ESBWR⁵.

downcomer section) and enters the reactor core several degrees below the saturation temperature. As it flows upwards along the fuel assemblies, the temperature increases, and the coolant starts to boil. Part of the coolant, which remains in liquid state, flows through the core by-pass channels and mixes with the coolant from inside the assemblies at the core outlet. As a result of the whole heating process, approximately 17% of the coolant mass is converted into steam. This steam-water mixture flows through the chimney section (located right above the core) until it is separated in the steam separators. Unlike in forced circulation systems, in natural circulation BWRs, the flow is only driven by buoyancy forces created by the difference in weight between the hot section (core + chimney) and the cold section (downcomer). The steam leaves the vessel via the main steam line and drives the turbines. The axis of the cascade of turbines is coupled with an electric generator to produce electricity. The water which is separated from the steam flows downwards through the downcomer section and mixes with the recirculated condensate water from the turbines, closing the flow circuit. The expected thermal output of the ESBWR is approximately 4500 MWth. A typical efficiency of 33% is applicable to this reactor resulting in around 1480 MWe. This tremendous amount of energy is generated in a relatively small volume of only 60 cubic meters, i.e. the average core power density is 55 kW/l. Hence, cooling of the reactor core has to be assured under all circumstances to avoid excessively high temperatures of fuel and structure materials.

1.3 Classification of BWR instabilities

The highly complex phenomena occurring in BWRs has motivated extensive research programs with a strong emphasis in stability studies. As a result of these, important knowledge has been generated which helped to understand the main instability mechanisms. It was shown that the most important instabilities in currently operating BWRs are due to purely thermal-

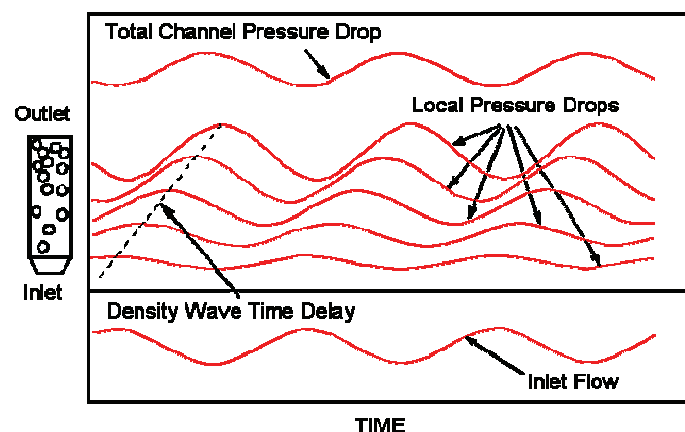


Figure 1-2: Illustration of the local pressure drop delay induced by the density wave mechanism.

hydraulic effects and also to coupled neutronic-thermal hydraulic effects^{7,8}. These instability types are basically induced by the 'density-wave' character of the two-phase flow in the coolant channels. The mechanism of density wave oscillations (DWO) in boiling channels can be

explained in a number of equivalent ways^{7,8,9} from which the most accepted explanation is as follows. Consider having a boiling channel with a constant pressure difference between inlet and outlet (see Figure 1-2). If the inlet flow rate is reduced at a constant heating power, bubbles produced in the channel will travel upwards as a packet, forming a propagating density wave. This traveling density wave causes a change in the local pressure drop at higher axial positions, with a certain delay due to the finite velocity of the propagating wave. The frictional pressure drop is particularly large in the region with a high (volumetric) amount of steam (void fraction), e.g. close to the core outlet. The major part of the total pressure drop will therefore be delayed with respect to the initial flow perturbation. Hence, if the inlet flow is perturbed sinusoidally as in Figure 1-2, the total pressure drop over the channel (being the sum of the delayed local pressure drops) will be delayed with respect to the inlet flow perturbation. In Figure 1-2 the total pressure drop is delayed 180 degrees with respect to the inlet flow i.e. a decrease in the inlet flow results in an increase of the total pressure drop (and vice versa). Perturbations of the inlet flow thus receive a positive feedback, and the oscillations grow at a specific frequency.

In a pioneer theoretical work¹⁰, Fukuda and Kobori investigated the dependence of the density-wave instability on the operating conditions by linearizing the governing equations and performing a frequency-domain stability analysis. These authors demonstrated that at least eight 'types' of DWO exist, three of them being static or 'Ledinegg' flow excursions and the remaining five all being dynamic instabilities. It is usual to divide the DWO into two main instability types: low-frequency Type-I instabilities induced by the gravitational pressure drop term, and high-frequency Type-II instabilities due to frictional pressure losses. Type-II instabilities have been thoroughly

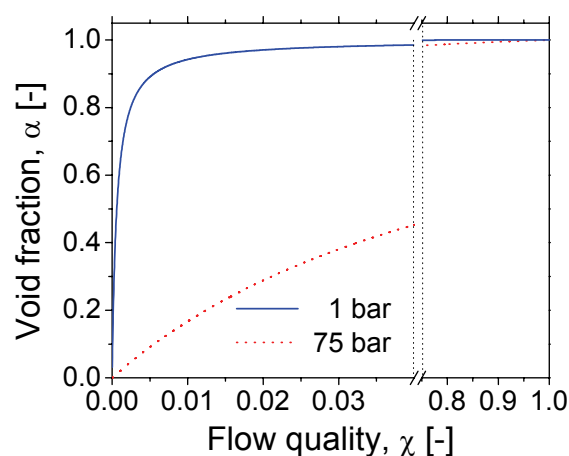


Figure 1-3: Void fraction vs. Flow quality at two pressures. The void fraction is very sensitive at small flow quality values and low pressures.

studied in the past because of their importance under low-flow-high-power (reactor accident) conditions. The previous discussion focused on Type-II oscillations since only variations in the frictional pressure drop were considered. The Type-I instability mechanism becomes dominant in natural circulation reactors operating at low power and pressure conditions, e.g. during the reactor startup. Under these conditions, the mass percentage of steam (the flow quality) at the core

outlet becomes very small. For small flow qualities and low pressures, the volumetric amount of steam (the void fraction) increases very rapidly as a function of the flow quality. A small decrease in the core inlet flow then leads to a large increase of the volume of steam produced at the core outlet. In a natural circulation reactor, this causes a low-density wave traveling through the chimney. This enhances the driving head, and the inlet flow will increase. Then the opposite process occurs, and the void fraction in the chimney decreases. Consequently, the driving head becomes smaller, and the flow rate will decrease. This completes one cycle of a Type-I oscillation. The main time constant governing this type of DWO is the transit time of the voids through the chimney section (~5-10 s).

1.4 High Pressure vs. Low Pressure stability

BWRs make use of the vapor created in the core to maintain the pressure at the nominal value of around 70 bar. During the start-up phase, however, such vapor simply does not exist and, therefore, the reactor needs to be operated at low pressure (most of the designs do not include external pressurization systems, which would elevate the total cost). Due to mechanical and neutronic safety reasons the power is kept at low levels during this stage. At low pressures (< 5 bar), which is the case for start-up conditions in a BWR, the dependence of the saturation temperature on the pressure is relatively strong for water.

Natural circulation BWRs can be represented as a loop, see Figure 1-4, with a cold section (the downcomer), a heated section (the core), an adiabatic section (the chimney) and a heat exchanger. Density differences between the cold and hot sections cause water to flow without using pumps. Natural circulation is thus enhanced in these systems by using a tall chimney.

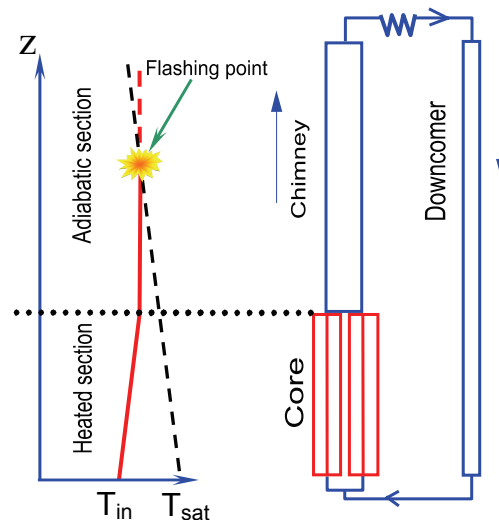


Figure 1-4: Schematic of a natural circulation BWR and the occurrence of flashing.

As the heated coolant flows upwards, the hydrostatic pressure will decrease. Hence, the saturation temperature will also decrease. If the saturation temperature becomes equal to the (constant) fluid temperature in the chimney, boiling out of the heated reactor core starts (see Figure 1-4). This ex-core boiling is not likely to occur at high pressures, because the saturation temperature is in good approximation independent of the axial position. Vapor production in the chimney directly affects the gravitational pressure drop over this section. Hence, it can be expected that the Type-I feedback mechanism is amplified by the occurrence of void flashing, especially in natural circulation BWRs with a tall chimney section^{11, 12}.

1.5 Coupled Neutronics-Thermal-hydraulics

Thermal reactors take advantage of the much larger fission cross-section of $^{235}\text{U}^+$ at low energies (<1 eV) than for energies above 1 keV (over two orders of magnitude larger for the first one). In each fission, on the average 2.5 high-energy neutrons are released in the MeV range. These ‘fast’ neutrons lose their kinetic energy as they collide with the nuclei from the coolant which also act as moderator. After several collisions, the neutrons have lost most of their kinetic energy and have a higher probability to cause new fissions. As a result of the leakage and absorptions in the non-fissile materials, neutrons which are not moderated have a small chance to cause fissions. For this reason, by reducing the moderation of neutrons in a BWR (for instance by increasing the amount of vapor in the reactor core) the number of fissions are decreased and

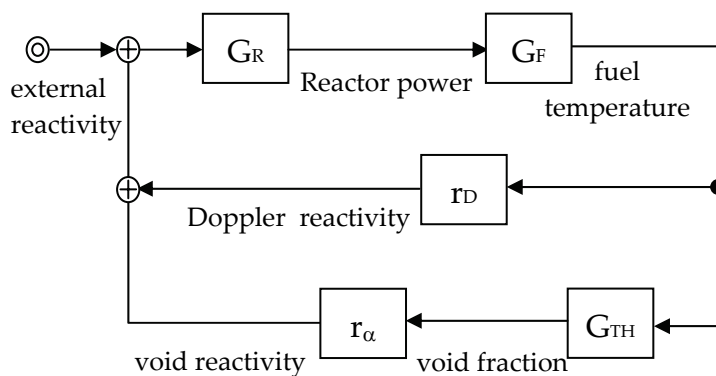


Figure 1-5: Block diagram of the main mechanisms relevant for BWRs dynamics³.

so the power produced.

The influence on the reactor power due to void fraction changes in the coolant channels is depicted schematically in Figure 1-5. The impact of the void fraction on the reactivity is described with the void reactivity coefficient r_α in this block diagram. The thermal-hydraulic subsystem is

described by G_{TH} . Figure 1-5 shows that overall BWR stability is determined by the interaction between neutronics (the zero-power reactor transfer function G_R), fuel dynamics (G_F) and thermal-hydraulics (G_{TH}). For instance,

[†] The symbolic form is used, where the number of nucleons is denoted as a superscript prefix to the chemical symbol of the specimen, e.g. ^yX refers to the isotope y of the specimen X .

by increasing the external reactivity, the reactor power will increase (via G_R). This causes an increase of the fuel temperature (via G_F) and the void fraction (via G_{TH}). An increase in the void fraction reduces the resonance escape probability, and therefore causes a negative void reactivity effect (ρ_α is negative). Furthermore, an increase of the fuel temperature will broaden the width of the capture resonances, increasing the resonance absorption. This Doppler effect is accounted for in the Doppler reactivity coefficient ρ_D (which is also negative). Hence, an increase of the reactor power results in a subsequent decrease of the reactivity via the void and Doppler feedback paths. These negative feedback mechanisms make a BWR a very stable system during fast and also slow transients. However, during middle-frequency transients (~ 0.5 -1 Hz) the (stabilizing) negative feedback in a BWR can become positive (destabilizing), in particular when the feedback processes occur with a certain time delay. When the feedback gain then exceeds a critical value, coupled neutronic-thermal-hydraulic instabilities can occur in a BWR¹³.

1.6 Motivation behind the present work

Large research programs on nuclear-thermal-hydraulic stability have been performed worldwide in the last three decades, after instability events in several commercial forced BWRs were reported^{1,3,14}. In particular, many investigations have been conducted regarding natural circulation BWRs stability in the Department of Physics of Nuclear Reactors from the Delft University of Technology. For instance, Van der Hagen carried out stability measurements at the Dodewaard reactor which helped to understand the basic instability mechanisms existent in that reactor¹⁵. Stekelenburg used such measurements to perform simple models and to further explain those mechanisms¹⁶. Van Bragt derived a simple numerical model with which he performed parametric studies that helped to gain more insight into the dynamics of natural circulation BWRs¹³.

Since experiments in a real reactor are difficult to assess, it was decided to develop a test facility to simulate the Dodewaard reactor¹⁷. Experiments on neutronic dynamical systems, however, are usually hard to implement and involve radiation-related safety issues. For this reason thermal-hydraulic facilities with simulated neutronics are a valuable option to experimentally study BWRs¹⁷. As a result, the DESIRE facility was designed and constructed in Delft using the fluid-to-fluid downscaling concept to considerably reduce the size, power and the pressure needed in the experiments. Kok and Zboray derived an artificial void reactivity feedback system which was added to the DESIRE facility^{17,18}. Different methods for reconstructing the void fraction core axial profile were tested by Zboray. As a result of such a study Zboray found that integral sensors (i.e. not local) are a good option for estimating the core

axial void fraction (when there is no axial weighting for the reactivity calculation) since they add a much smaller phase than local sensors do¹⁸. Furuya constructed a water-based facility, the so-called SIRIUS-N facility at the CRIEPI laboratories in Japan, which design was based on a natural circulation BWR prototype¹⁹. Furuya successfully implemented a void reactivity feedback system in his facility which used pressure drop sensors to estimate the void content. In his case, however, the use of water as working fluid limited the maximum available power for the facility and, therefore, the whole reactor core was simulated by only two annular channels. On top of this, the total chimney length was too short to represent the chimney of novel natural circulation BWRs concepts. As pointed out by many authors^{13,18,19}, a taller chimney destabilizes the thermal-hydraulic mode which would result in non-conservative estimations of the reactor stability performance of those reactors if SIRIUS facility is used for such a task.

Nowadays highly-sophisticated BWR stability codes have been developed with state-of-the-art models for the three-dimensional neutron kinetics, heat transfer and thermal-hydraulics²⁰. Besides the significant progress made in this field, still important uncertainties have to be considered in the numerical results, which are greatly due to the modeling of the two-phase flow dynamics^{21,22,23}. For this reason performing experimental work is of great relevance when investigating the stability of novel BWR designs. For instance, as a requirement for the licensing of the ESBWR, the U.S. Nuclear Regulatory Commission requested GE to validate their numerically based stability investigations with experiments²⁴. Existing experimental test facilities such as those from Zboray and Furuya cannot accurately represent the dynamics of novel natural circulation BWRs. Because of this, it was decided to design and construct a completely new experimental facility with an artificial void reactivity feedback system, with which the desired similarity with a prototypical natural circulation BWR dynamic behavior is optimized. Continuing the path followed with the DESIRE facility, a fluid-to-fluid downscaled Freon version of the real reactor is proposed to simulate the thermal-hydraulic system. The valuable experience gained from the works of Zboray and Furuya is used to develop a refined representation of the void reactivity feedback mechanism. The flexible design of such an artificial feedback system allows performing parametric investigations which could be used to validate numerical results. In addition, investigations such as the influence of low-frequency Type-I oscillations on coupled neutronic-thermal-hydraulic stability and the construction of stability maps for these reactors can be experimentally investigated.

Efforts have been done in the past to investigate possible start-up procedures with which instabilities could be avoided. Manera and Furuya performed experiments at low-pressure conditions to investigate natural

circulation BWRs start-up procedures. From their studies they concluded that an unstable region has to be crossed during the start-up phase of natural circulation BWRs if no external pressurization is used^{12,19}. Due to difficulties in downscaling the reactor at start-up conditions with a fluid different than water, a second facility, so-called CIRCUS, is used for investigations at such conditions. In modern natural circulation BWRs the steam separation is performed in sophisticated sections placed on top of the chimney section⁵. The introduction of such devices creates large pressure drops which are mainly concentrated at the swirlers²⁵. The effect of having a large restriction at the chimney exit may degrade the stability of the reactor regarding Type-I flashing-induced oscillations. This important subject was not investigated in the past and therefore needs to be assessed in order to assure a stable start-up procedure of these reactors.

Another characteristic of modern natural circulation BWRs is that the chimney is divided into smaller channels. The coupling between these channels may induce flashing-induced instabilities which may be different than those taking place in a single channel. Investigations in this topic are thus necessary to understand the mechanism behind those possible instabilities. Experiments in this topic need to be performed since such a mechanism was never experimentally investigated for reactor start-up conditions.

1.7 Outline of this thesis

Seven chapters form this thesis, the first one being the Introduction and the last one the Conclusions and Recommendations. Each of these chapters has its own introduction, conclusions and reference section, and can be read almost independently from the other chapters.

The complete design of the so-called GENESIS experimental facility based on fluid-to-fluid scaling of a natural circulation BWR is presented in Chapter 2. The ESBWR introduced in Section 1.2 is used as the reference design of a natural circulation BWR. The downscaling is performed in such a way that the dynamics of the thermal-hydraulics is as similar as possible to that existing in the reactor. The thermal-hydraulic stability performance of the reference ESBWR is analyzed in this chapter.

In Chapter 3, the void reactivity feedback mechanism is artificially implemented in the aforementioned facility. Such an improvement allowed investigating the *reactor* stability performance for different operational conditions. Complete stability maps regarding the thermal-hydraulic and the neutronic-thermal-hydraulic stability performance of the ESBWR are

constructed from the experiments and afterwards compared with numerical simulations obtained from the TRACG²⁶ and the ATHLET²⁷ system codes.

In Chapter 4 the GENESIS test facility with the void reactivity feedback system is used to perform an extensive study aimed to investigate the effect on the stability when varying some parameters. In addition, by varying the void reactivity coefficient, it was possible to investigate the characteristics of the interaction between the Type-I low frequency oscillations with the Type-II high frequency oscillations.

In Chapter 5 the water-based CIRCUS facility is used to perform very detailed experiments used to further investigate the so-called Type-I flashing-induced instabilities occurring in a single channel, which are of importance at start-up conditions of natural circulation BWRs. The phenomenon taking place in a single-chimney configuration is then numerically simulated by using a nodal model. The model is afterwards used to investigate the stability effect of the friction distribution in the channel.

Flashing-induced instabilities in parallel channels are experimentally investigated in the CIRCUS facility equipped with two separate chimneys placed on top of the heated section. The results of such a study are reported in Chapter 6.

1.8 References

- ¹ USDOE Nuclear Energy Research Advisory Committee and the Generation IV Int. Forum "A, Technology Roadmap for Generation IV Nuclear Energy Systems", GIF-002-00, (2002).
- ² European Nuclear Society, www.euronuclear.org, February 2007.
- ³ March-Leuba, J. and Rey, J.M., Coupled Thermal-hydraulic-Neutronic Instabilities in Boiling Water Reactors: A Review of the State of the Art, *Nucl. Eng. Des.*, 145, 97, (1993).
- ⁴ McCandless, R.J. and Redding, J.R., Simplicity: the key to improved safety, performance and economics (SBWR reactor), *Nucl. Eng., Int.*, 34:20–24, (1989).
- ⁵ Rao A.S. and Gonzalez, A., ESBWR Program–Development of Passive Plant Technologies and Designs, *Proc. Int. Cong. of Advanced NPPs (ICAPP)*, Florida, USA, N°1170, (2002).
- ⁶ Cheung, Y.K., Shiralkar, B.S. and Rao, A.S., Design Evolution of Natural Circulation in ESBWR, 6th Int. Conf. on Nuclear Engineering (ICONE-6), San Diego, USA, (May 1998).
- ⁷ Boure, J.A., Bergles, A.E. and Tong, L.S., Review of Two-Phase Flow Instability, *Nucl. Eng. Des.*, 25, 165, (1973).
- ⁸ Lahey, R.T. Jr. and Moody, F.J., The Thermal-Hydraulics of a Boiling Water Nuclear Reactor, American Nuclear Society, LaGrange Park, Illinois, (1979).
- ⁹ Yadigaroglu, G., Two-phase flow instabilities and propagation phenomena, Chapter 17, 353–403, Hemisphere Publishing Corporation, (1981).
- ¹⁰ Fukuda K. and Kobori, T., Classification of Two-Phase Flow Instability by Density Wave Oscillation Model, *J. Nucl. Sci. Tech.*, 16, 95, (1979).
- ¹¹ Furuya, M., Inada, F. and Yasuo, A., Density Wave Oscillations of a Boiling Natural Circulation Loop Induced by Flashing, *Proc. 7th NUREG/CP-0142*, 2:923–932, (1995).
- ¹² Manera, A. and Van der Hagen, T.H.J.J., Stability of Natural-Circulation-Cooled Boiling Water Reactors During Startup: Experimental Results, *J. Nuc. Tech.*, 143(1):77–88, (2003).
- ¹³ Van Bragt, D.D.B. *et al.* Stability of Natural Circulation BWRs: Part II-Parametric Study of Coupled Neutronic-Thermal-hydraulic Stability", *Nucl. Tech.*, Vol. 121, (1998).
- ¹⁴ Offerein, J.F. and Winters, L., Final Technical Report NACUSP Project Natural Circulation and Stability Performance of BWRs, (2005).
- ¹⁵ Van der Hagen, T.H.J.J., Stability Monitoring of a Natural-Circulation-Cooled BWR, Delft University of Technology PhD thesis, (1989).
- ¹⁶ Stekelenburg, A.J.C, Statics and Dynamics of a Natural Circulation Cooled BWR, Delft University of Technology PhD thesis, IOS Press, (1994).
- ¹⁷ Kok, H., Experiments on a Natural Circulation Loop - from Void-fraction to Coupled Nuclear Thermal-Hydraulics, Delft University of Tech. PhD thesis, IOS Press, (1998).
- ¹⁸ Zboray R., An Experimental and Modeling Study of Natural-Circulation BWR Dynamics, Delft University of Technology, PhD thesis, IOS Press, (2002).
- ¹⁹ Furuya M., Experimental and Analytical Modeling of Natural Circulation and Forced Circulation BWRs, Delft University of Technology PhD thesis, IOS Press, (2006).
- ²⁰ Shiralkar, B. S., State of the Art Report on Boiling Water Reactor Stability (SOAR on BWRs), OECD/CSNI report, Ch.4: Modelling Features and assessment, OECD/GD, 13, (1997).
- ²¹ AEN/NEA., Ringhals 1 Stability Benchmark, final report, (1996.).
- ²² Lin, H-T., Wang, J-R., Hsieh, C-L., Shin, C., Chiang, S-C. and Weng, T-L., Kuosheng BWR/6 stability analysis with LAPUR5 code, *Ann. Nucl. Energy*, Vol. 33, No. 3, (2006).
- ²³ Rohde, M. *et al.* Experimental and Numerical Investigations on the ESBWR Stability Performance. NURETH-12, Sep 30-Oct 4 2007, Pittsburg, USA (2007).
- ²⁴ Marquino, W., personal communication, (2006).
- ²⁵ Shiralkar, B.S., Personal communication, (2005).
- ²⁶ Andersen, J.G.M. *et al.* TRACG Model Description, Lic. Topical Rep., NEDO- 32176, (1976).
- ²⁷ Lerchel, G. and Austregesilo, H., ATHLET Mode 1.2 Cycle A, User's Manual, GRS-p-1/Vol.1, Rev. 1, GRS, (1998).

Chapter 2

Downscaling the thermal-hydraulics of natural circulation BWRs: The GENESIS facility

2.1 Introduction

In order to enhance the safety of the next generation of nuclear reactors, special emphasis is made on replacing active safety systems by passive ones. The Economic Simplified Boiling Water Reactor (ESBWR) is taken as the reference natural circulation BWR since it represents the most advanced design and it has the highest chances to be built in the near future. This reactor is therefore used in this work. The ESBWR, being a next generation nuclear reactor, eliminates the need for circulation pumps and associated piping and systems since cooling takes place by natural circulation. This cooling method is simple, extremely reliable (since it does not rely on active systems or components), and results in reduced overall maintenance costs. In such a reactor, the flow depends on the amount of vapor present in the system. It may therefore occur that perturbations in the void content cause the system to exhibit so-called thermal-hydraulic instabilities. The ESBWR is

designed to have large margins to instabilities¹. Such margins, however, are only numerically verified and experimental evidence is therefore required to certify that finding.

To experimentally investigate the stability performance of the modern ESBWR design, the most direct way is to carry out measurements on the reactor itself. The ESBWR, however, has not been built yet and, therefore, its thermal-hydraulic stability was never demonstrated experimentally. In addition, real plant tests have many limitations related to safety reasons, lack of sensors and limited operative range².

To fill this gap, an experimental facility, designed to have a similar stability behavior to the ESBWR, is developed. The working conditions of BWRs, however, involve high power, high pressure and, particularly in the ESBWR case, large dimensions. A fluid-to-fluid scaling approach is therefore used, which allows representing the ESBWR at a lower pressure, temperature and by using considerably less power.

The flow inside a BWR assembly may vary from unsaturated single-phase flow to annular two-phase flow. In order to design a downscaled version of the ESBWR with a coolant different than water, scaling criteria are necessary that cover all flow regimes present in the assembly. The work of Van de Graaf on flow pattern similarity³ is therefore used as a starting point. In the lower part of the assembly the coolant is not in equilibrium. The development of the flow quality in this subcooled boiling regime and the required inlet enthalpy of the liquid can be scaled properly if the phase change number N_{PCH} and the subcooling number N_{Sub} are used as scaling parameters. Consequently, these parameters fix the development of the quality in the upper part of the assembly, where the coolant is in thermal equilibrium. Van de Graaf found that the Froude number N_{Fr} and the Weber number N_{We} , as given by Ishii⁴ should be used as scaling parameters to ensure proper scaling of all flow regimes³. The results of this flow pattern scaling approach are in agreement with those of Symolon, who simulated the slip ratios as a function of the void fraction using a one-dimensional, fully developed two-fluid model. In such analysis the similarity in the predicted slip ratios for water and Freon is excellent⁵. Symolon experimentally showed that similar flow regime transition boundaries occur in Freon liquid/vapor as in steam/water if the Weber and Froude numbers are kept the same.

Van de Graaf focused on the proper downscaling of the reactor core bundle³. To achieve a successful similarity of the thermal-hydraulic stability performance of the ESBWR, however, more attention has to be paid to the proper scaling of the rest of the sections of the loop. For this reason, the work of Van de Graaf needs to be extended to cover a global fluid-to-fluid downscaling design that guarantees a similar stability performance for the

original and downscaled systems. Since dynamic similarity has to be achieved, the time scaling also needs to be analyzed.

In this chapter the main design steps followed to develop a downscaled version of the ESBWR, the so-called GENESIS facility, are shown, thereby taking the dynamics of the whole loop into account. Moreover, a way of diminishing the distortions that arise from the fluid-to-fluid downscaling is presented and numerically tested. Finally, a comparison of the resulting GENESIS facility with the ESBWR is addressed.

2.2 Design philosophy – The scaling

Figure 2-1 presents a schematic view of the ESBWR and the proposed design for the experimental GENESIS facility.

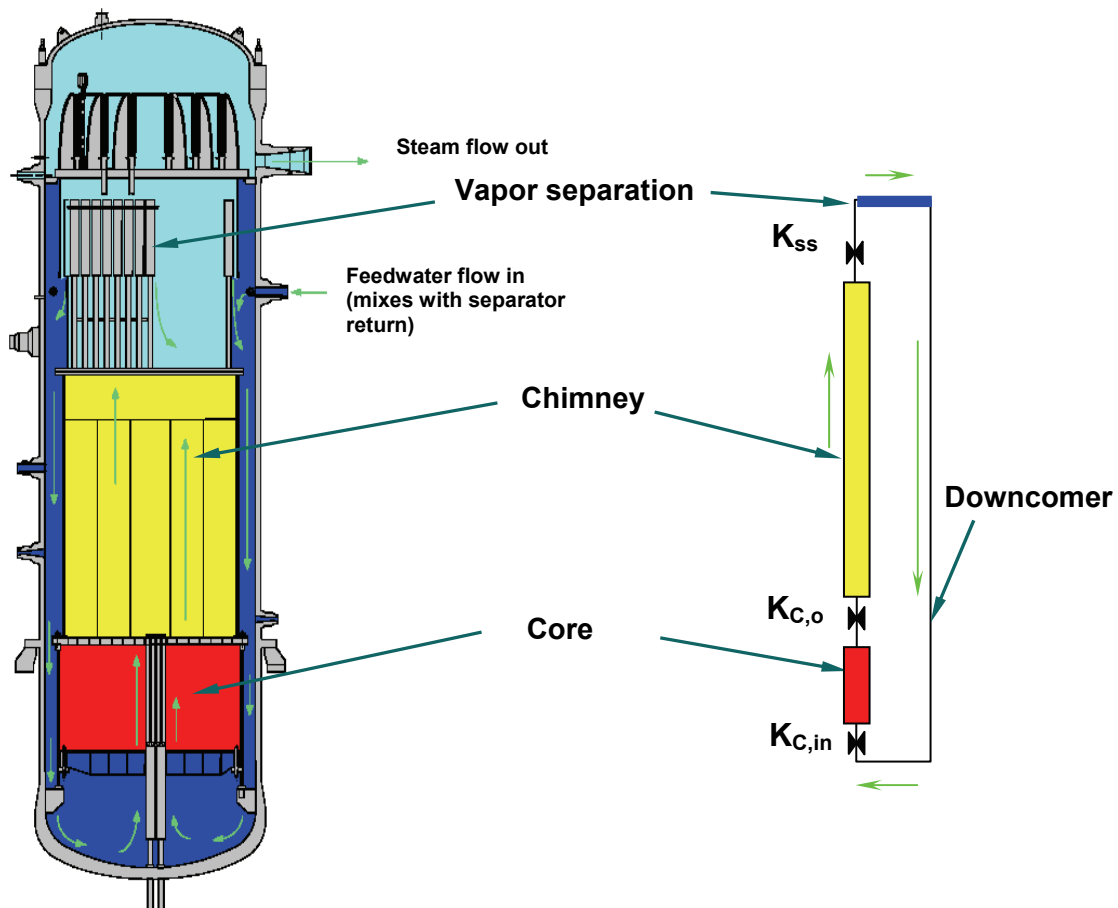


Figure 2-1: The ESBWR and the proposed GENESIS facility designed to emulate its stability performance (radially not to scale).

This figure shows the basic flow direction indicated by arrows and the most important sections that play a role in the stability analysis. As can be seen, all the sections of the ESBWR (except for the steam separators) are present in the downscaled system. A relatively taller chimney is placed in GENESIS which accounts for the extra driving force produced by the steam

separators. The steam separators are not included because of the large uncertainties lying in the liquid/vapor separation process and the technical difficulties in trying to reproduce this process. As a consequence, the friction associated with this section in the ESBWR (in which the swirlers play a major role⁶) is concentrated at the chimney exit now.

The scaling is based on the fact that two systems which can be represented by analogous differential equations should have the same type of solution, and thus similar physical behavior. Based on this, the mass, momentum and energy conservation differential equations, together with two more equations derived from the drift-flux model³, are mathematically manipulated in order to find the intrinsic parameters and variables that define the problem. The scaling procedure is schematically presented in Figure 2-2.

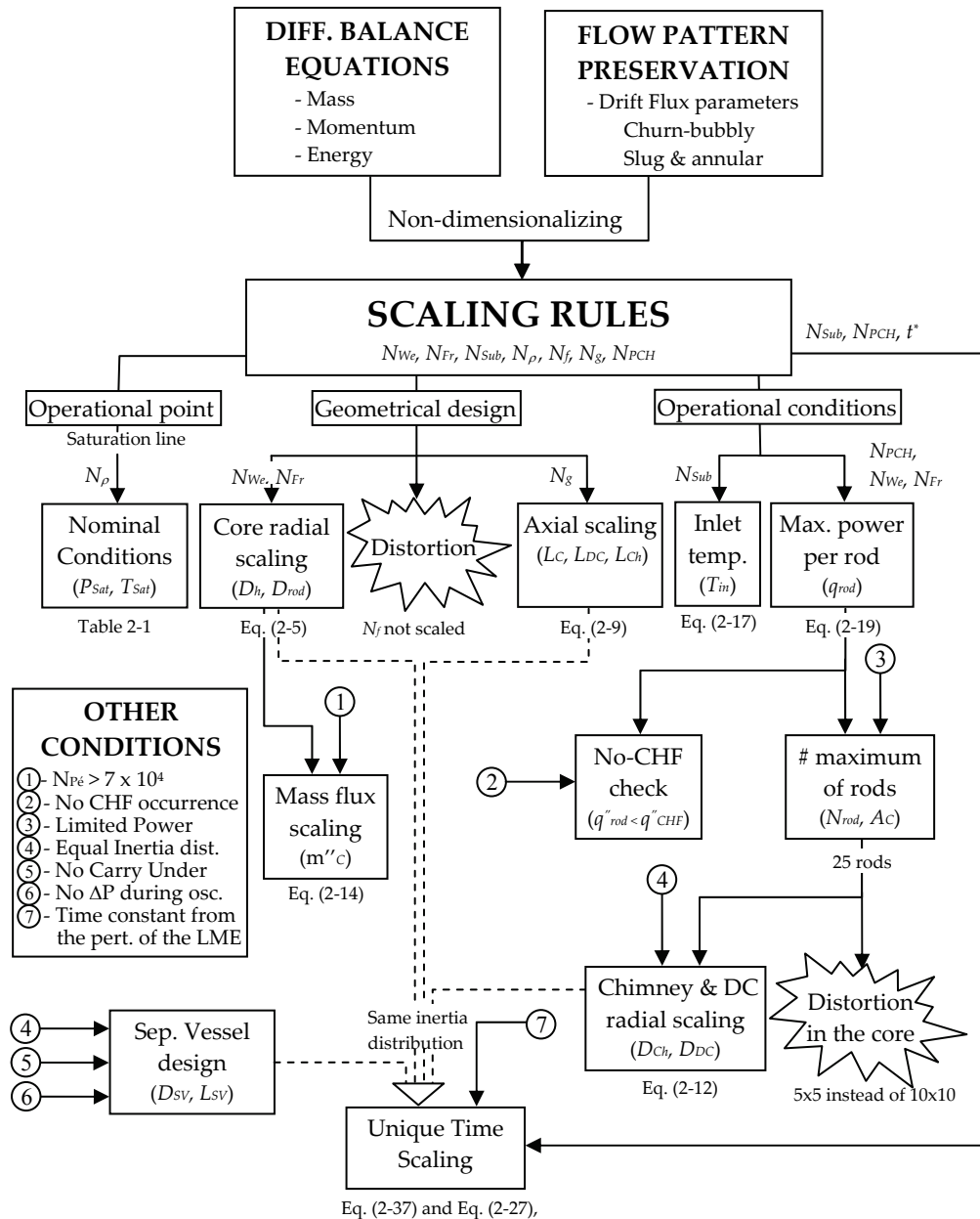


Figure 2-2: A schematic block diagram of the scaling procedure.

In the scaling procedure it is assumed that the reactor can be represented by three different sections: the core, the chimney and the downcomer. Thus, the mass, momentum and energy differential balance equations are expressed for each of these sections.

From the manipulation of the balance equations, a number of dimensionless numbers are found. These dimensionless numbers are the subcooling number N_{Sub} ; the density ratio N_ρ ; the friction number N_f ; the geometry number N_g and the phase change number $N_{PCH}^{7,3,8}$. These numbers need to be the same in both the facility and the reactor if similarity is to be achieved.

The drift-flux model parameters C_o and \bar{v}_{gj} (the distribution parameter and the weighted mean drift velocity respectively) are assumed to correctly describe the flow transitions in the reactor and are therefore used to characterize the flow pattern³. To assure the same flow pattern in the facility as in the reactor, the equations describing the C_o and the \bar{v}_{gj} are converted into their dimensionless form. In this way, two more scaling parameters arise, being the Froude and the Weber dimensionless numbers, N_{Fr} and N_{We} , respectively³.

In the GENESIS facility, Freon R-134a (CH_2FCF_3) is chosen as a coolant instead of others liquids because of its physical properties (which allow a great power, pressure and size reduction) and environmental properties.

Figure 2-2 shows that three main branches arise from the scaling rules: the operational point of the fluid is defined in the first branch, the second branch shows the geometrical scaling and the last one presents the scaling of the power and the inlet temperature.

2.2.1 Defining the operational conditions

The starting point of the whole scaling procedure is the matching of the so-called density number N_ρ from which the operational point (namely P_{sat} and T_{sat}) can be determined (see Figure 2-2 left hand branch). This matching gives a unique solution since the density number is a monotonical function of the pressure along the saturation line. This is

$$\frac{N_{\rho,R-134a}}{N_{\rho,water}} = 1 \rightarrow N_\rho = \frac{\rho_v}{\rho_l} = 5.03 \times 10^{-2} \text{ (at 71 bar)}. \quad (2-1)$$

As a result, the ESBWR operational nominal pressure of 71 bar can be reduced to 11.4 bar in the downscaled GENESIS facility. Hence, the pressure scaling factor X_{Press} , is found to be

$$X_{Press} = \frac{P_{R-134a}|_{GENESIS}}{P_{water}|_{ESBWR}} = 0.16. \quad (2-2)$$

Once the operational downscaled pressure is found, all Freon fluid properties are known. A comparison between the Freon and the water fluid properties is shown in Table 2-1.

	Symbol, Unit	Freon R-134a [†]	Water [‡]
Sat. temperature [†]	$T_{sat}, (^\circ\text{C})$	44.27	286.6
Sat. pressure	$P_{sat}, (\text{bar})$	11.38	71
Liquid density	$\rho_l, (\text{kg}/\text{m}^3)$	1128.3	738.23
Vapor density	$\rho_v, (\text{kg}/\text{m}^3)$	56.49	37.117
Liquid heat capacity	$C_p, (\text{kJ}/\text{kg}\cdot\text{K})$	1.525	5.42
Latent heat	$h_{fg}, (\text{kJ}/\text{kg})$	158.39	1499
Surface tension	$\sigma, (\text{N}/\text{m})$	5.66×10^{-3}	17.3
[†] Properties calculated at 11.4 bar; [‡] Properties calculated at 71 bar			

Table 2-1: Physical properties of Freon R-134a and water at saturated conditions.

2.2.2 Geometrical scaling

Moving rightwards in Figure 2-2, the second branch describing the geometrical scaling can be found.

Radial scaling of the core

The correct scaling of the flow pattern in the assembly is attained by keeping the Weber and Froude dimensionless numbers in the two systems the same^{3,8}, when the departure of bubbles is hydrodynamically controlled ($N_{Pe} > 7 \times 10^4$).

Conventionally the Eötvös number $N_{Eö}$, defined as the ratio between the Weber and the Froude number, is used. For the ESBWR its value is

$$N_{Eö}|_{ESBWR} = \frac{N_{We}}{N_{Fr}} = \frac{\frac{(\dot{m}_0'')^2 D_h}{\rho_l \sigma}}{\frac{(\dot{m}_0'')^2}{\rho_v^2 g D_h}} = \frac{D_h^2 \rho_v^2 g}{\rho_l \sigma} = 0.085. \quad (2-3)$$

By keeping this dimensionless number the same, the following relation is found.

$$\frac{N_{Eö}|_{ESBWR}}{N_{Eö}|_{GENESIS}} = 1 \Rightarrow \frac{D_h^2 \rho_l}{\sigma}|_{ESBWR} = \frac{D_h^2 \rho_l}{\sigma}|_{GENESIS} = 3.46 \frac{\text{s}^2}{\text{m}} \quad (2-4)$$

Equation (2-4) fixes the GENESIS core radial dimensions since the physical properties of the working fluids are constant (at the operational point) and are already known. Thus, the core radial scaling factor $X_{Core,r,g}$ is

$$X_{Core,r,g} = \frac{D_{h,R-134a}}{D_{h,water}} = \left(\frac{\sigma_{R-134a} \rho_{l,water}}{\sigma_{water} \rho_{l,R-134a}} \right)^{1/2} = 0.46. \quad (2-5)$$

From the dimensionless form of the momentum balance equation of the flow in the core, it can be seen that the radial and axial dimensions are related by the geometry number. This number is defined as

$$N_g = \frac{D_h}{L_c}, \quad (2-6)$$

which needs to be kept the same for a proper scaling. Thus, the core axial and radial geometry scaling factors $X_{C,a,g}$ and $X_{C,r,g}$ respectively, also need to be the same. Consequently,

$$X_{C,r,g} = X_{C,a,g} = \frac{L_{C,R-134a}}{L_{C,water}}. \quad (2-7)$$

Axial scaling of all sections

Since the mass flow rate is driven by natural circulation, the axial scaling is very important in the GENESIS facility. This scaling is derived from achieving a similar balance of buoyancy-to-drag forces in GENESIS as in the ESBWR. Such a balance can be found by integrating the steady state momentum balance equations over the length of the loop. As a result, the following relation for the square of the dimensionless mass flow rate is found, which needs to be equal for the two systems.

$$M^2 = \frac{\frac{L_{DC}^*}{N_{Fr}} - \frac{L_c^*}{N_{Fr}} [N_p \alpha + (1-\alpha)] - \frac{L_{Gh}^*}{N_{Fr}} [N_p \alpha + (1-\alpha)]}{\frac{1}{2A_c^{*2}} \left[\left(N_{f,C,TP} + \sum_j K_{j,C,TP} \right) + \frac{A_c^{*2}}{A_{Gh}^{*2}} \left(L_{Gr}^* N_{f,Gh,TP} + \sum_j K_{j,Gh,TP} \right) + \frac{A_c^{*2}}{A_{DC}^{*2}} N_{f,DC} L_{DC}^* \right]} \quad (2-8)$$

In the numerator, the Froude and density numbers, together with the void fraction (to be shown later in this section), are kept the same in the GENESIS facility and the ESBWR. In addition, the dimensionless lengths of all the sections need to be matched. This means that all lengths in the facility need to be downscaled following the same rule. Consequently, Equation (2-7) has to be applied to all lengths present in the GENESIS facility. Especially the chimney section needs to be properly scaled since both the core and the chimney length (and therefore the downcomer length also) determine the driving head. The axial geometry scaling factor $X_{a,g}$ is therefore the same for all sections (see Figure 2-2),

$$X_{a,g} = X_{C,a,g}. \quad (2-9)$$

The radial and axial core dimensions are related to the dimensionless core area by the so-called geometry non-dimensional number, N_g (see Equation (2-6)). Note that this scaling criterion is not unique since the friction non-dimensional number N_f , also relates the same dimensions (see the denominator of Equation (2-8)) via

$$N_f = f_{TP} \frac{L}{D_h}. \quad (2-10)$$

Since the two-phase friction factor (and its dependence with the quality) is not equal for Freon R-134a and for water, an inevitable distortion exists. All distortions, however, are treated separately further in section 2.2.4. of this chapter.

Once the core radial scaling has been completed, the same procedure must be applied to the other sections. The radial scaling of the downcomer and the chimney are particularly important since they strongly contribute to the inertia of the loop which is of importance for the dynamics of the system.

Radial scaling of the chimney and downcomer sections

In a natural circulation loop, the mass flow rate $M(t)$ is described by the loop momentum equation, which in its non-dimensional form can be written as

$$\frac{dM^*(t)}{dt^*} = \frac{\Delta P_{driv}^*(t) - \Delta P_{loss}^*(t)}{\sum_i \frac{l_i^*}{A_i^*}}, \quad (2-11)$$

with $\Delta P_{driv}^*(t)$ being the driving force of the flow and $\Delta P_{loss}^*(t)$ the pressure losses⁹. From Equation (2-11) it is clear that the inertia of the loop is determined by the summation in the denominator of all non-dimensional length-to-area ratios present in the loop. Hence, to get the same dynamic response in the downscaled system as in the ESBWR, all radial dimensions in the facility have to be scaled by the same rule as the lengths¹⁰. Consequently, a unique geometrical scaling factor X_g , exists for all dimensions of the facility.

$$X_g = X_{a,g} = X_{r,g} = \left(\frac{\sigma_{R-134a} \rho_{l,water}}{\sigma_{water} \rho_{l,R-134a}} \right)^{1/2}. \quad (2-12)$$

The inertia contribution of each section in the case of the ESBWR, expressed by the ratio in the denominator of Equation (2-11) is presented in Figure 2-3.

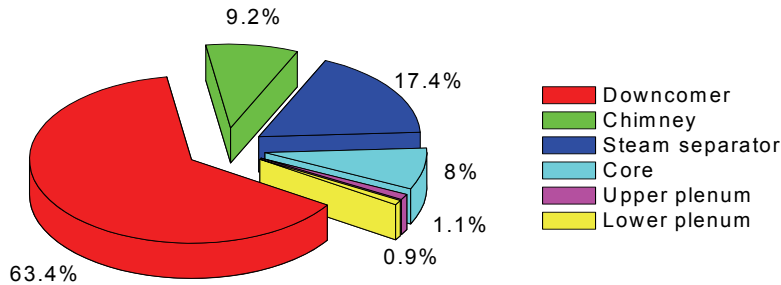


Figure 2-3: Inertia distribution in the ESBWR per section.

As can be observed, almost two thirds of the total inertia in the ESBWR is induced by the downcomer. This shows that a correct scaling of this section is very important in order to achieve the stability similarity.

Design of the separation vessel

Figure 2-3 also shows the small contribution of the upper and lower plenum to the total inertia in the ESBWR. This finding allows designing the separation vessel to achieve an optimum vapor-liquid separation. This means that the cross-sectional area of the separation vessel can be enlarged, such that its inertia contribution remains small (see Equation (2-11)), in order to enhance the vapor-liquid separation process.

Because of the complexity of the two-phase flow in the steam separation of the ESBWR, the transit time associated to the flow in the separators plus the upper plenum (UP) cannot be accurately predicted. Due to this uncertainty the length of the separation vessel is decided to be equal to the downscaled mean flow path in the UP in the ESBWR¹⁰. As the contribution of the UP to the total inertia can be neglected, the area of the separation vessel is designed on the basis of avoiding carry-under under all possible operational conditions instead of proper scaling of the associated inertia.

Mass flux scaling

The second result from matching the Weber and the Froude numbers is the scaling rule for the mass flux. By equalling the product of N_{We} and N_{Fr} for the GENESIS facility and the ESBWR, the next relation can be written,

$$1 = \frac{N_{We} N_{Fr}|_{ESBWR}}{N_{We} N_{Fr}|_{GENESIS}} = \frac{\dot{m}_0''^4}{\rho_l^3 \sigma} \bigg|_{ESBWR} \frac{\rho_l^3 \sigma}{\dot{m}_0''^4} \bigg|_{GENESIS}. \quad (2-13)$$

The mass flux scaling factor $X_{m''}$ is thus given by

$$X_{m''} = \frac{\dot{m}_{0,R-134a}''}{\dot{m}_{0,water}''} = \left(\frac{\sigma_{R-134a}}{\sigma_{water}} \right)^{1/4} \left(\frac{\rho_{l,R-134a}}{\rho_{l,water}} \right)^{3/4} = 1.007. \quad (2-14)$$

Scaling the operational conditions

From the non-dimensional equations it is found that the quality profile has to be preserved in the GENESIS facility. The thermodynamic quality profile according to the homogeneous equilibrium model (HEM), (in the case of an axial uniform heat flux in the rods) can be written as

$$\chi_{(z)} = N_{PCH} \left(\frac{z}{L_C} \right) \frac{N_\rho}{1 - N_\rho} - N_{Sub} \frac{N_\rho}{1 - N_\rho}. \quad (2-15)$$

Thus, to properly scale the quality profile in the heated section, the subcooling number N_{Sub} , and the phase change number N_{PCH} , need also to be matched.

The inlet temperature of the Freon R-134a is determined by matching the subcooling number N_{Sub} .

$$N_{Sub}|_{GENESIS} = N_{Sub}|_{ESBWR} = \frac{h_{in} - h_{sat}}{h_{fg}} \frac{\rho_l - \rho_v}{\rho_v} = 0.95. \quad (2-16)$$

Thus, the inlet temperature in the GENESIS facility representing the ESBWR nominal condition is

$$T_{in}|_{GENESIS} = 39.8 \text{ } ^\circ\text{C}|_{R-134a}. \quad (2-17)$$

The phase change number N_{PCH} , fixes the power to be applied per rod (via the power scaling factor, X_p), see the right hand branch of Figure 2-2.

$$\frac{N_{PCH}|_{GENESIS}}{N_{PCH}|_{ESBWR}} = 1 \rightarrow X_p = \frac{q_{GENESIS/rod}}{q_{ESBWR/rod}} = \left(\frac{\rho_{l,water}}{\rho_{l,R-134a}} \right)^{1/4} \left(\frac{\sigma_{R-134a}}{\sigma_{water}} \right)^{5/4} \left(\frac{h_{fg,R-134a}}{h_{fg,water}} \right) = 0.023 \quad (2-18)$$

Therefore, the power for one GENESIS heating rod[†] is

$$q|_{GENESIS/rod} = 1.01 \text{ kW}|_{R-134a}. \quad (2-19)$$

The N_{PCH} together with the N_{Sub} defines the operational point in the stability plane¹¹, hence stability comparisons can be made between the GENESIS and the ESBWR when these two numbers are the same.

As can be noted from Equation (2-18), the power scaling factor refers to the power *per rod*. An external constraint exists, which is related to the maximum available power to operate the GENESIS facility, which fixes the number of heating rods, N_{rod} (see Figure 2-2, third branch).

Once N_{rod} is fixed, the cross sectional core area can be calculated via Equation (2-5). Consequently, the rest of the radial geometries (e.g. the chimney diameter D_{Ch} , and the downcomer diameter D_{DC}) can also be accounted.

In the GENESIS particular case, the power available allowed to have a maximum of 25 downscaled ESBWR heating rods. These rods are arranged in a 5x5 square lattice, following a typical BWR arrangement.

Other requirements that need to be fulfilled by the facility are: vapor separation without the introduction of carry-under in the separation vessel (condition 5 in Figure 2-2) and the Péclet number, N_{Pe} , being larger than 7×10^4 in the GENESIS core (condition 1 in Figure 2-2). The latter condition assures the void ejection being hydrodynamically controlled which implies that the Weber and the Froude numbers correctly describe the flow pattern¹². In addition, the critical heat flux phenomenon (CHF) needs to be absent (condition 2 in Figure 2-2). The latter is discussed in the following section.

[†] The power of an average ESBWR fuel rod is found as the total reactor thermal power divided by the total number of fuel of pins. It equals to 43.2 kW (= 4500 Mw/1132 x 92).

Margin to the Critical Heat Flux (CHF) occurrence

The critical heat flux (CHF) is a well known phenomena that enormously degrades the heat transfer from rod to coolant and therefore needs to be avoided in real plant conditions. CHF does not occur in the ESBWR, but since this phenomenon is not scaled, the absence of CHF in the GENESIS facility needs to be proved. For this reason a study based on the look-up table and on experimental investigations especially performed by Pioro¹³ in small tubes with Freon R-134a is performed. In this study the GENESIS nominal core exit condition (in terms of quality, heat flux and mass flux) is compared with those experiments for which CHF is reached. Figure 2-4 presents the results of such research investigation. This figure, extracted from the work of Pioro¹³, shows the experimental relations found between the critical value of the heat flux and the critical value of the local quality (i.e. those values for which the CHF point is reached) for different mass fluxes. Superimposed to these results is the most critical operational point for the GENESIS facility expressed in terms of the core exit quality and the heat flux at the surface of the heating rods.

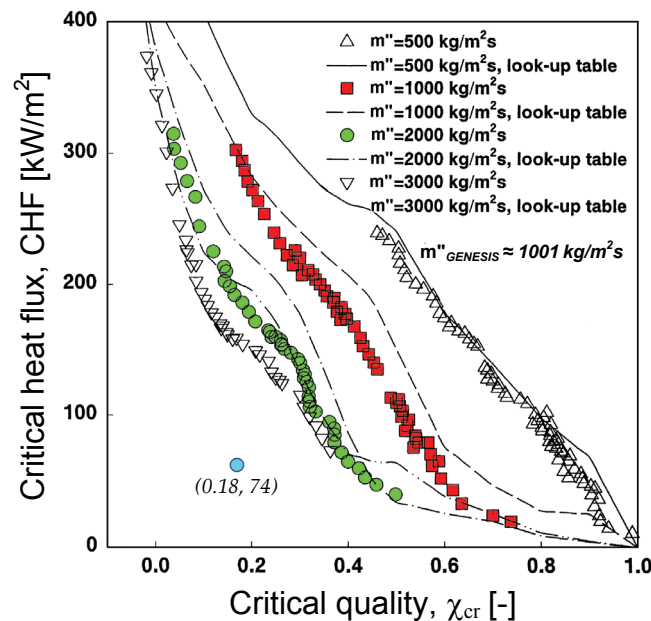


Figure 2-4: Experimental relations found for Freon R-134a between the critical heat flux and the critical quality. A sufficient CHF margin of occurrence was proven for all the GENESIS facility operational conditions.

As can be observed from Figure 2-4, a large margin to CHF can be assured in the GENESIS facility (at any realistic operational condition), since the CHF occurrence for both, a mass flux equal to 1000 kg/m²s and a mass flux equal to 2000 kg/m²s are far from the most critical GENESIS operational point which corresponds to a mass flux of ~1000 kg/m²s.

2.2.3 Scaling of the dynamics

From the scaling equations, it follows that in the GENESIS facility time is not a scaled parameter. In other words, the time in GENESIS could run at a different speed than in the ESBWR. Since we are interested in the dynamics of the reactor, the determination of the correspondence between the two times (defined by the time ratio, X_t), becomes an important issue. In this section, X_t is addressed by using a steady state approach (based on the transit time through the core plus chimney section) and an approach based on dynamic considerations (by making use of perturbation theory analysis of the linearized version of the loop momentum equation). For completeness, the time ratio derived from the non-dimensionalization process, is also presented.

Time ratio from the flow transit-time

Many authors have pointed out the importance of the transit time through the heated plus chimney sections in the physics involving density wave oscillations (DWO). DWO are the most common type of instability mechanism found in BWRs at high pressure which, as result of the scaling process, are expected to be also present in the GENESIS facility. Consequently, an expression for the steady state time ratio $X_{t,ss}$, can be derived from the transit times calculated for the ESBWR and the GENESIS facility.

The non-dimensional steady state coolant transit time, estimated from the operational conditions, can be calculated from the following set of equations^{14,15}.

- Core section

- - Single phase region $\tau_{1\phi} \equiv \frac{N_{Sub}}{N_{PCH}}$ (2-20)

- - Two-phase region $\tau_{2\phi} \equiv \frac{1}{N_{PCH}} \ln(1 + N_{PCH} - N_{Sub})$ (2-21)

- - Chimney section $\tau_{Ch} \equiv \frac{L_{Ch}^* A_{Ch}^*}{1 + N_{PCH} - N_{Sub}}$ (2-22)

Where the non-dimensional chimney length and area are respectively defined as

$$L_{Ch}^* \equiv \frac{L_{Ch}}{L_C} \text{ and } A_{Ch}^* \equiv \frac{A_{Ch}}{A_C}. \quad (2-23)$$

The transit time can thus be calculated by

$$t_t = (\tau_{C,1\phi} + \tau_{C,2\phi} + \tau_{Ch}) \frac{L_C}{v_0}, \quad (2-24)$$

where v_0 is the velocity of the coolant at the core inlet.

The ratio between the transit time for the GENESIS facility and the ESBWR is

$$\frac{t_t|_{GENESIS}}{t_t|_{ESBWR}} = \frac{(\tau_{C,1\phi} + \tau_{C,2\phi} + \tau_{Ch})|_{GENESIS}}{(\tau_{C,1\phi} + \tau_{C,2\phi} + \tau_{Ch})|_{ESBWR}} \frac{\left. \frac{L_C}{v_0} \right|_{GENESIS}}{\left. \frac{L_C}{v_0} \right|_{ESBWR}} = \frac{\left. \frac{L_C}{v_0} \right|_{GENESIS}}{\left. \frac{L_C}{v_0} \right|_{ESBWR}}. \quad (2-25)$$

The first terms cancels out because all the non-dimensional parameters that determine the different contributors to the non-dimensional transit times are the same for the two systems (see Equations (2-20), (2-21) and (2-22)). Thus,

$$X_{t,ss} = \frac{t_t|_{GENESIS}}{t_t|_{ESBWR}} = \frac{L_C \rho_{l,0}}{\dot{m}_0''} \bigg|_{GENESIS} \frac{\dot{m}_0''}{L_C \rho_{l,0}} \bigg|_{ESBWR}. \quad (2-26)$$

By expressing the velocity in terms of the mass flux and using equation (2-14), equation (2-27) is found.

$$X_{t,ss} = \left(\frac{\sigma_{R-134a}}{\sigma_{water}} \frac{\rho_{l,water}}{\rho_{l,R-134a}} \right)^{1/4} = 0.68. \quad (2-27)$$

Equation (2-27) shows that at steady state conditions, the time ratio is not equal to 1 but time runs $1/0.68=1.45$ times faster in the downscaled GENESIS facility than in the ESBWR.

By comparing Equations (2-12) and (2-27), it is found that a direct relation exists between the steady state time ratio $X_{t,ss}$, and the geometrical scaling factor X_g . This relation is

$$X_{t,ss} = X_g^{1/2}. \quad (2-28)$$

As the above findings are based on steady-state quantities (i.e. transit times), in order to investigate whether the dynamic response of the GENESIS facility follows the same rule as that expressed by Equation (2-27), the time ratio estimated by making use of dynamic considerations is also addressed.

Time ratio from the perturbation of the linearized momentum equation (LME)

The dimensional version of Equation (2-11) derived from the momentum balance equation of the whole loop is

$$\frac{dM(t)}{dt} = \frac{\Delta P_{driv}(t) - \Delta P_{loss}(t)}{\sum_i \frac{l_i}{A_i}}, \quad (2-29)$$

where the driving forces can be estimated as

$$\Delta P_{driv}(t) = \langle \alpha \rangle L_{tot} \Delta \rho \cdot g, \quad (2-30)$$

where $\langle \alpha \rangle$ represents the average void-fraction over the core plus chimney sections and L_{tot} is the correspondent total length. The frictional pressure drop is modeled as $\Delta P_{loss}(t) = a \cdot M^2$ where the parameter a originates from the requirement that $dM/dt = 0$ at the stable operating point.

The loop momentum balance equation is linearized by making use of the following set of equations.

$$\begin{aligned} \langle \alpha \rangle_{(t)} &= \langle \alpha \rangle_0 + \delta \langle \alpha \rangle_{(t)} \\ M_{(t)} &= M_0 + \delta M_{(t)} \end{aligned} \quad (2-31)$$

and the steady state momentum balance can be written as

$$a.M_0^2 = \langle \alpha \rangle_0 L_{tot} \Delta \rho \cdot g. \quad (2-32)$$

By Laplace transforming, the transfer function from void fraction fluctuations to flow rate fluctuations can be found as,

$$\frac{\delta \hat{M}}{\delta \hat{\alpha}} = \frac{M_0}{2 \langle \alpha \rangle_0} \frac{1}{1 + s\tau}, \quad (2-33)$$

where \hat{M} and $\hat{\alpha}$ are the Laplace transforms of M and α respectively and s the Laplace variable. The time constant of this transfer function is thus,

$$\tau = \frac{M_0 \sum_i \frac{l_i}{A_i}}{2 \langle \alpha \rangle_0 L_{tot} \Delta \rho \cdot g}. \quad (2-34)$$

The dynamic time ratio $X_{t,d}$, can now be determined by taking the ratio of the time constants, as expressed in Equation (2-34), for the GENESIS facility and the ESBWR cases. Thus

$$X_{t,d} = \frac{\tau|_{GENESIS}}{\tau|_{ESBWR}} = \left[\frac{\frac{A_C \sum_i \frac{l_i}{A_i}|_{GENESIS}}{L_{tot} \sum_i \frac{l_i}{A_i}|_{ESBWR}} \right] \frac{\dot{m}_0''|_{GENESIS} \frac{2 \langle \alpha \rangle_0 \Delta \rho \cdot g|_{ESBWR}}{\dot{m}_0''|_{ESBWR} \frac{2 \langle \alpha \rangle_0 \Delta \rho \cdot g|_{GENESIS}}}}{\quad} \quad (2-35)$$

The term within brackets cancels out since a unique scaling rule exists for scaling the geometry (see Equation (2-12)). The mean void fraction terms also cancel out since the void profile in the GENESIS facility is kept the same as in the ESBWR (this is one of the most important requirements of the scaling). By using the definition of the mass flux scaling factor $X_{\dot{m}''}$, Equation (2-35) can be expressed as

$$X_{t,d} = \frac{\tau|_{GENESIS}}{\tau|_{ESBWR}} = X_{\dot{m}''} \frac{\Delta \rho_{water}}{\Delta \rho_{R-134a}} = X_{\dot{m}''} \frac{\rho_{water,l} (1 - N_{\rho,water})}{\rho_{R-134a,l} (1 - N_{\rho,R-134a})}. \quad (2-36)$$

The operational point of the GENESIS facility is chosen so that the density number N_ρ is kept the same as in the ESBWR (see Equation (2-1)). By using Equation (2-14), the dynamic time ratio, $X_{t,d}$, is therefore found as

$$X_{t,d} = \frac{\tau|_{GENESIS}}{\tau|_{ESBWR}} = \left(\frac{\sigma_{R-134a} \rho_{l,water}}{\sigma_{water} \rho_{l,R-134a}} \right)^{1/4} = 0.68. \quad (2-37)$$

As can be seen, Equation (2-37) is identical to Equation (2-27). This finding means that, in the case the same geometrical scaling rule is used for all the sections in the facility, the time ratio from both steady state considerations and dynamic considerations is the same, i.e. a unique time ratio exists.

By calculating the breaking frequency associated to the ESBWR time constant of the void-to-flow transfer function at nominal conditions, as expressed by Equation (2-34), the following result is obtained.

$$\tau|_{\text{ESBWR}} = \frac{M_0 \sum_i \frac{l_i}{A_i}}{2 < \alpha >_0 L_{\text{tot}} \Delta \rho \cdot g} = \frac{12000 \frac{\text{kg}}{\text{s}} 3.2 \frac{1}{\text{m}}}{2 \times 0.7 \times L_{\text{tot}} \cdot \Delta \rho \cdot g} = 0.23 \text{ s} \rightarrow f|_{\text{ESBWR}} = \frac{1}{2\pi \tau|_{\text{ESBWR}}} \approx 0.7 \text{ Hz} . \quad (2-38)$$

This frequency is in the order of magnitude of the typical frequencies of BWRs Type II oscillations (~ 1 Hz) and therefore cannot be neglected as other authors recommended¹⁶. Furthermore, the downcomer section contributes with roughly two thirds of the summation in the numerator, which means the preservation of the inertia in this section is particularly important in order to achieve a correct scaling of the dynamical behavior.

Time ratio from the non-dimensional time

From the non-dimensionalization process, the same non-dimensional time is found from the three balance equations (for the mass, momentum and energy) for all the sections. This non-dimensional time is expressed as

$$t^* \equiv \frac{t}{\frac{L_C \rho_{l,0}}{\dot{m}_0}} . \quad (2-39)$$

By equating the non-dimensional time for the GENESIS facility and the ESBWR, the following relation is obtained for the time ratio X_t ,

$$\frac{t|_{\text{GENESIS}}}{t|_{\text{ESBWR}}} = \frac{\dot{m}_0}{L_C \rho_{l,0}} \bigg|_{\text{ESBWR}} \frac{L_C \rho_{l,0}}{\dot{m}_0} \bigg|_{\text{GENESIS}} = \frac{\dot{m}_{0,\text{ESBWR}}}{\dot{m}_{0,\text{GENESIS}}} \frac{L_{C,\text{GENESIS}}}{L_{C,\text{ESBWR}}} \frac{\rho_{l,0,R-134a}}{\rho_{l,0,\text{water}}} . \quad (2-40)$$

By using the scaling rules expressed in equations (2-12) and (2-14), equation (2-40) can be rearranged to find equation (2-41).

$$\frac{t|_{\text{GENESIS}}}{t|_{\text{ESBWR}}} = \left(\frac{\sigma_{R-134a} \rho_{l,\text{water}}}{\sigma_{\text{water}} \rho_{l,R-134a}} \right)^{1/2} \left(\frac{\rho_{l,\text{water}}}{\rho_{l,R-134a}} \right)^{3/4} \left(\frac{\sigma_{\text{water}}}{\sigma_{R-134a}} \right)^{1/4} \frac{\rho_{l,R-134a}}{\rho_{l,\text{water}}} = \quad (2-41)$$

$$\frac{t|_{\text{GENESIS}}}{t|_{\text{ESBWR}}} = \left(\frac{\sigma_{R-134a}}{\sigma_{\text{water}}} \frac{\rho_{l,\text{water}}}{\rho_{l,R-134a}} \right)^{1/4} = X_t = X_g^{1/2} . \quad (2-42)$$

As it can be seen, Equation (2-42) is identical to Equations (2-27) and (2-37) and therefore the same scaling rule is obtained from this method.

Conclusions and remarks regarding the time ratio

As a result of the previous analysis, it was proven that the time ratio obtained from the approaches based on the transit time through the channel and the non-dimensional time, are equivalent if the N_{PCH} , N_{Sub} are the same, and the core and chimney areas are scaled in the same manner. From the dynamic analysis, however, an extra requirement needs to be fulfilled: the downcomer area has to be downscaled following the same rule as in the core and chimney cases. This result indicates that the inertia of each section in the loop has to be properly scaled in order to obtain a unique relation for the time ratio. Hence, a scaling based on merely the core and the chimney sections (as performed by Van de Graaf³) leads to an erroneous dynamic scaling since the time ratio is not well defined (i.e. a different time ratio is obtained from static and dynamic considerations).

In the case the geometry scaling is correctly performed the time ratio is merely described by the physical properties of the two fluids. In addition, a simple equation is found which relates the time ratio and the geometrical scaling factor. An important implication of this finding is that the geometrical scaling factor and the time ratio are not independent in buoyancy driven systems.

It has to be mentioned that the difference in the time speed is a distortion that cannot be corrected by changing the geometry since, with such a change, the stability characteristics (e.g. the decay ratio) will also change and the dynamic similarity will be lost. The best way to correct this distortion in the time is to convert the experimental results to the water time frame by using the relation found for the time ratio X_t (Equation (2-37)).

2.2.4 Treatment of the distortions

In sections 2.2.1, 2.2.2 and 2.2.3, the scaling of the operational conditions, the geometry and the time is shown. As a result of that scaling some undesired effects (so-called 'distortions') appeared. The most important distortions are because of:

- limitations in the available power allow to simulate a 5x5 fuel bundle only (instead of a 10x10 ESBWR fuel bundle)
- the friction non-dimensional number N_f , is not properly scaled
- a small additional friction exists in the downscaled chimney and the downcomer sections, and
- the core by-pass channels are not included in the GENESIS simulated core.

These distortions and their influence on the thermal-hydraulic stability of the system need to be analyzed and, if possible, compensated for.

Core friction distortions

As result of the downscaling process, two main effects contribute to have a relative higher friction in the GENESIS core than in the ESBWR core.

First, the use of a reduced number of rods in the GENESIS bundle representing a complete ESBWR fuel bundle (5x5 instead of 10x10) creates a higher friction in the GENESIS core because of the increment in the wetted perimeter per rod (~15%).

The second contribution is related to the larger value of the friction factor coefficient for Freon 134a than for water and is explained as follows. Since two different non-dimensional numbers link the radial dimensions to the axial dimensions, namely

$$N_g = \frac{D_h}{L_c} \quad \text{and} \quad N_f = f \frac{D_h}{L_c}, \quad (2-43)$$

by using the geometry non-dimensional number N_g as scaling parameter may imply the friction number N_f , to be different for the GENESIS facility and the ESBWR^{7,10}.

To analyze the above distortion, the two-phase friction factor for the operational conditions, both for water and Freon R-134a, is determined by using the correlations suggested by Zhang¹⁷ (developed for Freons) and Müller¹⁸. Figure 2-5 shows that, for the same quality value, the friction factor is indeed higher in the GENESIS facility than in the ESBWR.

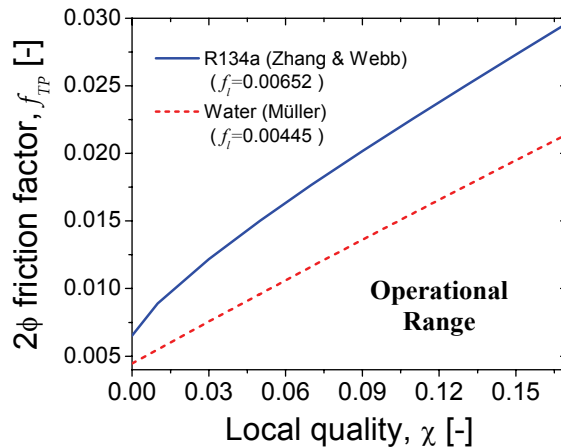


Figure 2-5: Two-phase friction factor for water and Freon R-134a as a function of the local quality.

Hence, the GENESIS facility has extra friction which may play a role in the stability of the system.

The net effect of the aforementioned distortions is that a higher friction exists in the GENESIS facility. This extra friction is particularly important in the core because of the high quality combined with the relatively small hydraulic diameter.

It can be shown that in a forced circulation system¹⁹ and in a natural driven system²⁰, in which the local restrictions are concentrated at the inlet and outlet of the channel (K_{in} and K_o respectively), the stability performance regarding the friction distribution is mainly controlled by a non-dimensional friction factor Υ defined as

$$\Upsilon = \frac{K_{in} + K_o}{1 + K_o}. \quad (2-44)$$

By preserving the scaling non-dimensional factor Υ , the stability of the scaled GENESIS facility and the ESBWR (in the non-dimensional plane) can be made similar by adjusting the chimney exit friction in such a way that Equation (2-44) is kept the same for both systems. Hence by increasing the outlet friction factor K_o , the effect of the higher inlet friction can be compensated.

To check the validity of the proposed correction, a reduced order model²¹ is used to calculate three different cases:

- the *ideal* one with the exact core inlet friction,
- a *distorted* one (i.e. with an extra friction placed at the core inlet) without any correction, and
- a second *distorted* one, in which the chimney outlet restriction is used to compensate the extra friction, according to Equation (2-44).

In this analysis a value of 8% extra friction in the core (which is the extra friction found in the GENESIS core) is assumed and later on corrected for. The resulting thermal-hydraulic stability boundaries (SBs) for the three cases are shown in Figure 2-6.

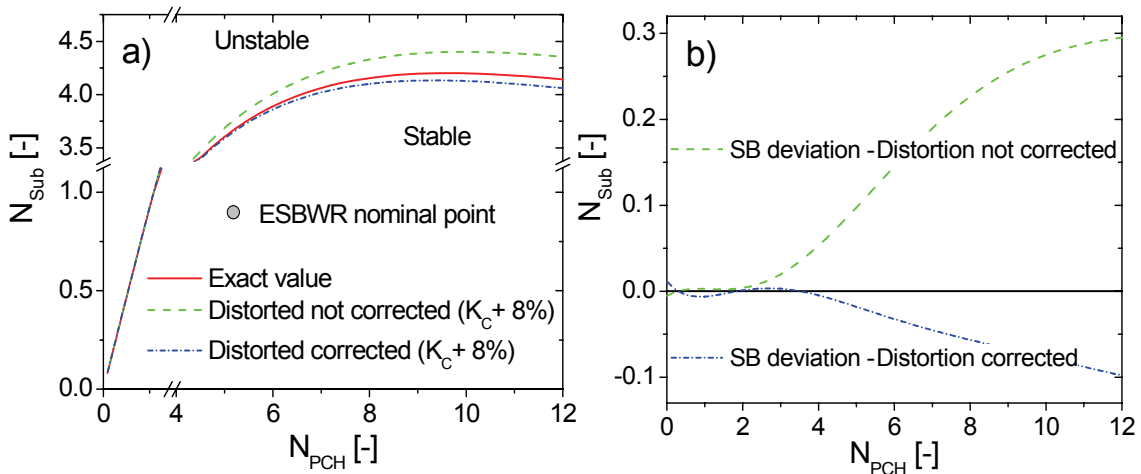


Figure 2-6: a) Thermal-hydraulic SBs calculated for the three different friction distributions in the loop: ideal case in which the friction is exactly downscaled (red solid line); scaled case with no correction of the distortion (green dotted line); corrected scaled system (blue dashed line). b) Deviation in the SBs for the corrected and not corrected cases (blue dashed and green dotted lines).

As can be seen in Figure 2-6, ignoring the distortion caused by the core extra friction leads to a non-conservative determination of the stability performance of the ESBWR, since the stable region enlarges. By keeping the non-dimensional number Υ the same, it can be assured that from the thermal-hydraulic stability point of view the experimental results performed in GENESIS will be slightly conservative.

From the results of the reduced order model shown in Figure 2-6b) it can be concluded that the proposed correction method significantly diminishes the distortion caused by the extra core friction.

Although equation (2-44) is derived from a simplified model (the core friction is concentrated only at the inlet), its application in the ESBWR downscaling is considered to be valid since the chimney section is very long and therefore the axial core friction distribution does not play an important role in the thermal-hydraulic stability.

Influence of the core by-pass channels

Since the presence of the core by-pass channels may influence the GENESIS stability, the absence of such channels in the GENESIS facility needs to be analyzed from both the neutronic and the thermal-hydraulic point of view. The neutronic feedback is simulated in GENESIS by using the same void reactivity feedback coefficient as in the ESBWR (see Chapter 3). This coefficient was estimated *including* the core by-pass channels. Hence, the similarity in the feedback mechanism is guaranteed by correctly simulating the void fraction in the core only. The effect of power deposition in the single-phase water from the by-passes is small and can therefore be neglected. From the thermal-hydraulic point of view, the lack of the core by-pass channels creates a slightly higher quality in the chimney section and therefore a slightly higher buoyancy force which has a destabilizing effect. For this reason, the absence of the core bypass channels has a slight conservative effect.

Chimney and downcomer extra friction

Another consequence of the radial reduction in GENESIS (together with the higher friction caused by Freon R-134a) is a higher frictional pressure drop in the chimney and the downcomer sections. Because of these pressure drops being uniformly distributed along the corresponding sections, they do not strongly influence the stability of the system. In addition, the increased friction is somewhat compensated by the higher buoyancy force created by the slightly higher void fraction in the GENESIS chimney caused by the absence of the core bypass channels (see Figure 2-13).

2.2.5 Scaling sensitivity to the operational pressure

A novel method for controlling the power in the ESBWR by means of varying the operational pressure has been suggested by some researchers²². It is therefore of importance to study the stability performance of the ESBWR at a pressure different than the operational one. The GENESIS facility, however, is designed to be operated at the point in which the density number is correctly matched (see Equation (2-1)). For different pressures, the operational conditions (i.e. power and temperature inlet conditions) and geometry would need to be modified in order to scale the reactor in this new situation. The geometry of the facility, however, cannot be easily adjusted.

In order to investigate how the geometrical scaling, given by Equation (2-12), should be modified when the operational pressure of the ESBWR is changed, Figure 2-7 is constructed. This figure shows the correspondence between the pressure in the ESBWR and the downscaled pressure in the facility. The figure has to be interpreted as follows: for a given ESBWR-water pressure at the right hand side scale, the corresponding downscaled Freon R-134a pressure is presented at the bottom scale (via the dotted line). The downscaled pressure can then be used to read the change in the geometrical scaling factor X_g , indicated by the left hand side scale (via the solid line).

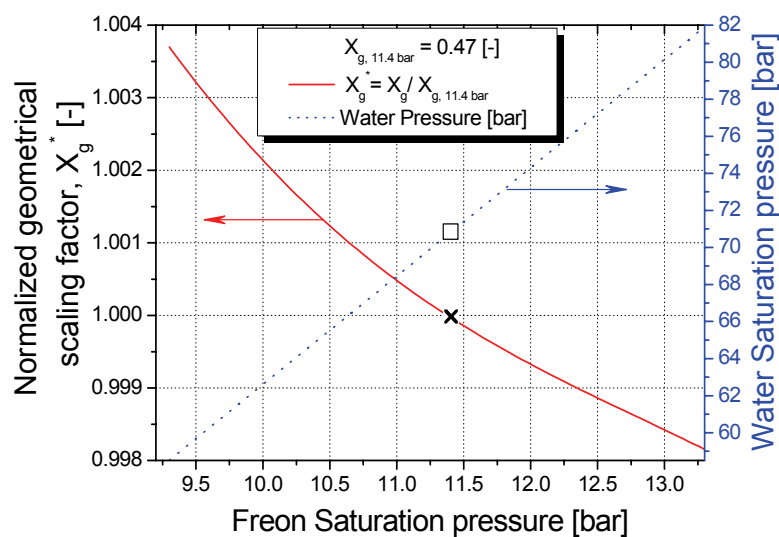


Figure 2-7: Pressure relation between the ESBWR (water) and the downscaled facility (Freon R-134a). The resulting change in the geometrical scaling factor with respect of the original conditions (71 bar in water) is also shown (indicated by □ and x).

For instance, to investigate the geometry scaling of the reactor at 64 bar, the water-Freon saturation pressure line can be used to read the correspondent Freon operational pressure which in turn accounts to ~10.25 bar. This Freon pressure is thus used to read the normalized scaling factor which in this example is ~1.0016.

Figure 2-7 shows that, for a wide range of pressures, the change in the geometrical friction factor is less than 0.5% and therefore can be neglected. In other words, the stability of the ESBWR can be studied with a facility using Freon R-134a for a wide range of pressures without geometrical changes. Thus, the change in the time scaling is also negligible, see Equations (2-27) and (2-37). The new scaling factors for the mass flux scaling, the power and the inlet subcooling, however, must be recalculated with the fluid properties at the new pressure, by using Equations (2-14), (2-16) and (2-18) respectively.

2.3 Application of the proposed scaling design approach

In order to analyze the proposed scaling design, the GENESIS facility is constructed according to the scaling rules described in the previous sections. Figure 2-8 shows a schematic view of the GENESIS test facility.

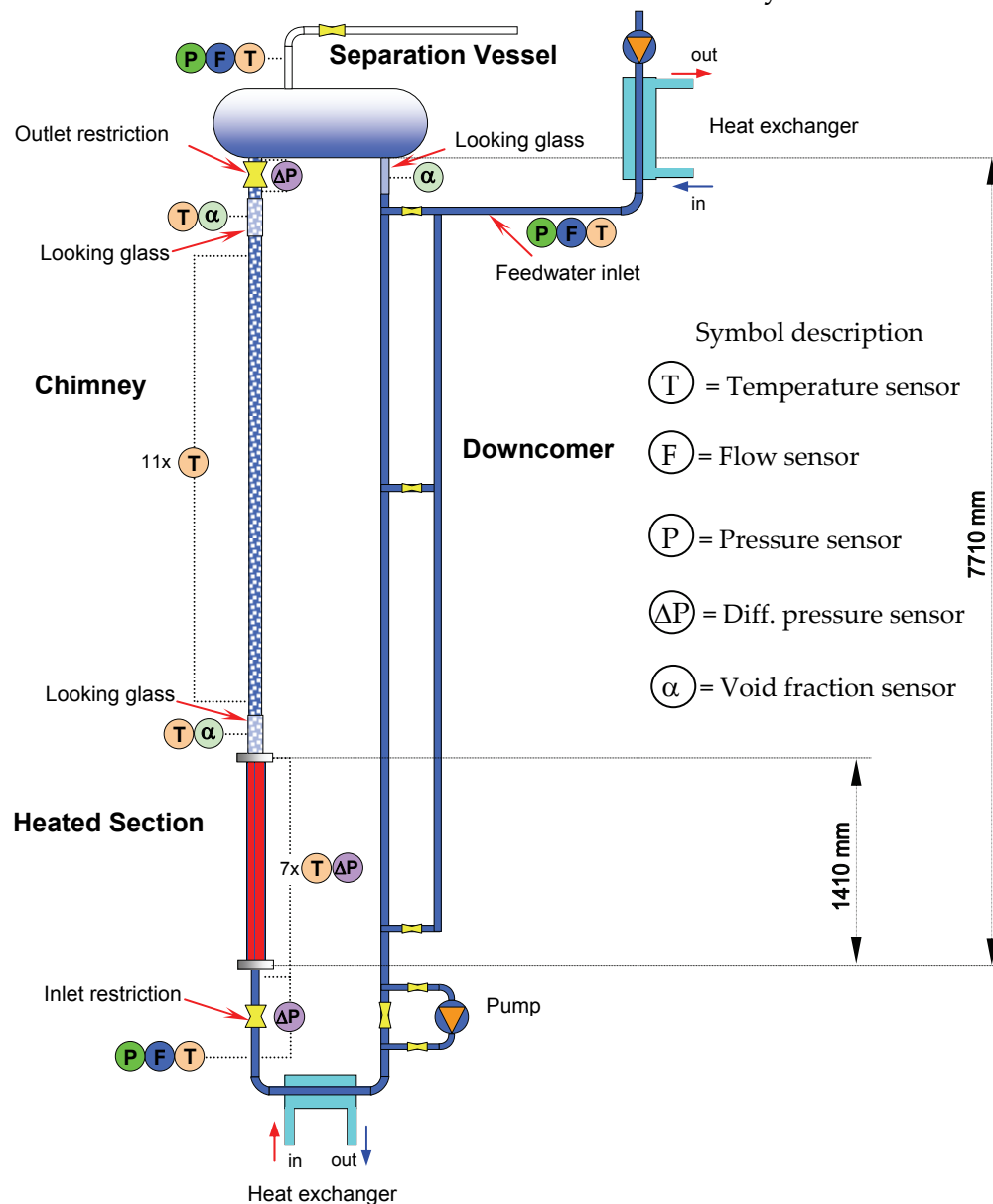


Figure 2-8: Schematic view of the GENESIS facility (not to scale)

The primary loop consists of a heated section, a chimney and a downcomer section. The vapor separation takes place in the separation vessel which design assures that no carry-under occurs. The heated section consists of a fuel bundle with 5x5 rods which represents a fuel bundle of the ESBWR. The core spacers and the tie plates are located in the same place as in the ESBWR. Numerous sensors located at different positions (thermo-couples, capacitance void fraction sensors, magnetic flowmeters and absolute and differential pressure sensors) allow characterizing the operational status of the facility (see the work of Marcel²⁰ for a complete description of the GENESIS facility). The GENESIS facility can be operated with natural or forced circulation. For this latter case, the primary pump needs to be used.

The two-phase flow created in the bundle enters the long chimney section, after which it flows into the separation vessel. The liquid Freon flows to the downcomer section, while the vapor flows upward towards the condenser. A regulator system controls the pressure in the separation vessel by means of a valve. The vapor leaving the separation vessel is condensed in the condenser, after which it is introduced into the facility by the feed "water" pump. The variable speed of this pump allows keeping the mass balance in the system. The temperature at which the liquid Freon is introduced can be controlled by the cooling system in order to satisfy the requirements regarding the inlet temperature. A heat exchanger placed in the horizontal part of the downcomer can enlarge the operation temperature range by heating/cooling the liquid just before it enters the heated section again.

Three transparent sections (looking glasses) placed at the core and chimney outlet and downcomer inlet allow visual inspection during operation. From the looking glass placed at the downcomer inlet, it is observed that carry-under does not take place as long as the liquid level is kept above a certain minimum value.

Technical details of the GENESIS facility are given in APPENDIX A.

The fictional pressure drop component distribution

In order to check whether the geometrical scaling and the treatment of the distortions resulted in a similar pressure drop distribution in the GENESIS facility and in the ESBWR the following study is conducted. Figure 2-9 shows the numerically estimated pressure drop for each section for both the ESBWR and the GENESIS facility.

In the figure the pressure drop contributions are grouped into two categories: the friction associated to the core (labeled as CORE) and the friction at the top of the chimney mainly associated to the void separation process (named as SS). It has to be mentioned that, even when the core pressure drop in GENESIS is 8% higher than in the ESBWR, the proper

adjustment of the exit chimney restriction allowed having the same value of the non-dimensional friction number Υ (see Equation (2-44)), for both systems.

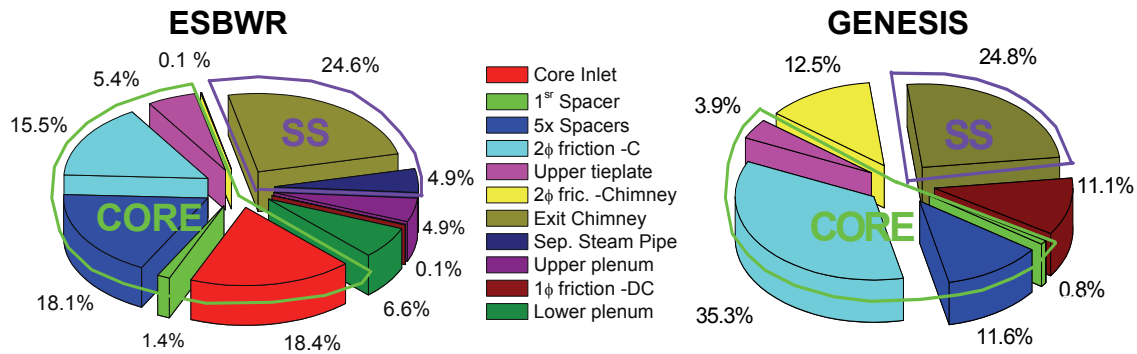


Figure 2-9: Calculated frictional pressure drop distribution at nominal conditions for the ESBWR and the GENESIS facility.

Note the relatively higher friction in the chimney and downcomer sections in the GENESIS facility which, however, do not influence the stability.

Core frictional pressure drop distribution

It is interesting to discuss more in detail the different friction pressure drop components in the core section for both the ESBWR and the GENESIS facility.

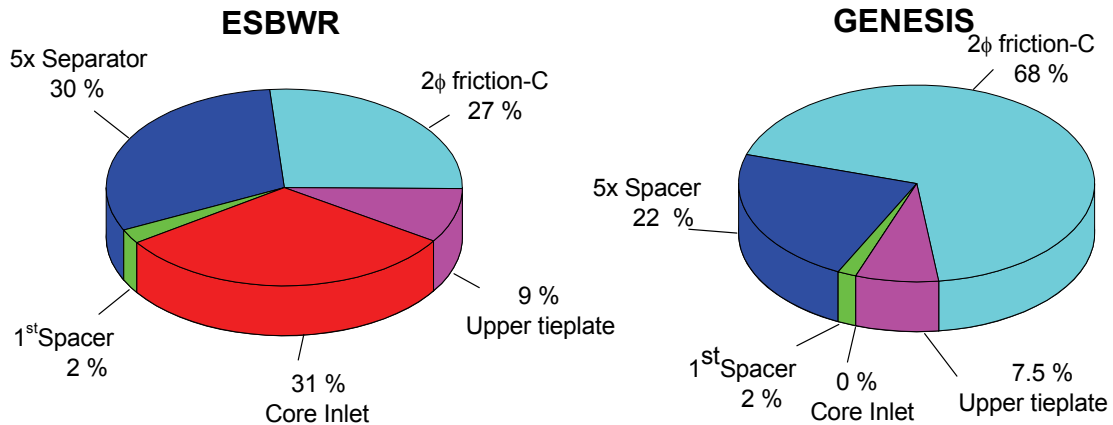


Figure 2-10: Calculated core frictional pressure drop contributors at nominal conditions for the ESBWR and the GENESIS facility.

From Figure 2-10, it can be seen that there exists a relatively larger friction caused by the Freon R-134a flow than by the water flow. This difference can be explained as follows:

- the larger single and two-phase friction factors for Freon than for water,
- the relatively smaller core hydraulic diameter in the GENESIS core section, and
- the slightly larger mass flux in GENESIS (see Equation (2-14)).

For the neutronic-thermal-hydraulic stability, the axial core friction pressure drop distribution is important since it may influence the resulting void fraction distribution. For this reason, the axial core friction pressure drop distribution for GENESIS and the ESBWR, need to be compared. This characteristic plays a role in GENESIS when the so-called void reactivity feedback (VRF) system is applied. Figure 2-11 shows the pressure distribution of both systems, thereby assuming nominal conditions and by applying an axially uniform power profile. To facilitate the comprehension, the comparison is done in terms of the normalized core frictional pressure drop and the normalized core axial length.

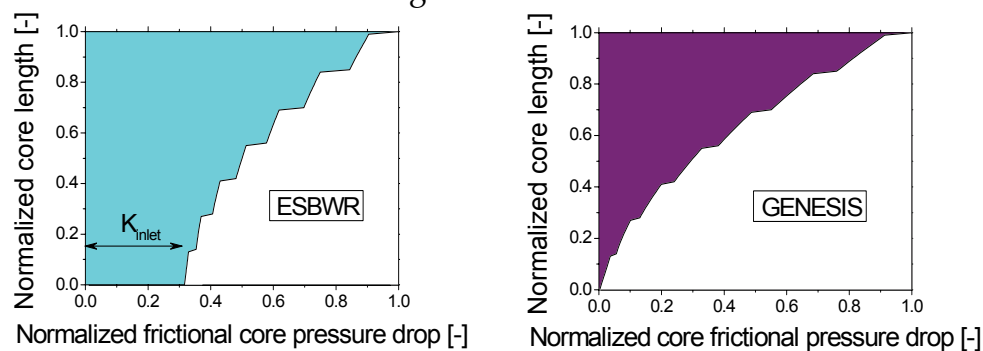


Figure 2-11: Normalized core axial frictional pressure drop distribution at nominal conditions for the ESBWR and the GENESIS facility.

As a result of the scaling process and the absence of core inlet friction in the facility, the GENESIS core section exhibits a more top-peaked frictional pressure drop distribution than the ESBWR. Consequently, the GENESIS facility shows smaller stability margins (i.e. conservative results) than the ESBWR from the neutronic-thermal-hydraulic point of view¹⁸.

System inertia distribution

The inertia distribution calculated for all the sections is shown in Figure 2-12 for the ESBWR and the GENESIS facility. From the figure it is clear that the inertia distribution is approximately the same in the two systems, which is a result of the use of the same scaling rule for radial and axial dimensions for all sections. As in the ESBWR, the downcomer inertia significantly contributes to the total inertia in GENESIS, being roughly two thirds of the total inertia.

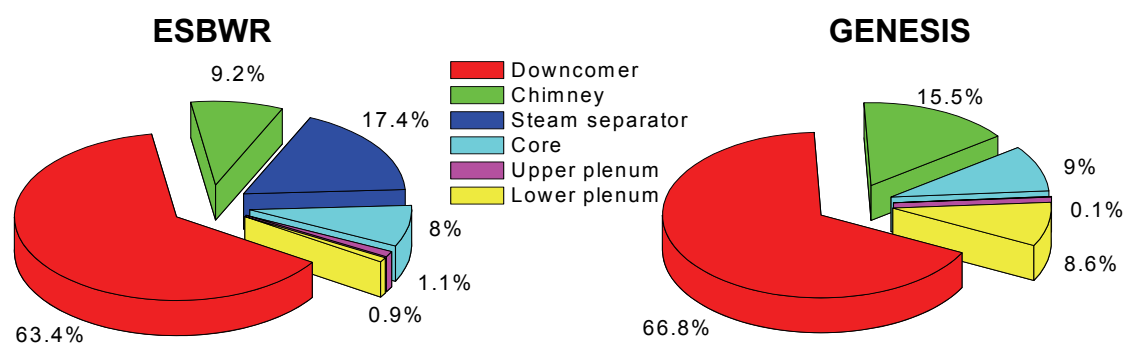


Figure 2-12: Inertia distribution for the ESBWR and the GENESIS facility.

Experimental results

In order to test the behavior of the facility, the GENESIS facility was run at different operational conditions. The experimental results obtained in GENESIS are compared with numerical simulations of the ESBWR by using the ATHLET system code²³ and the TRACG system code²⁴. These results comprise the mass flux (which is an independent parameter) and the stability characteristics of the nominal point. In order to perform such a comparison, the same operational conditions, defined by the non-dimensional phase change number N_{PCH} , and subcooling number N_{Sub} , are used.

In Figure 2-13 the obtained mass flow and fluxes for different power conditions are shown.

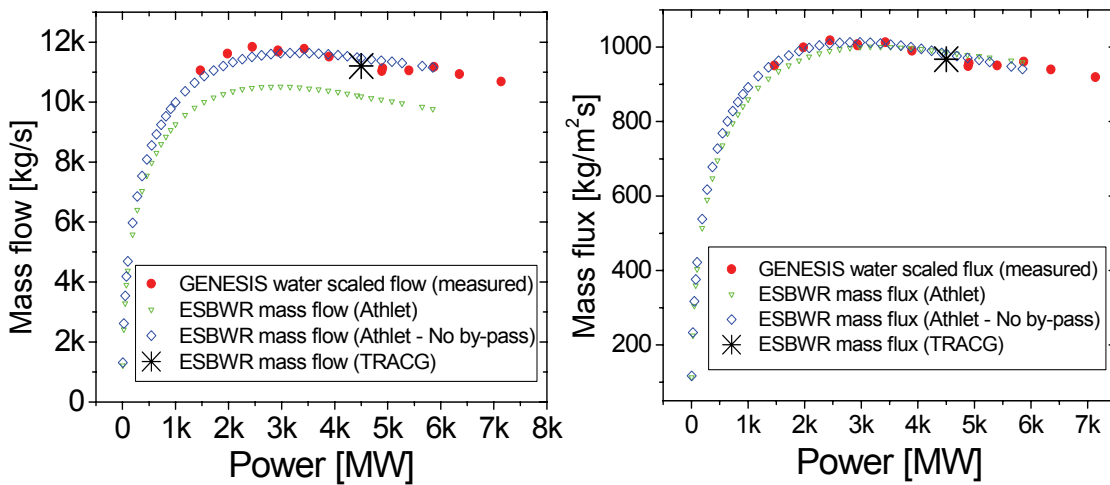


Figure 2-13: The power mass flow and the power-mass flux map at the core inlet as found in the numerical and experimental studies. The experimental results are rescaled to ESBWR scale.

In the ESBWR, core bypass channels are installed which are also included in the numerical simulation. These bypasses, however, are not present in the facility due to the fact they do not significantly influence the stability. Nevertheless, the cases with and without the bypass channels (i.e. those obtained from ATHLET and GENESIS respectively), show a very good agreement for the whole investigated range of powers, which indicates the friction in GENESIS correctly represents the reactor. The agreement between TRACG, ATHLET and GENESIS is also good for the nominal point (TRACG results were only available for the ESBWR at the nominal point).

The absence of experimental points at low power conditions is due to the difficulty to operate the GENESIS facility at low subcooling temperatures (close to the saturation point) since limitations exist on the maximum temperature at which Freon can be introduced at the feedwater sparger position.

Besides the relation between the power and the mass flux, the thermal-hydraulic stability of the GENESIS facility and the ESBWR is investigated for nominal conditions. The parameters characterizing the dynamics, are extracted by analyzing the flow response of the GENESIS facility running at nominal condition when slightly perturbing the steady state (power steps with a magnitude being only a few percent of the nominal power and randomly distributed in time were used for this purpose). These parameters are the decay ratio DR, and the resonance frequency f_{res} . The same method is used regarding the numerical experiments performed in ATHLET code which allowed characterizing the ESBWR thermal-hydraulic stability performance. In addition to the GENESIS and ESBWR-ATHLET results, the expected natural frequency for density wave oscillations (DWO) is calculated from the TRACG results. The results of that study are presented in Table 2-2.

	GENESIS	ESBWR [†]	ESBWR [‡]
Decay-ratio, DR (-)	0.12	0.11	-
Resonance frequency, f_{res} (Hz)	0.11*	0.13	0.083-0.17
<p>* Rescaled to <i>real time scale</i> by using Equation (2-37). [†] Obtained from numerical simulations performed in ATHLET code. [‡] Estimated from the typical period found for DWO being between one to two times the fluid transit time through the channel based on TRACG results.</p>			

Table 2-2: Thermal-hydraulic stability characteristics for the nominal operational point.

It is found that the experimental and numerical results show a good agreement for both the decay ratio and the natural frequency. This good agreement between the resonance frequencies certifies the correct time scaling proposed in section 2.2.3. As a matter of completeness it can be mentioned that the resulting frequencies from both ATHLET and GENESIS correspond well with the expected natural frequency estimated from the transit time of the fluid through the hot channel. This finding is in accordance with the expectable behavior of density wave oscillations (DWO).

2.4 Conclusions

The fluid-to-fluid scaling method for the simulation of the thermal-hydraulics phenomena taking place in the natural circulation BWR has been revised and discussed in detail. As a result of this approach, an experimental facility (GENESIS) was designed and constructed in which thermal-hydraulic stability performance was found to be similar to that of the downscaled ESBWR which was taken as the reference natural circulation BWR. The importance of correctly scaling the inertia and the friction distribution in the loop has been shown. It is found that for stability investigations with fluid-to-fluid downscaled systems, the same geometrical scaling factor has to be applied to properly scale both the axial and radial dimensions of all sections in the loop. As a consequence, the time in the downscaled facility was found not to be scaled one-to-one with the time of the reference reactor. An explicit rule applies for the time instead. In addition, it was found that the time ratio is not independent of the geometrical scaling.

Scaling distortions have been discussed and a way of diminishing their consequences in the case of higher friction in the core has also been presented. By using the proposed methodology, it was shown that core friction-related distortions can be reduced.

It was proven that the geometrical scaling is weakly dependent on the operational pressure, allowing investigating the stability performance of the original system in a wide range of pressures, without significant geometrical modifications.

Experimental results, obtained with the help of the GENESIS facility, were compared with numerical results obtained by using two different codes (the ATHLET system code and the validated TRACG system code). This comparison shows a very good agreement from both the steady state and dynamic points of view. This finding confirms the validity of the downscaling methodology for stability analysis proposed in this work.

In order to investigate the neutronic-thermal-hydraulic stability of natural circulation BWRs void reactivity feedback needs to be implemented in the GENESIS facility. The details of such implementation, and further analysis regarding stability performance of natural circulation BWRs are presented in Chapter 3.

2.5 References

- ¹ Cheung, Y.K., Shiralkar, B.S. and Marquino, W., Analysis of ESBWR Startup in Natural Circulation, Proceedings of ICAPP (2005).
- ² Van der Hagen, T.H.J.J., Exploring the Dodewaard Type-I and Type-II stability, From start-up to shut-down, from stable to unstable, *Ann. Nuc. Energy*, 24 - 8, 659-669, (1997).
- ³ Van de Graaf, R. and van der Hagen, T.H.J.J., Two-phase flow scaling laws for a simulated BWR assembly, *Nuclear Engineering and Design*, 148, 455-462, (1994).
- ⁴ Ishii M. and Jones Jr., O.C., Derivation and application of scaling criteria for two-phase flows, in Kakaç, S. and Veziroghi (eds.) *Two-Phase Flows and Heat Transfer*, Vol. I, Hemi- sphere, Washington, 163-185, (1977).
- ⁵ Symolon P.D., Scaling of Two-Phase Flow Regimes in a Rod Bundle with Freon, *Trans. Am. Nucl. Soc.*, 62, 705- 706, (1990).
- ⁶ Shiralkar, B.S., Personal communication (2005).
- ⁷ Lahey, R. and Moody, F.J., *The thermal-hydraulics of a Boiling Water Reactor*, 284, (1993).
- ⁸ Marcel C. P., Development of the scaling laws for a natural circulation loop, GE Proprietary Report, (2004).
- ⁹ Todreas N.E. and Kazimi M.S., *Nuclear systems I, Thermal Hydraulics Fundamentals*, Taylor & Francis Ed, (1992).
- ¹⁰ Marcel C.P., Rohde, M. and van der Hagen, T.H.J.J., Fluid-to-fluid modeling of natural circulation loops for stability analysis. In press in the *Int. J. of Heat and Mass Tran.*, (2007).
- ¹¹ Van Bragt D.D.B., Stability of Natural Circulation Boiling Water Reactors: Part I – Description Stability Model and Theoretical Analysis in terms of Dimensionless Groups, *Nuc. Technology*, 121, 40-51, (1998).
- ¹² Saha, P. and Zuber, N., Point of net vapor generation and vapor fraction in subcooled boiling. Proceedings 5th Int. Heat Transfer Conf., Tokyo, Japan, September 3-7, Vol. 4, (1974).
- ¹³ Pioro, I.L., D.C. Groeneveld, S.C. *et al.*; Comparison of CHF measurements in R-134a cooled tubes and the water CHF look-up table. *Int. J. Heat and Mass Tran.*, 44, 73-88, (2001).
- ¹⁴ Rizwan-uddin, On density-wave oscillations in two-phase flows. *Int. J. Multiphase Flow*, 20:721-737, (1994).
- ¹⁵ Zboray R., An experimental and modeling study of natural-circulation boiling water reactor dynamics Delft University of Technology PhD thesis, IOS Press, (2002).
- ¹⁶ Kok, H., Experiments on a Natural Circulation Loop - from Void-fraction to Coupled Nuclear Thermal-Hydraulics, Delft University of Tech. PhD thesis, IOS Press, (1998).
- ¹⁷ Zhang M. and Webb, R.L., Correlation of two-phase friction for refrigerants in small-diameter tubes, *Exp. Thermal and Fluid Science* 25, 131-139, (2001).
- ¹⁸ Müller-Steinhagen H. and Heck K., A simple friction pressure drop correlation for two-phase flow in pipes, *Chem. Eng. Process*, 20, 297-308, (1986).
- ¹⁹ Guido G., Converti, J. and Clausse, A., Density-wave oscillations in parallel channels - an analytical approach, *Nuclear Engineering and Design*, 125, 121-136, (1991).
- ²⁰ Marcel C. P and Rohde, M., Application of the scaling laws to the design of a natural circulation loop based on the ESBWR, GE Proprietary Report, (2005)
- ²¹ Van Bragt D.D.B., Analytical modeling of BWRs Dynamics. Delft University of Technology PhD thesis, IOS Press, (1998).
- ²² Marquino, W. personal communication, (2006).
- ²³ Manera A., Deliverable 2 (FZR) of the GENESIS project, Revised input deck and power flow map for ESBWR, (2005).
- ²⁴ Andersen, J.G.M. *et. al.*, TRACG Model Description, Lic. Topical Report, NEDO- 32176, (1976).

Chapter 3

Experimental investigations on the stability of natural circulation BWRs

3.1 Introduction

Numerous investigations have shown that modeling of two-phase flows is still a difficult task which involves large uncertainties. In the particular case of nuclear reactors, these uncertainties are extremely important since they may lead to underestimations of the reactor safety margins of operation. Due to this, experimental investigations on nuclear reactors involving two-phase flows are very important since they can help to understand the interaction between the complex mechanisms and also to validate numerical tools and models. In BWRs a strong coupling exists between the vapor production in the core and the resulting fission power, since the boiling coolant also works as moderator. Therefore, the void reactivity feedback mechanism needs to be taken into account in order to investigate the stability of those reactors. For this reason large efforts have been done to obtain BWRs experimental data relevant for stability studies. The limited operational range in which reactor

experiments can be performed and also a lack in sensors present in the reactors (which are mainly aimed for system monitoring), however, limits such a task. Particularly difficult is the case of the natural circulation BWR which may exhibit a characteristic dynamical behavior due to the fact that the two-phase mixture is also responsible for driving the coolant flow. In this case, the lack of natural circulation BWRs hinders the realization of reactor experiments. The exceptions are the Dodewaard reactor tests which helped to start understanding the stability of natural circulation BWRs^{1,2}. Novel natural circulation BWRs produce more power and have larger cores than that of the Dodewaard reactor. On top of this, they include a much taller chimney and a different steam separation process which induces a large pressure drop at the chimney outlet. These two last characteristics are known to destabilize the thermal-hydraulic stability mode³. How those differences may affect the reactor stability performance i.e. when considering neutronic feedback, however, is not clear. For that reason, a number of projects involving numerical simulations and experiments have been carried out (see e.g. Offerein⁴). Up to now, however, no good agreements have been obtained between numerical and experimental results regarding stability of natural circulation BWRs including the void reactivity feedback effect. The reason for that may be found in the numerous difficulties numerical codes encounter to accurately simulate complex two-phase systems together with some limitations from the previous experimental facilities (e.g. they did not achieve a proper dynamic thermal-hydraulic similarity^{5,6}, limitations in the simulation of the void reactivity feedback mechanism, a simplified representation of the flow pattern⁷). On top of this, previous experimental facilities were designed to obtain general knowledge about BWR stability issues. Now we aim at represent as accurately as possible a reference natural circulation BWR prototype, i.e. the ESBWR⁸.

In this chapter, an experimental attempt is performed with the GENESIS test facility presented in Chapter 2. The design of such a facility is optimized to simulate the thermal-hydraulics of the ESBWR by making use of fluid-to-fluid scaling modeling. In order to simulate the reactor neutronics, an artificial void reactivity feedback system is added to GENESIS. Details regarding the implementation of such a system are given at the beginning of this chapter. Experimentally obtained stability maps regarding the thermal-hydraulic mode (obtained without accounting the neutronic feedback) and the reactor-kinetic mode (including the neutronic feedback effect) are compared afterwards with numerical simulations obtained from the TRACG code⁹ (which is optimized for representing BWRs for a broad range of situations) and the ATHLET code¹⁰ (specially developed for simulating nuclear reactor safety-related incidents and accidents¹¹) for exactly the same conditions. The results of such a comparison are further presented at the end of the chapter.

3.2 The VRF system

3.2.1 The VRF system design

To simulate the reference ESBWR, the GENESIS facility needs to be extended with a system simulating the reactor neutronics, the so-called void reactivity feedback (VRF) system^{12,13}. The experience learnt from the VRF systems developed by Kok¹⁴, Zboray⁶ and Furuya⁷ is used in order to accurately simulate the neutronic feedback mechanism in GENESIS. In some test facilities, e.g. in SIRIUS⁷, the reactor fuel bundle is simulated by an annular channel. The following analysis shows that such a simplification may cause the flow pattern to be different than that present in the reactor. Table 3-1 presents a comparison of the core hydraulic diameter D_h and the subchannel diameter D_{s-ch} (defined as the diameter of the largest circumference which fits into the channel) between the ESBWR, SIRIUS and the GENESIS facility.

	ESBWR (10x10)	SIRIUS (1x1)	GENESIS (5x5) ‡
$D_{h,C}$ (mm)	9.5	6.5	7.5
$D_{s-ch, C}^+$ (mm)	10.5	3.3	8.4
† Diameter of the largest circumference fitting into the channel			
‡ Upscaled to water			

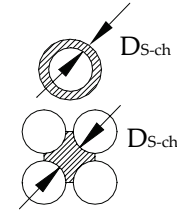


Table 3-1: Geometrical core comparison of the ESBWR, SIRIUS and the GENESIS facility.

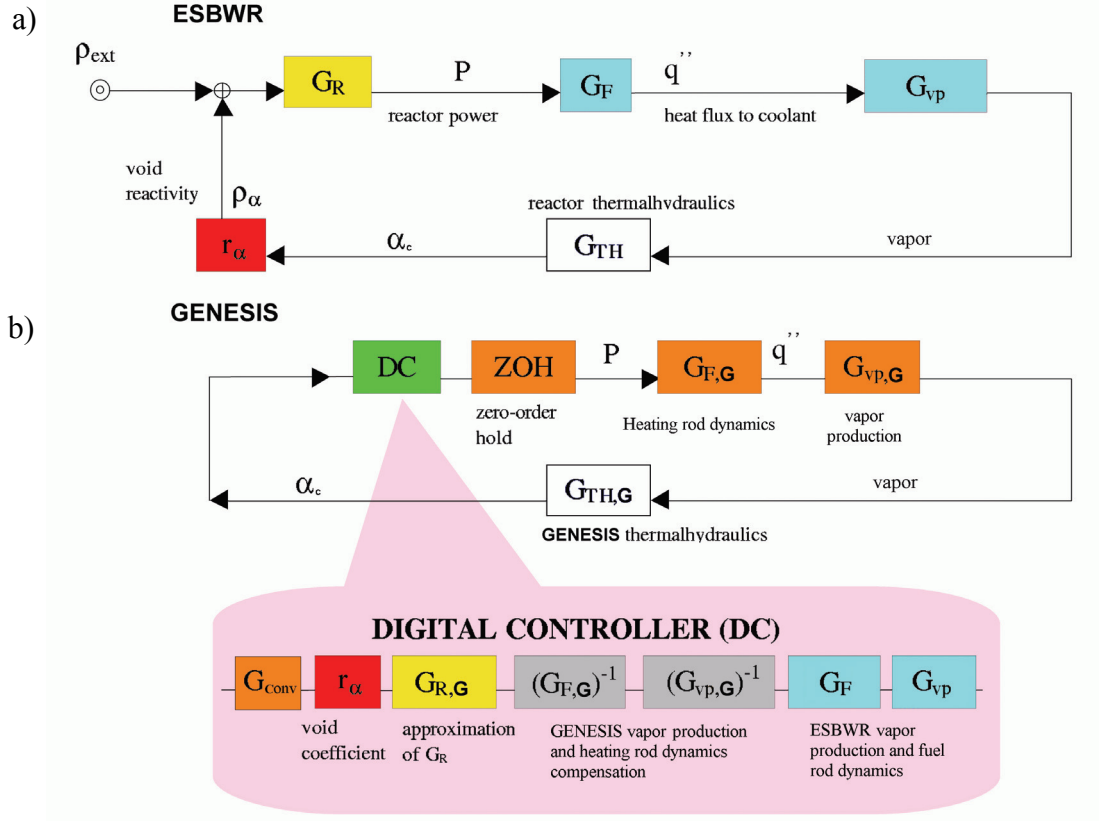
Many investigators have pointed out the importance of the hydraulic diameter and the subchannel diameter on determining the characteristics of the two-phase flow^{15,16}. In particular, it is observed a tendency for the vapor to seek the less obstructed, higher velocity regions of the channel. The flow pattern is important for the neutronic-thermal-hydraulic stability since it affects the core pressure drop and also the axial void fraction profile. Table 3-1 shows that GENESIS more accurately represents the ESBWR core than an annular channel such as it was used in SIRIUS.

The VRF system developed here estimates the core void fraction by measuring the core pressure drop obtained from fast dP sensors. This choice is based on to the small phase difference with respect to the actual core-averaged void fraction found for such a measurement system^{6,7}. This is related to the fact the core pressure drop is an integral quantity.

As in the former implementations^{6,7}, the VRF simulation is implemented in the form of a digital controller (DC) running on a single PC. The DC controls the power of the electrically heated rods, based on the simulated reactivity effect of the measured void-fraction fluctuations. The design of the digital controller allows studying BWR dynamics for different fuel types and reactor parameters like the void-reactivity coefficient, the delayed-neutrons fractions and decay constants and also the neutron generation time (e.g. important for studying MOX fuels).

3.2.3 The VRF system implementation

The block diagram from Figure 3-1 shows the interaction between the physical mechanisms taking place in the ESBWR and in the GENESIS facility.



NOMENCLATURE

G_R	= Reactor transfer function from reactivity to power
$G_{vp} \ G_F$	= Total transfer function from power to heat transfer to the coolant
G_{TH}	= Thermal-hydraulic transfer function from power to void production
r_α	= Transfer function from void fraction to reactivity
G_{Conv}	= Void fraction determination transfer function
ZOH	= Zero-Order Hold
α_c	= Void fraction in the core

Subscripts

G	= GENESIS facility
---	--------------------

Figure 3-1: a) The feedback mechanism of the ESBWR and b) the feedback system as implemented in the GENESIS facility (adapted from Zboray⁵).

The thermal-hydraulics is represented by the G_{TH} block. Since the scaling of GENESIS (represented by $G_{TH,G}$) is designed to simulate the reactor thermal-hydraulics, it is assumed that the ESBWR thermal-hydraulics is correctly reproduced by the GENESIS facility ($G_{TH,G}=G_{TH}$). The mean void fraction in the GENESIS core is estimated (process represented by G_{Conv}) and afterwards used to calculate the void reactivity feedback due to the variation in the neutronic moderation. This feedback effect is calculated via the void reactivity coefficient (represented with r_α). In GENESIS the neutronics is simulated by a

numerical model which is solved in real time (represented by $G_{R,G}$). As a result, the applied power is adjusted according to the estimated fission rate. Since the ESBWR fuel rods dynamics and the steam bubbles creation mechanism (represented by G_F and G_{VP} , respectively) influence the dynamics of the system, they are artificially simulated in the algorithm. Some mechanisms present in GENESIS (which are absent in the ESBWR) need to be removed or compensated for (e.g. the effect of the GENESIS heating rods and the Freon vaporization, represented by $G_{F,G}$ and $G_{vp,G}$, respectively). These compensations are implemented by adding the inverse transfer functions of the mechanisms that need to be eliminated. All the transfer functions added artificially are implemented in a discrete time form due to the discrete time characteristics of the DC. For this reason, the Z transform is used instead of the more common Laplace transform.

Determination of fluctuations of the core averaged void fraction (G_{Conv})

The axial average void fraction in the core is determined, as suggested by Furuya⁷, by measuring the pressure drop over the core ΔP_C , and by applying an iteration step regarding the momentum balance over the entire core, thereby adjusting the core outlet quality χ_o step by step ($\delta\chi_o = 0.0005$). The next assumptions are made in the implemented algorithm.

- The homogeneous equilibrium model (HEM) is used. The use of this simplification is supported by the homogenizing effect of the (6X) GENESIS core spacers placed at the same location as in the ESBWR core.
- The quality profile $\chi_{(z)}$ is linear, starting from the boiling boundary position, z_{bb} .
- No void accumulation exists near the spacers.
- Subcooled boiling is neglected.
- The coolant physical properties are found by using the (estimated) local pressure and temperature in correlations which are specially developed for that purpose. Those correlations are obtained by performing a high order fitting of the coolant physical properties.

The online determination of the average core void fraction takes place according to the following steps:

- 1) The value of the boiling boundary position z_{bb} is needed for determining the void fraction profile $\alpha_{(z)}$. The location of z_{bb} is calculated by performing a heat balance in the single-phase section of the core. The input power signal is filtered with the dynamics introduced by the GENESIS rods (given by $G_{F,G}$) since the power applied to the rods is not instantaneously transferred to the coolant. Furuya⁷ did not comment on this effect in his VRF implementation and therefore, most probably he

did not consider it. The heat flux and the mass flow are then used in the energy balance to predict z_{bb} . In order to validate this procedure, the resulting value of z_{bb} was compared with the location of the breaking point of the core axial temperature profile (reconstructed by using 7 thermocouples located in the core section) showing a good agreement.

- 2) The core pressure drop, ΔP_c is measured.
- 3) ΔP_c is used in the core momentum balance equation to find the best fitting parameter b of the equation describing the linear quality profile $\chi(z) = b(z - z_{bb})$. The iteration algorithm (with an average calculation speed of 0.001 s per converged solution) starts from high quality values (to avoid spurious solutions) and runs until the convergence criterion is fulfilled ($|\Delta P_{C,Calc} - \Delta P_{C,Meas}| = \text{minimum}$). In the implemented algorithm, the core is divided into two parts: a single-phase region and a region with two-phase flow. The different terms from the momentum balance considered in each of these regions are the following.

Single-phase region

- Friction due to the rods and the walls, estimated by using the Blasius formula¹⁷,

$$f_l = 0.079 \text{ Re}^{-0.25} \quad (3-1)$$

- Friction due to the spacers $K_{sp} = 0.69$ (experimentally found) (3-2)

- Gravitation

Two-phase region

- Friction due to the rods and the walls, $f_l = 0.079 \text{ Re}^{-0.25}$. The following correlation¹⁷ specially developed for Freons in small tubes, is used to estimate the two-phase friction multiplier

$$\phi_{LO}^2 = (1 - \chi)^2 + 2.87 \chi^2 \left(\frac{P}{P_c} \right)^{-1} + 1.68 \chi^{0.8} (1 - \chi)^{0.25} \left(\frac{P}{P_c} \right)^{-1.64}, \quad (3-3)$$

- Friction due to the spacers, $K_{sp} = 0.69$, $\phi_{LO}^2 = \left(1 + \left(\frac{1}{N_p} - 1 \right) \chi \right)$, (3-4)

- Acceleration,
- Gravitation,

being f_l the liquid friction factor, K_{sp} the spacers friction coefficient obtained from experiments, ϕ_{LO} the two-phase multiplier and $P/P_c = 0.26$ the reduced pressure (P_c is the critical pressure). The inertial term is neglected since it is estimated to be small compared to the others (<2.5 %) for all conditions. Temperature gradients affecting the Freon density have been considered in the connecting tubes of the dP sensors used in the algorithm.

- 4) $\chi_{(z)}$ is then used to calculate the void fraction axial profile $\alpha_{(z)}$. Due to the HEM assumption, $\alpha_{(z)}$ can be found from $\chi_{(z)}$ by using

$$\alpha = \frac{1}{1 + \left(\frac{1}{\chi} - 1 \right) \frac{\rho_v}{\rho_l}}. \quad (3-5)$$

- 5) $\alpha_{(z)}$ is then integrated to find the space averaged core void fraction, $\langle \alpha \rangle = \frac{1}{L_c} \int_{L_c} \alpha_{(z)} dz$. (3-6)

Reactivity response to fluctuations in the average void fraction (r_α)

Deviations from the power at critical conditions are calculated and applied according to reactivity changes. Using a one-dimensional, axial, model of the reactor and assuming small variations in the cross sections around the equilibrium value, i.e. assuming a linear dependence on the fluctuations in the void fraction, the void reactivity variation $\delta\rho$ is given by¹⁸

$$\delta\rho = C \int_0^{L_c} \phi_0^2(z) \delta\alpha_{(z)} dz, \quad (3-7)$$

where $\delta\alpha$ is the void fraction fluctuation regarding the average void fraction in the core corresponding to a critical reactor ($\delta\alpha_{(z,t)} = \alpha_{(z,t)} - \alpha_{0(z)}$) and ϕ_0 is the critical flux shape; C is a constant of proportionality.

For a flat power profile, Equation (3-7) can be expressed as

$$\delta\rho = r_\alpha \delta\alpha, \quad (3-8)$$

where r_α is the void reactivity feedback coefficient. The value of r_α used in this study corresponds to a middle of cycle (MOC) profile condition of the ESBWR¹⁹, which is $r_\alpha = -1.03 \times 10^{-3}$.

Power fluctuations from the reactivity fluctuations ($G_{R,G}$)

As in former implementations^{6,7}, power changes are estimated by using the point-kinetic equations for the neutron density and the six neutron precursor densities²⁰.

$$\begin{aligned} \frac{dn(t)}{dt} &= \frac{\rho(t) - \beta}{\Lambda} n(t) + \sum_i \lambda_i c_i(t) \\ \frac{dc_i(t)}{dt} &= \frac{\beta_i}{\Lambda} n(t) - \lambda_i c_i(t). \end{aligned} \quad (3-9)$$

It needs to be pointed out that all the time dependent parameters from Equation (3-7) had to be converted into the proper time frame, according to the relation given by the time ratio, Equation (2-37) derived in Chapter 2,

$$X_t = \frac{\tau|_{\text{GENESIS}}}{\tau|_{\text{ESBWR}}} = 0.68. \quad (3-10)$$

Dynamics of the GENESIS rods plus vapor production mechanism ($G_{F,G}$ $G_{vp,G}$)

The dynamics of the power-to-heat flux regarding the GENESIS facility is modeled as a first-order process in this chapter. In Chapter 4, this simplification is discussed in detail. Therefore,

$$G_{vp,G} G_{F,G} = \frac{1}{\tau_{FG}s + 1} \quad (3-11)$$

where $G_{F,G}$ represents the heat transport through the GENESIS heating rods and $G_{vp,G}$ the vapor production process taking place in the surface of the rods. Experimental investigations performed in the DESIRE facility, have shown that the time constant associated with the power to void creation in such a facility can be approximated by a first order model with a typical time constant $\tau \approx 0.5s$ ¹³. Since the rods from GENESIS are similar to those from DESIRE as well as the Freon R-12 and the Freon R-134a fluid properties, the power to void creation mechanism in GENESIS ($G_{F,G}$ $G_{vp,G}$) is modeled with a transfer function as the one given by Equation (3-11) with $\tau_{F,G} = 0.5s$. The dynamics of the heating rods and the void creation in GENESIS are eliminated from the feedback mechanism by implementing in the algorithm the inverse of Equation (3-11), expressed in z domain.

Dynamics of the ESBWR rods plus vapor creation mechanism (G_F G_{vp})

Once the dynamics of the heating rods plus vapor generation in Freon is eliminated, the dynamics of the simulated ESBWR in water has to be artificially implemented. The dynamics of the power to the rod surface heat flux taking place in the ESBWR rods (indicated by G_F) cannot be described by a first-order system²¹. For this reason, in the GENESIS VRF system the reactor fuel rods are not modeled as first order processes like in the previous implementations^{6,7}. The solution for the temperature response within the rod due to a step in power can be described by the following analytic relation²¹,

$$T'(r',t') = \sum_{n=1}^{\infty} \frac{2Bi}{\lambda_n^2 (\lambda_n^2 + Bi^2)} \frac{J_0(\lambda_n r')}{J_0(\lambda_n)} (1 - \exp(-\lambda_n^2 t')) \quad (3-12)$$

where $Bi=h.D/k$ is the Biot number, with h being the heat transfer coefficient from fuel-to-coolant, k the rod heat conductivity and D the rod diameter; λ_n is the n^{th} root of $Bi=\lambda_n[J_1(\lambda_n)/J_0(\lambda_n)]$ with J_0 and J_1 the first kind Bessel function of the zero and first order respectively. All quoted quantities are non-dimensional. The heat flux at the surface of the rods q'' , is found from $q''=f(T'(r',t'))$. The heat flux from the analytic relation is approximated by a second-order model with a response described by

$$G_F = \frac{1}{\tau_F^2 s^2 + 2\zeta\tau_F s + 1}, \quad (3-13)$$

obtaining, for an ESBWR fuel rod at MOC condition, two fitted time constants $\tau_1=5.42s$ and $\tau_2=0.188s$ (corresponding to $\tau_F=1.01s$ and $\zeta=2.78$).

The analytical solution and the second order approximation of the resulting heat flux at the rod surface, resulting from a power step is shown in Figure 3-2 in terms of the Fourier number, which is defined as

$$N_{Fo} \equiv t \frac{4k}{\rho C_p D^2}, \quad (3-14)$$

where ρ is the pellet density and C_p its constant pressure heat capacity.

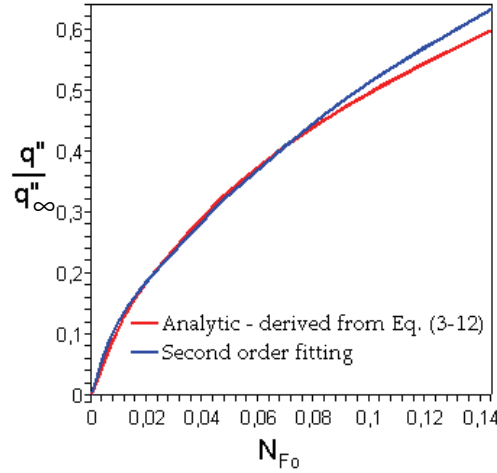


Figure 3-2: Evolution of the non-dimensional heat flux at the surface of the ESBWR rod after a power step is applied. The time scale is given in terms of the Fourier number (0.0288 (N_{Fo})=1 s, thus 0.144 (N_{Fo})=5 s).

The approximation to the analytic solution is in good agreement for a broad range of N_{Fo} numbers assuring a good representation of the rods dynamics for the region of interest. When applying this transfer function, the associated two time constants are converted into the GENESIS time frame by using the factor expressed in Equation (3-10).

The heat transfer process from the surface of the rods to the bulk of the boiling water is much faster than the heat transfer within the ESBWR rods. A simple analysis of the heat resistance of each material (fuel pellets, gap and cladding) and the boiling water boundary layer shows that most of the heat resistance is due to the fuel pellet (~98.5%). The transfer function G_{vp} can therefore be neglected¹³. Hence, $G_{vp} \approx 1$. Equation (3-13) is Z transformed for its implementation in the discrete-time based algorithm.

The dynamic response of other devices like the power supplies, the differential pressure sensors and the calculation time of the core average void fraction are also taken into consideration. However, these are orders of magnitude faster than the dynamic processes mentioned above and, therefore, can be considered as instantaneous processes.

3.3 Stability performance of natural circulation BWRs

In this section, the stability performance of the reference natural circulation BWR, the ESBWR, is investigated by using the GENESIS facility. Two stability modes are investigated: the thermal-hydraulic mode and the neutronic-thermal-hydraulic mode, the so-called reactor-kinetic mode. These results are then compared with simulations performed with the TRACG and the ATHLET numerical codes.

In order to present the stability performance for conditions different from nominal, the so-called stability maps are constructed. These maps represent contour plots of the decay-ratio DR, and the main resonance frequency f_{res} for all investigated reactor conditions in terms of the power, the flow rate and the core inlet temperature. However, in order to simplify the representation, the phase-change number N_{PCH} , and the subcooling number N_{Sub} , are used instead. Both the DR and the f_{res} are determined from the experimental results by using a third order model to fit the flow response to step perturbations in reactivity. Details of the theoretical basis of such a model can be found in APPENDIX B.

To simplify the notation, in the following a system with void-reactivity feedback will be indicated with the '-R' suffix from 'Reactor'. For a purely thermal-hydraulic system, the '-TH' suffix will be used instead.

3.3.1 Thermal-hydraulic stability

The DRs and the f_{res} obtained from experiments carried out in the GENESIS facility without using the VRF system are shown in Figure 3-3.

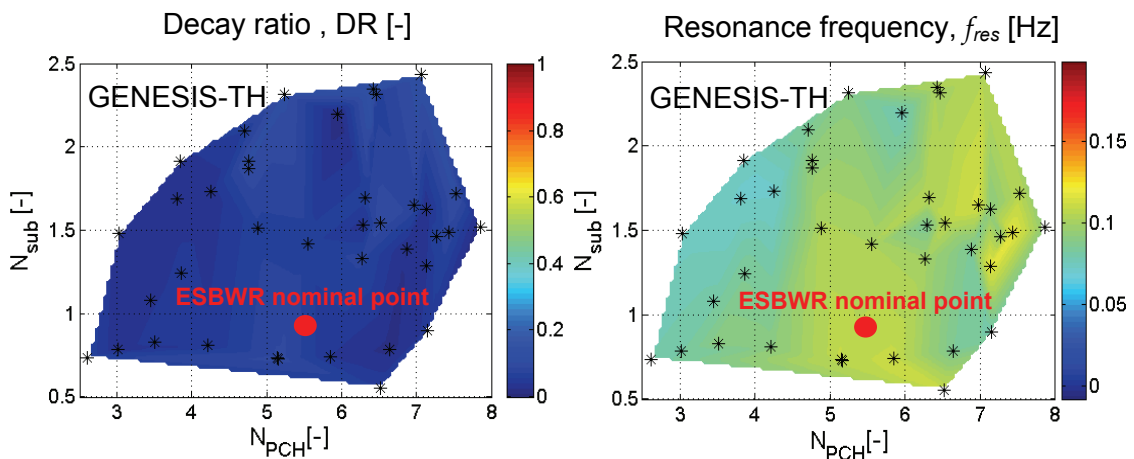


Figure 3-3: Stability maps of the experimentally found decay-ratio and resonance frequency without reactivity feedback obtained from GENESIS.

From the experimental investigations it can be concluded that the GENESIS facility representing the ESBWR is very stable for a wide range of operational conditions and shows large margins to instabilities regarding the

thermal-hydraulic instability mode. Since no unstable cases are observed in the experiments, quantifying the (obviously large) margin to instabilities for this oscillatory mode is difficult.

An area of discussion between GE people and the (US) Nuclear Regulatory Commission (NRC), has been the effect of the thermal-hydraulic mode of oscillation in the ESBWR; i.e. the low frequency mode driven by changes in the coolant density in the chimney. This mode cannot be observed in the TRACG calculations because with the neutronic feedback this mode is very stable relative to the higher frequency density wave oscillations for the ESBWR configuration (as it will be clarified in Chapter 4). As it was shown in Chapter 2, the f_{res} for the nominal operational point corresponds well to typical frequencies found for density wave oscillations traveling through the core plus chimney sections (about 5 s in the ESBWR at rated conditions). It is thus clear that the transport time is important at the high power level of rated conditions, indicating a static head dominated phenomenon instead of the more common core friction dominated density wave oscillations. This result is very important since it indicates the two oscillatory modes present in the natural circulation BWR (the thermal-hydraulic and the neutronic-thermal-hydraulic mode) seems to be decoupled, characterized by very different resonance frequencies. This issue will be further investigated in Chapter 4.

Note that distortions arising from the downscaling procedure may influence the similarity between the GENESIS-TH and the ESBWR-TH stability. From these distortions, the most relevant ones are the difference in the axial power profile and the core axial pressure drop profile (see Figure 2-11). These two, however, have little influence on the thermal-hydraulic instability mode (see Chapter 2). Because of this, a good agreement between the GENESIS-TH and the ESBWR-TH stability performances is to be expected.

3.3.2 Reactor-kinetic stability

To investigate the reactor-kinetic stability of the reference reactor, the VRF system detailed in Section 3.2 is applied in GENESIS using a constant value for r_{α} , which is an approximation since it is well known that such a coefficient varies with the operational conditions ($r_{\alpha,BOC}=-0.107$; $r_{\alpha,MOC}=-0.103$; $r_{\alpha,EOC}=-0.113$)¹⁹. The results of such experiments are presented in Figure 3-4.

Regarding the f_{res} , since the oscillation mode is driven by the interplay between the friction in the core section and the neutronic response due to void changes in the core, the frequency is much higher than in the case of a system without void-reactivity feedback (see Figure 3-3). These frequencies correspond well with what is to be expected for Type-II DWOs, i.e. the oscillation period being between 1.5 and 2 times the transit time through the core section (about 1 s in the ESBWR at rated conditions).

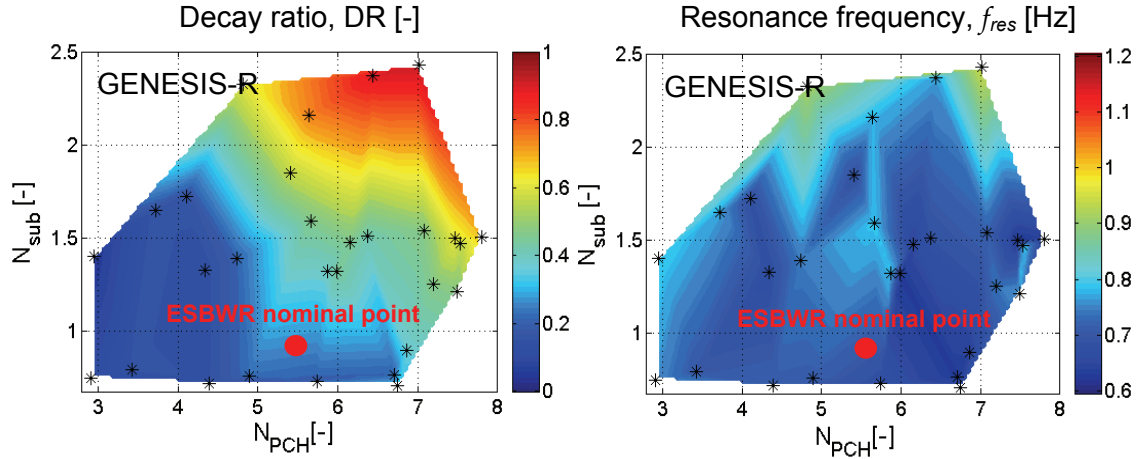


Figure 3-4: The experimentally found decay-ratio and resonance frequency with reactivity feedback, represented in a stability map.

Because the stability characteristics at the nominal point are also calculated by the GE validated TRACG code²², a comparison between the GENESIS experiments and the TRACG calculations (regarding the reactor-kinetic stability) can be made. TRACG is a General Electric (GE) proprietary version of the Transient Reactor Analysis Code (TRAC)²³. TRACG uses advanced one-dimensional and three-dimensional methods to model the phenomena that are important in evaluating the operation of BWRs. TRACG has been approved by the USNRC for ESBWR stability analysis since it has been extensively qualified against separate effects tests, component performance data, integral system effects tests and operating BWR plant data. The TRACG thermal-hydraulic instability modeling using the semi-explicit integration scheme has been evaluated for adequacy by comparison to experimental data from the FRIGG facility²³. Plant data from operating BWRs (e.g. LaSalle 2, Leibstadt, Peach Bottom) have been used to validate TRACG predictions of core-wide and regional stability. The uncertainties in the TRACG calculations have been quantified through extensive validation, and Monte-Carlo analysis yields an uncertainty of the order of 0.1 in the core decay ratio²⁴. Hence, even with a very detailed description of the ESBWR and its physical phenomena taking place (e.g. multi-channels, 3-D neutronics, component-specific thermal-hydraulics models), a certain, non-negligible uncertainty has to be taken into account.

The stability results found for the ESBWR at rated conditions are given in Table 3-2.

REACTOR	GENESIS	TRACG ¹⁹
DR (-)	0.30	0.33
f_{res} (Hz)	0.73	0.74

Table 3-2: The reactor-kinetic stability characteristics for the ESBWR at the nominal operational point as obtained from GENESIS and TRACG.

Although the results for the nominal conditions agree very well, a few points need to be mentioned about possible deviations that might occur for other operational points. Besides the differences resulting from the downscaling discussed in Chapter 2, the following may cause differences between the GENESIS-R and the TRACG results:

- The HEM model used in the VRF system for estimating the mean void fraction in the core.
- The power profile (axially uniform profile in GENESIS and bottom peaked in TRACG).
- The core axial frictional pressure drop (less bottom peaked in GENESIS than in the modeled ESBWR, see Figure 2-11).

As a result of the HEM model used in the GENESIS-R experiments, the void perturbations are slightly overestimated. Consequently, the reactivity perturbations are also slightly larger which, as it will be shown in Chapter 4, leads to a less stable system and therefore conservative results.

In their works, Rizwan-uddin²⁵ and Zboray⁶ showed that a BWR having a bottom-peaked power profile results in a slightly less stable system than one with a top-peaked power profile for both natural and forced circulation. In a forced circulation BWR, the stability boundary for the uniform power profile is found to be situated somewhere between those two extremes. Based on this, the use of a uniform power profile in GENESIS-R experiments would lead to slightly more stable predictions than those from the TRACG calculations.

The GENESIS core creates a pressure drop profile which is more concentrated at the top than that for the ESBWR case at similar conditions (see Figure 2-11). As discussed in section 2.3, this effect would result in less stable estimations and therefore conservative results.

Regarding the neutronic modeling, TRACG uses 3-D neutronics whereas in GENESIS a point-kinetic approximation is assumed. In the AEN/NEA Ringhals Benchmark Report²⁶ and the recent Kuosheng study²⁷, however, no evident distortion in the DR was found due to the use of less than three spatial dimensions for the neutronics.

Table 3-2 shows that at rated conditions, the GENESIS-R and the TRACG results for the DR and the f_{res} are in very good agreement. A possible explanation for this similarity is that the stabilizing effect of the uniform power profile is canceled out by the destabilizing effect of the less bottom-peaked core friction distribution, and the HEM used in the VRF system.

3.3.3 The ATHLET numerical results

ESBWR numerical simulation results are presented in this section. The simulations are performed by Manera¹³ who used the ATHLET system code¹⁰ (Analysis of the Thermal-Hydraulics for Leaks and Transients). The ATHLET code is a general system code that has been validated for a number of cases (see e.g. Krepper, *et al.*²⁸) which mainly involve reactor accidents. ATHLET uses a 1-D, two-phase fluid dynamic model based on the conservation equations of the mass, the energy and the mixture momentum, together with the drift-flux model²⁹. The neutronics is modeled with the point-kinetics equations with six groups of precursors in which data corresponding to the ESBWR at MOC condition is used. The obtained numerical results are shown in Figure 3-5.

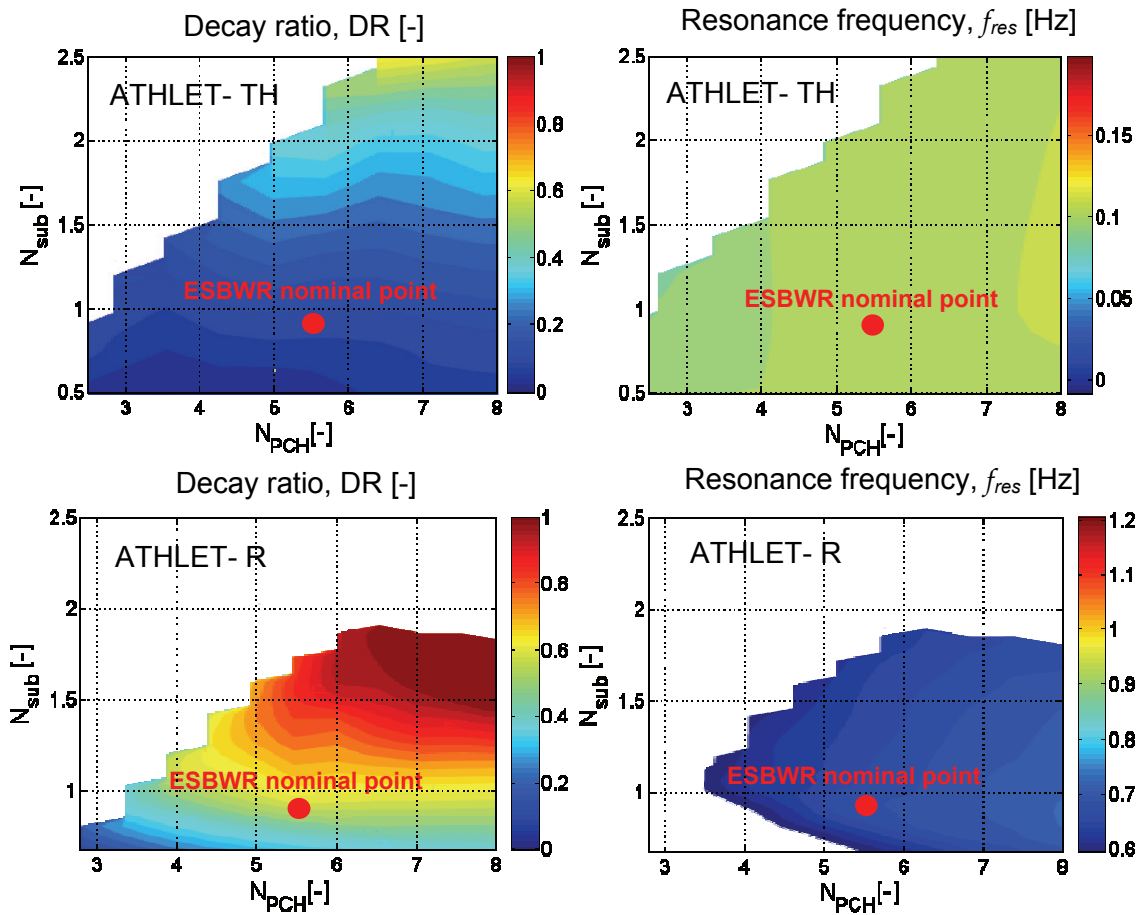


Figure 3-5: Numerical stability results for the thermal-hydraulic and the reactor mode.

As can be seen, the numerical results also show that the ESBWR is stable. In addition, the trend of the iso-decay-ratio lines is roughly the same as that one found in the GENESIS experiments. This trend is to be expected, as can be seen in numerous stability studies^{6,3}. The resonance frequencies are roughly the same for both the numerical and the experimental studies. It can also be seen that for the reactor system, the ATHLET calculations predict a less stable

system than the experiments do. The ATHLET stability boundary is situated around the subcooling-number $N_{sub} \approx 1.5$ (corresponding to a margin for inlet temperature of 6 K) for the largest range of Zuber-numbers, whereas a stability margin for the inlet temperature > 30 K is found in the experiments.

In order to understand this result, the stability at the nominal point is discussed in more detail. The ATHLET results for this point are compared with those from the GENESIS experiments and the TRACG code in Table 3-3.

	GENESIS (TH)	TRACG (TH)	ATHLET (TH)	GENESIS (REACTOR)	TRACG (REACTOR)	ATHLET (REACTOR)
DR (-)	0.12	-	0.11	0.30	0.33	0.64
f_{res} (Hz)	0.11	0.083 -0.17	0.13	0.73	0.74	0.66

Table 3-3: Thermal-hydraulic and reactor stability performance of the ESBWR at rated conditions obtained by using GENESIS and the ATHLET and the TRACG codes.

A large difference in the DR is observed when comparing the ATHLET-Reactor results with the TRACG results regarding the nominal point.

Since the uncertainties in the core decay ratio calculated by ATHLET are not known, we can only speculate on this issue. Sources of uncertainties are the single-channel approximation (the conditions in all modeled 1132 parallel channels are the same), the fixed pressure boundary condition and the point-kinetic neutronics. Due to the fixed pressure boundary in the steam dome, the ATHLET results are conservative, since the feedback due to the compression of the steam cushion in the steam dome has not been taken into account¹³. Based on this, the differences in the numerical results from the two models are most probably due to the uncertainties of the ATHLET numerical simulations of the reactor thermal-hydraulics. This result should recall the attention to the limitations existing in the codes to accurately predict the stability performance of complex two-phase systems.

The same argumentation regarding the uncertainties in the ATHLET thermal-hydraulics can be used to explain the differences in the stability maps obtained from the experiments performed in GENESIS-R and the ATHLET-R simulations. The scaling distortions and assumptions performed in the VRF system, however, have also to be mentioned. Since it is not possible to quantify these effects, a more detailed comparison is difficult to draw here and need to be studied in the future.

3.4 Conclusions

The stability performance of a natural circulation BWR has been addressed by using a test facility and two numerical codes. For such a study, the ESBWR is taken as the reference reactor. Special care has been taken to reduce the differences regarding the experimental system and the real reactor.

The GENESIS test facility, being a downscaled version of the ESBWR, is successfully equipped with a so-called void reactivity feedback system which includes some improvements compared to systems developed in the past.

The experimentally found characteristic resonance frequency of the thermal-hydraulic mode is found to be much lower (~ 0.11 Hz) than in forced-circulation BWRs (~ 1 Hz). This result indicates a static head dominated phenomenon for this instability mode since it corresponds well with typical frequencies of DWOs traveling through the core-plus-chimney sections.

Complete stability maps for the thermal-hydraulic and neutronic-thermal-hydraulic mode are experimentally obtained for a wide range of conditions. The resonance frequency for the reactor case corresponds well with typical frequencies of DWOs traveling through the core.

Results from the TRACG code and from the ATHLET code are used for the numerical investigations. It is found that the experimental results for the reference reactor at the nominal point agree very well with the numerical estimations obtained with the validated TRACG code. Since a number of (conservative and non-conservative) distortions and assumptions are done in the GENESIS case, it is most probably that the good agreement found with the TRACG code is a result of a compensation of the aforementioned differences. For the nominal point it is experimentally found that the GENESIS facility, representing the ESBWR, is stable with a large margin to instabilities (>30 K).

Besides the approximations used in the VRF simulation and the limitations from the downscaling, it is shown that, if properly designed, facilities with an artificial neutronic feedback implementation can represent the stability behavior of nuclear reactors. To gain more confidence in the comparison between numerical and experimental results it is suggested to numerically simulate (e.g. by using the TRACG code) a water-based up-scaled version of the GENESIS facility and benchmark the results to quantify the simulation capabilities of the code and also the scaling rules.

The differences found between the ATHLET results and the GENESIS and the TRACG results, indicate that stability predictions regarding BWRs are still a challenging task for thermal-hydraulic codes and therefore, considerations based on numerical results only have to be taken with care.

3.5 References

- ¹ Van der Hagen, T.H.J.J., Stekelenburg, A. J. C., and Van Bragt, D. D. B. (2000). Reactor experiments on Type-I and Type-II BWR stability. *Nucl. Engng. Design*, 200:177–185.
- ² Van der Hagen, T.H.J.J. and Stekelenburg, A. J. C. The low-power low-pressure flow resonance in a natural circulation cooled BWR., NUREG/CP-0142, 4:2785–2795, (1995).
- ³ Van Bragt, D.D.B., Rizwan-uddin and van der Hagen, T.H.J.J., Stability of Natural Circulation Boiling Water Reactors: Part II-Parametric Study of Coupled Neutronic-Thermal-hydraulic Stability. *Nucl. Techn.*, Vol. 121, (1998).
- ⁴ Offerein, J.F., Winters, L., Final Technical Report NACUSP Project Natural circulation and stability performance of BWRs, (2005).
- ⁵ Kok, H., Experiments on a Natural Circulation Loop – from Void-fraction to Coupled Nuclear Thermal – Hydraulics, Delft University of Technology PhD thesis, IOS Press, (1998).
- ⁶ Zboray R., An experimental and Modeling Study of Natural-Circulation Boiling Water Reactor Dynamics. Delft University of Technology PhD thesis, IOS Press, (2002).
- ⁷ Furuya M., Experimental and Analytical Modeling of Natural Circulation and Forced Circulation BWRs, Delft University of Technology PhD thesis, IOS Press, (2002).
- ⁸ Cheung, Y.K., Shiralkar, B.S. and Rao, A.S., Design Evolution of Natural Circulation in ESBWR, 6th Int. Conference on Nuclear Engineering (ICONE-6), San Diego, USA, (1998).
- ⁹ Andersen, J.G.M. *et al.*, TRACG Model Description, Lic. Top. Report, NEDO- 32176, (2001).
- ¹⁰ Lerchel, G. and Austregesilo, H., ATHLET Mode 1.2 Cycle A, User's Manual, GRS-p-1/Vol.1, Rev. 1, GRS, (1998).
- ¹¹ Steinhoff, F. Validation of the computer code ATHLET by means of PKL experiments. GRS Annual Report (2002/2003)
- ¹² Marcel, C.P. and Kaaijk, C.N.J. Neutronic feedback implementation in the GENESIS facility (GE proprietary document), (2005).
- ¹³ Rohde, M. Marcel, C.P. Manera, A. *et al.* Experimental and Numerical Investigations on the ESBWR stability Performance. NURETH-12, Pittsburg, USA, Sep. 30 Oct. 4 (2007).
- ¹⁴ Kok, H.V. and Van der Hagen, T.H.J.J., Design of a simulated void-reactivity feedback in a boiling water reactor loop. *Nucl. Techn.* Vol. 128, (1999).
- ¹⁵ Lahey, R.T. Moody, F.J. The thermal-hydraulics of a BWR. ANS, second edition, (1993).
- ¹⁶ Whalley, P.B., Boiling, Condensation, and Gas-Liquid flow. Oxford University Press, (1987).
- ¹⁷ Zhang, M. and Ralph, L., Webb; Correlation of two-phase friction for refrigerants in small-diameter tubes. *Experimental Thermal and Fluid Sciences*, 25, 131-139, (2001).
- ¹⁸ Ott, K. O. and Neuhold, R. J. Nuclear Reactor Dynamics. American Nuclear Society, La Grange Park, Illinois, USA (1985).
- ¹⁹ Shiralkar, B.S., Personal communication, (2005).
- ²⁰ Duderstadt J.J., and L.J. Hamilton, Nuclear Reactor Analysis, J. Wiley & Sons, NY, (1976).
- ²¹ Van der Hagen, T.H.J.J., Experimental and theoretical evidence for a short effective fuel time constant in a boiling water reactor, *Nucl. Technol*, 83, 171, (1988).
- ²² United States Nuclear Regulatory Commission (USNRC) Computer Codes, <http://www.nrc.gov/aboutnrc/regulatory/research/comp-codes.html>.
- ²³ Andersen J. G. M. *et al.*, Time Domain Analysis of Thermal Hydraulic Stability with TRACG-Sensitivity to Numerical Methods and Qualification to Data. BWR Stability Symposium, Idaho, (1989).
- ²⁴ Shiralkar, B., Marquino, W., Klebanov L. and Cheung Y.K., "Natural Circulation in ESBWR", *Proceedings of ICONE 15*, Nagoya, Japan, April 22-26 (2007).
- ²⁵ Rizwan-uddin and Dorning, Nonlinear Stability Analyses of Density-Wave Oscillations in Non-uniformly Heated Channels. *Trans, Am. Nucl. Soc.*, Vol. 54, (1987).

- ²⁶ AEN/NEA, Ringhals 1 Stability Benchmark, final report, (1996).
- ²⁷ Lin, H-T., Wang, J-R., Hsieh, C-L., Shin, C., Chiang, S-C. and Weng, T-L., Kuosheng BWR/6 stability analysis with LAPUR5 code, *Ann. Nucl. Energy*, Vol. 33, No. 3, (2006).
- ²⁸ Krepper, E. Pre- and post-test calculations to natural circulation experiments at the integral test facility ISB-VVER using the thermalhydraulic code ATHLET, *Nucl. Eng. Des.*, 190, pp. 341-346, (1999)
- ²⁹ Sonnenburg, H.G., Berechnung der Phasendifferenzgeschwindigkeit von Wasser und Dampf in geometrisch unterschiedlich berandeten Kanälen. ISBN 3-923875-59-2, (1994).

Chapter 4

An experimental parametric study on natural circulation BWRs stability

4.1 Introduction

During the design and optimization phases of novel reactor concepts, many parameters and configurations are varied and investigated. Numerical simulations and large scale experiments^{1,2} are commonly used for that purpose. Those experiments, however, are extremely expensive and usually do not include the reactivity feedback mechanism. As a result, a lack of experimental evidence confirming numerical findings exists.

Another less expensive possibility is to use an experimental facility with a simulated neutronic feedback system. Besides the advantage regarding the operational costs of such a tool, a test facility can offer a large degree of flexibility allowing studying different configurations. Operating experimental facilities for long time allow using noise analysis techniques in order to get accurate results. This approach has been successfully used by some investigators as, for instance, Zboray and Furuya who have studied the effect

on the stability of BWRs when varying some parameters, such as the void reactivity coefficient and the inlet restriction value^{3,4}.

With the current GENESIS facility, being a downscaled version of the most advanced natural circulation BWR prototype, i.e. the ESBWR, further relevant investigations and parametric studies can be assessed. For instance, the presence of a very long chimney section in novel designs may lead to new instability features.

In this chapter, the flexible capabilities of the GENESIS facility are used to study the aforementioned coupling and also the effect on the reactor stability when varying some parameters such as the operational pressure, the void reactivity coefficient, the geometry and the fuel rods.

4.2 GENESIS improvements

In previous chapters many experiments have been presented for different operational points of the reference natural circulation BWR in the non-dimensional plane. Due to the fact only little differences may be expected in the stability performance when varying a parameter, it was decided to use noise analysis techniques to investigate the stability performance of a certain configuration. From the experiments presented in Chapter 3, it was found to be difficult to operate GENESIS at a certain state for long time because of fluctuations of some input parameters (e.g. system pressure, inlet temperature, etc.). For that reason some modifications are introduced in the facility which improved its controllability. For that purpose a better pressure controller system is installed. On top of this, a by-pass system is added to the feedwater pump loop to better control cavitation of this pump together with the addition of two extra heat exchangers located at the core inlet. As a result of those improvements, the system pressure could be controlled within ± 0.02 bar and the inlet temperature within $\pm 0.1^\circ\text{C}$ of their respective set points.

In the same line, an investigation is conducted to more accurately identify and model the different mechanisms taking place within the GENESIS core which are afterwards used in the compensation functions of the VRF system. The void fraction is estimated in the VRF system by measuring the pressure drop over the core (see Chapter 3). This process can thus be described by a number of transfer functions as shown in Figure 4-1.

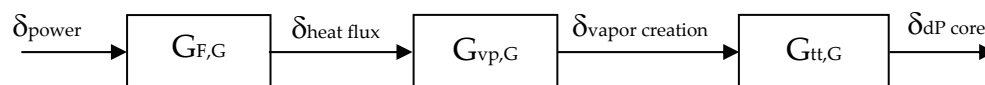


Figure 4-1: Schematic representation of the power to core pressure drop transfer mechanism.

The first two transfer functions, which need to be compensated for, correspond to the dynamics of the heated rods $G_{F,G}$, and the vapor production process in Freon $G_{vp,G}$. The last transfer function named $G_{tt,G}$, is related to the transport of the coolant through the core, which is responsible of the measured pressure drop. This last process associated to the mass transport through the core has not to be compensated because it is correctly simulated in GENESIS since the axial dimensions, the void fraction profile and the mass flow rate, are properly considered in the downscaling (see Section 2.2.3).

The investigation regarding the characterization of the processes shown in Figure 4-1 is divided into two parts. First, a numerical estimation of the dynamics of the heating rods and the mass transport in the core is performed. Second, the estimated time constants associated to those processes are used as initial guesses for the fitting of the parameters of the transfer function from δq -to- δdP_c , i.e. $G_{power-dP_c} = G_{F,G} G_{vp,G} G_{tt,G}$ presented in Figure 4-1.

A numerical 1D model⁵ is used to describe the GENESIS rod dynamics (represented by $G_{F,G}$ in Figure 4-1) following the same procedure as in the ESBWR fuel rods case, see Chapter 3 Section 3.2.1. A boundary condition of no heat resistance at the outside of the rod is assumed in the modeling. As a result of the simulation, it is found that the dynamics of the heating rods can accurately be represented by a second order transfer function. Therefore,

$$G_{F,G} = \frac{A_1}{(1+\tau_{F,G,1}s)(1+\tau_{F,G,2}s)} \quad (4-1)$$

After fitting the response of the heat flux at the rod surface, after a power step is applied to the rod, the following two time constants are found,

$$\begin{aligned} \tau_{F,G,1} &= 0.03 \text{ s} \\ \tau_{F,G,2} &= 0.28 \text{ s}. \end{aligned} \quad (4-2)$$

The boiling process is considered as a first order process. Thus,

$$G_{vp,G} = \frac{A_2}{(1+\tau_{vp,G}s)} \quad (4-3)$$

The transfer function representing the coolant flow through the core $G_{tt,G}$ can be approximated with a first order model with an associated time constant $\tau_{tt,G}$ equal to the effective transit time of the flow through the core⁶.

$$G_{F,G} = \frac{A_3}{(1+\tau_{tt,G}s)} \quad (4-4)$$

This transit time is calculated as in Section 2.2.3 by using the next set of conditions.

$$\begin{aligned} N_{PCH} &= 5.5 \\ N_{Sub} &= 1.65 \\ M &= 0.62 \text{ kg/s} \end{aligned} \quad (4-5)$$

The corresponding effective fluid transit time in the core is found to be

$$t_{Core} = 0.45 \text{ s.} \quad (4-6)$$

The transfer function for the mechanism described in Figure 1.4 is thus,

$$G_{\text{power-dPc}} = \frac{A}{(1+s0.03s^{-1})(1+s0.28s^{-1})(s\tau_{vp,G}+1)(1+s0.45s^{-1})} \quad (4-7)$$

where $A=A_1A_2A_3$.

For the second part of this study, two signals are used (which are obtained at the conditions detailed in Equation (4-3) and the VRF system turned off): the electrical power input, to which a white noise with amplitude of 6 % is added, and the signal from the dP sensor located across the core. The cross correlation between these two measured signals CCF_{meas} is calculated and presented in Figure 4-2.

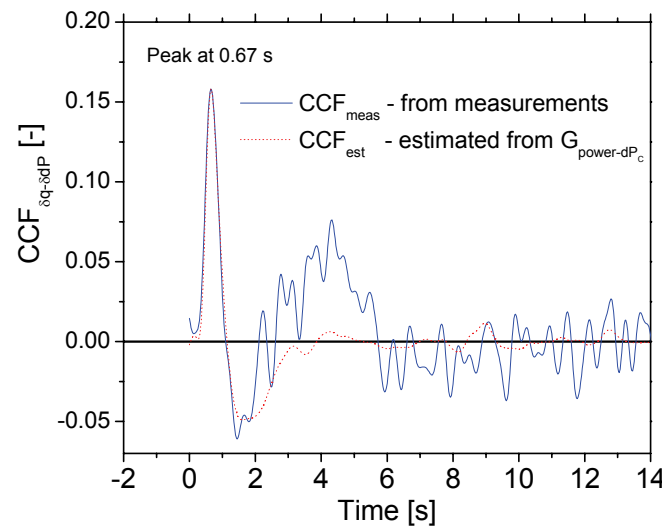


Figure 4-2: Cross correlation function of the noisy power input and the dP measured across the core (solid line) and the analytical estimation (dotted line).

The peak located at ~ 0.67 s is found to be associated to three phenomena:

- heat transport within the GENESIS heating rods (represented by $G_{F,G}$),
- Freon boiling process (represented by $G_{vp,G}$), and
- transport of the vapor-liquid through the core (represented by $G_{tt,G}$).

A relation exists between vapor and flow fluctuations. Since the measurements are performed without a pump, an increase in the vapor production influences the flow by increasing buoyancy in the system. The second peak located at ~ 4 s seems to reflect this feedback mechanism. This reasoning can be confirmed since the distance between the two positive peaks (~ 3.3 s) agrees well with the traveling time found for the chimney section (3.24 s). Since the feedback due to buoyancy can be well discriminated from the fast processes occurring in the core, it is ignored in the following analysis.

The estimated transfer function $G_{\text{power-dPc}}$ is used with the noisy power as input to obtain an estimated pressure drop over the core. The Simulink tool from the MATLAB environment is used for that purpose. A second cross

correlation CCF_{est} is calculated and compared with the previous CCF_{meas} . All the time constants present in $G_{power-dPc}$ (see Figure 4.1) are varied until the similarity between CCF_{meas} and CCF_{est} is optimized, i.e. the error of CCF_{est} for the first peak is minimal. The resulting CCF_{meas} is also plotted in Figure 4-2.

Table 4.1 summarizes the time constants estimated analytically and their correspondence with the ones found through the fitting. By comparing the experimental and analytical time constants it can be seen that a very good agreement exists for the first peak. It can therefore be concluded that the modeled physical mechanisms are well characterized.

Physical process	Parameter	Numerical value	Experimentally derived value	Previous implementation
Heat transport within the rod	$\tau_{FG,1}$	0.03 s	0.02 s	0.5 s
	$\tau_{FG,2}$	0.28 s	0.28 s	
Boiling process	τ_{vpG}	Unknown	0.31 s	
Void transport through the core	τ_{tG}	0.45 s	0.45 s	-

Table 4-1: Experimentally and analytically found parameters of the TF from Figure 4-1.

Since the processes occurring in the GENESIS core are successfully modeled, the compensation transfer function presented in Equation (4-9) (based on the experimental analysis presented above) can be expressed in the z domain and implemented in the VRF system algorithm.

$$G_{F,G}^{-1}(s)G_{vp,G}^{-1}(s)=G_{power-dPc,G}^{-1}(s)G_{t,G}(s)=\frac{(1+s3.2s^{-1})(1+s3.57s^{-1})(1+s49.9s^{-1})}{sA'} \quad (4-8)$$

with $A'=3.37 \times 10^{-3} \text{ 1/W}$.

The following results are obtained by using the improved compensation transfer function expressed in Equation (4-9).

4.3 Parametric study

In this section, the capabilities of the GENESIS facility are exploited by modeling different fuel rods, varying the void reactivity coefficient and changing some operational parameters, such as the pressure and the feedwater sparger location. Unless indicated, the power and inlet subcooling (defining the operational point in the non-dimensional plane) are the same for all experimental cases and correspond to a reference situation of the GENESIS facility, named as REFERENCE CASE, which is characterized by:

$$\begin{aligned} N_{PCH} &= 5.7 \\ N_{Sub} &= 1.2. \end{aligned} \quad (4-9)$$

All the results presented in this chapter are obtained by using noise analysis. Details of the treatment of the data and the procedure followed in the analysis are given in APPENDIX B.

4.3.1 Effect of the improved VRF system

This study is intended to investigate the influence of using the compensation function expressed in Equation (4-9) instead of the following one used in Chapter 3.

$$G_{vp,G}^{-1} G_{F,G}^{-1} = \frac{\tau_{F,G} s + 1}{1} \quad \text{with } \tau_{F,G} = 0.5 s \quad (4-10)$$

The stability obtained by using both algorithms is presented in Table 4-2.

$R_\alpha = -0.103$	DR [-]	f_{res} [Hz]
REFERENCE CASE (Eq. 4-6)	0.31 ± 0.02	0.66 ± 0.02
VRF from Chapter 3	0.26 ± 0.02	0.66 ± 0.03

Table 4-2: Experimental decay ratio and resonance frequency found for the reference case by using the VRF system with the compensation functions described in Chapter 3 and the more sophisticated ones developed in this chapter.

As can be seen, implementing the simple compensation function from Chapter 3 seems to have a non-conservative effect since the decay ratio (DR) is underpredicted compared with the one obtained from the improved implementation. The resonance frequency is unchanged. As it will be shown later, a slower dynamics of the heat transfer from the rods to the coolant increases the neutronic-thermal-hydraulic stability. From the results presented in the table it can be inferred that the time constant of the first order implementation is smaller than the *effective* time constant from the more sophisticated implementation developed in this chapter (defining the effective time constant as the time constant corresponding to a first order model which would give the same stability results as the real system). This result indicates that care has to be taken when compensating a higher order system by a lower order transfer function since non-conservative results may be obtained.

4.3.2 Effect of the modeling of the ESBWR fuel rods

Van der Hagen has proposed that the dynamics of heat transfer taking place in a BWR core during Type-II oscillations is governed by small fuel time constants that are associated with heat transfer from the outer region of the fuel rods⁷. It is therefore important to investigate the effect on stability when modeling the heat transfer within the fuel rods by using a first order model since in such a case the rod dynamics is described by only one time constant. The GENESIS facility is therefore used with a first order implementation of the ESBWR rods. The associated time constant is obtained as detailed in Section 3.2.1 but by using the solution of a first order system as a fitting function. Experiments obtained at the same operational conditions as the reference case are conducted by using this new rods implementation. As a

matter of completeness, such rods are also implemented and tested in the VRF algorithm used in Chapter 3. The results of this study are shown in Table 4.3.

Table 4-3 shows that by using a first order transfer function to model the ESBWR fuel rods stabilize the system for both cases, when using the sophisticated implementation presented in this chapter and also with the VRF model from Chapter 3. This effect is due to the fact that by using a slow representation for the fuel rods filters out the dynamics of the power-to-vapor production effect which is important in the neutronic-thermal-hydraulic instability mechanism.

$r_d = -0.103$	$\tau_{F,1}$ [s]	$\tau_{F,2}$ [s]	DR [-]	f_{res} [Hz]
2 nd order approx. REFERENCE CASE	0.57	6.55	0.31 ± 0.02	0.66 ± 0.02
1 st order approx.	4.86		0.24 ± 0.03	0.64 ± 0.02
1 st order approx. + VRF from Chapter 3	4.86		0.20 ± 0.02	0.64 ± 0.02

Table 4-3: Experimental decay ratio and resonance frequency found for the reference case (which uses a 2nd order representation of the fuel rods) and the case in which a 1st order model for describing the ESBWR fuel rods is used.

From the experiments it can be concluded that by using the first order approximation with the fitted time constant results in non-conservative results. It therefore can be confirmed that the effective time constant that has to be used in the first order model is associated to fast responses taking place in the fuel rods. It is thus recommended to represent the fuel rod dynamics as (at least) a second order system in order to avoid undesired effects originated from the modeling of such a component.

Table 4-3 also shows that the use of the VRF implementation from Chapter 3 reinforces the stabilization effect caused by approximating the fuel rods as first order systems, as discussed in section 4.3.1.

4.3.3 Effect of changing the rod diameter

The impact of changing the fuel rod diameter on the stability performance is investigated in this section. For this purpose two cases are studied and afterward compared with the reference case: a case in which the fuel rods diameter is twice the one from the reference case and a case in which the diameter is half of that. Different authors have predicted that when modeling the fuel rods as first order systems, large time constants (*large* compared to typical periods of thermal-hydraulic instabilities) have a stabilizing effect on Type-II oscillations because of a significant filtering of high-frequency oscillations in the void reactivity feedback loop^{8,9}. However, to what extent this holds for a second-order approximation of the fuel rod dynamics, is not known. The results of this study are condensed in Table 4-4.

$r_a = -0.103$	$\tau_{F,1}$ [s] [†]	$\tau_{F,2}$ [s] [†]	τ_F [s] [‡]	DR [-]	f_{res} [Hz]
$D_{rod} = 2.0 D_{rod REF}$	1.31	17.65	14.05	0.28 ± 0.02	0.62 ± 0.02
REFERENCE CASE	0.57	6.55	4.86	0.31 ± 0.02	0.66 ± 0.02
$D_{rod} = 0.5 D_{rod REF}$	0.22	2.04	1.67	0.34 ± 0.01	0.67 ± 0.03
[†] Obtained by fitting the analytical solution with the solution for a second order system.					
[‡] Idem before but with the solution for a first order system (not used in the experiments).					

Table 4-4: Experimental decay ratio and resonance frequency found for the reference case and two cases using different fuel rod diameters.

Having the doubled diameter fuel rods stabilizes the system while decreases the resonance frequency. This effect can be understood by the lower cut off frequencies associated to thicker rods, which filters more effectively the high frequency fluctuations induced by the void reactivity feedback dynamics. For the same reason, the typical frequency associated to this type of rod is lower. The opposite occurs in the experiments when modeling the fuel rods having a diameter being half the reference one. However, these differences are found to be less pronounced than those predicted by numerical models using a first order approximation for the rods dynamics⁵. This effect seems to be related to the larger time constant derived from the first order approximation which tends to amplify the differences in the dynamics of the rods. As a result of this, it is likely possible that numerical investigations using a first order approximation for the fuel rods (see for instance Reference 6) may overpredict the stability effect of the rods diameter.

4.3.4 Effect of using a MOX fuel

The recycling of plutonium as mixed oxide (MOX) has a promising potential for reducing the long-term radiotoxicity of disposed nuclear fuel. For this reason, the use of MOX fuel in light water reactors is an important part of the nuclear strategy in many countries worldwide. It is thus of importance to investigate the influence on the stability performance when MOX fuels are loaded in a BWR. In this section, the stability behavior of the reference reactor being fully loaded with a typical MOX fuel is investigated by slightly changing the VRF system implementation in the GENESIS facility. MOX fuel at the beginning of the cycle (BOC) is considered which is known to have the most different neutronic behavior regarding UO₂ fuel¹⁰. Since the geometrical and thermo-physical properties (relevant for the heat transfer mechanisms) of the MOX fuels are practically the same as those for a fuel filled with UO₂ pellets at BOC and MOC respectively¹¹ the implementation of the fuel rods remain unchanged. In order to account for the different neutronic behavior of the MOX fuel, the neutronic parameters needed for the six groups point kinetics model implemented in the algorithm are obtained from numerical simulations when using a reference neutron flux (the European Pressurized Reactor (EPR)¹² being also a thermal reactor was used).

The MOX fuel composition and the resulting neutronic parameters are given in Table C-II from APPENDIX C.

From SIMULATE-3 calculations, Demazière estimated the moderator temperature coefficient (for which the void reactivity coefficient is the largest contributor) to be 15% larger for a fully loaded MOX fuel core at BOC than the correspondent UO₂ one at MOC^{13,14}. In this investigation, the void reactivity feedback coefficient for the MOX experiment is therefore 1.15 times the void reactivity coefficient used for the reference case.

The results of the stability performance of a core fully loaded with MOX and the reference case in which UO₂ fuel is used are presented in Table 4-5.

	DR [-]	f_{res} [Hz]
REFERENCE CASE (UO ₂ fuel, $r_a=-0.103$, $\beta=0.00562$)	0.31 ± 0.02	0.66 ± 0.02
MOX case (MOX fuel, $r_a=-0.118$, $\beta=0.004079$)	0.33 ± 0.05	0.91 ± 0.02

Table 4-5: Experimental decay ratio and resonance frequency found for the reference case and the case simulating a core fully loaded with MOX fuel.

It can be seen that the MOX fuel causes the system to be slightly more unstable and shows a higher resonance frequency than that using a conventional UO₂ fuel. This difference can be attributed to the smaller effective delayed neutron fractions from MOX fuels, mainly caused by the ²³⁹Pu and ²⁴⁰Pu content.

4.3.5 Effect of the pressure

In Chapter 2 it has been shown that the scaling factors used in the design of the GENESIS facility are hardly dependent on the system pressure for pressures close to the design value (11.4 bar). Based on this, GENESIS can be used to explore the thermal-hydraulic stability performance of a natural circulation loop when the operational pressure shifts to higher or lower values. By changing the pressure, the fluid properties change, particularly the vapor density and the saturation temperature. The inlet subcooling and the power input were therefore adjusted in such a way the operational point in the non-dimensional plane was kept the same. If those parameters were not kept constant, the GENESIS working point would be different and therefore no comparison could be made between the cases. The results of the investigation regarding the pressure effect on the system stability (obtained without reactivity feedback) are shown in Table 4-6.

$r_a=0$	DR [-]	f_{res} [Hz]
Low Pressure (10.6 bar-Freon \equiv 66 bar-water)	0.02 ± 0.05	0.15 ± 0.03
REFERENCE CASE (11.4 bar-Freon \equiv bar 71-water)	0.09 ± 0.04	0.13 ± 0.03
High Pressure (12 bar-Freon \equiv 74 bar-water)	0.07 ± 0.03	0.16 ± 0.04

Table 4-6: Experimental decay ratio and resonance frequency found when varying the pressure while keeping the same operational point in the non-dimensional plane.

From the table, no clear change is observed in the resulting stability. This finding agrees well with numerical calculations obtained by Van Bragt who found very little dependency of the stability boundary when varying the system pressure in the modeled natural circulation channel¹⁵. Such a finding valid for natural circulation systems is due to the fact that there is no explicit pressure dependency on the non-dimensional parameters which determine the stability of the system (see Chapter 2). Since all the non-dimensional numbers are kept the same (the inlet coolant temperature and the power are adjusted to have the same N_{PCH} and N_{Sub}) the stability boundary location is also preserved.

4.3.6 Effect of the feedwater sparger position

Zboray and Podowski have shown that fluctuations in the core inlet coolant temperature can significantly influence the stability of closed-loop reactor systems^{16,17}. As a result of numerical investigations, Zboray has found that such thermal-hydraulic systems change their stability performance when the feedwater sparger position is varied¹⁶. In the case in which the sparger position is placed at the core inlet, he predicted the system to be unconditionally stable regarding the thermal-hydraulic stability mode. Zboray found that in his model the influence of flow variations on the boiling-boundary position is cancelled out by the influence of the core inlet-temperature variations if the sparger position approaches to the core inlet. In order to investigate such a prediction, the GENESIS facility is destabilized by increasing the chimney outlet local restriction which would amplify any instability mechanism effect. The thermal-hydraulic stability performance of this new configuration (the so-called DESTABILIZED CASE) is investigated for three feedwater sparger inlet positions, which are located at different heights regarding the core inlet (see Figure 2-8). The stability results for these experiments (obtained without reactivity feedback) are presented in Table 4-7.

DESTABILIZED CASE - $r_{\alpha}=0$	DR [-]	f_{res} [Hz]	φ [°]
[†] FW sparger at 7.3m (Nominal position)	0.60 ± 0.02	0.108 ± 0.002	-253
[†] FW sparger at 3.3 m	0.83 ± 0.02	0.106 ± 0.002	-168
[†] FW sparger at 0.3 m	0.75 ± 0.02	0.110 ± 0.003	-110
[†] With respect to the core inlet (See Figure 2-8)			

Table 4-7: Decay ratio and resonance frequency found for the destabilized case using three different feedwater sparger positions.

From the experiments it is seen that when lowering the feedwater sparger position, the stability performance is affected. By investigating the correlation between the signal from the coolant inlet temperature and the signals corresponding to the primary flow, and the feedwater flow and temperature, it is concluded that the core inlet temperature fluctuations are

induced by changes in the primary flow and not by the feedwater flow dynamics. Such an investigation is presented in APPENDIX D.

Zboray related the system stability to the phase between the core inlet temperature and flow fluctuations φ , which can be estimated by¹⁶,

$$\varphi = -2\pi f_{res} t_t, \quad (4-11)$$

where $t_t = \rho A_{DC} l_{Sparger} / M_{C,in}$ is the coolant transit time from the sparger position to the core inlet, A_{DC} is the downcomer cross sectional area and $l_{Sparger}$ is the distance between the feedwater sparger and the core inlet. Note that $l_{Sparger}$ is different from the height at which the sparger inlet is located because of the extra piping connecting the downcomer with the core inlet. The resulting phases for the three cases are shown in the last column of Table 4-7.

Clearly the most unstable case is the one having a phase close to -180° . For such a value, the inlet-temperature oscillations are out-of-phase with the flow oscillations and therefore reinforce their influence on the boiling boundary oscillations, which are known to have a destabilizing effect on the system. This result seems to confirm the instability mechanism predicted by Zboray. Unfortunately, the cases with $\varphi = n.2\pi$, with $n=0,1,\dots$ could not be examined which would make the conclusions stronger.

The stability effect of varying the sparger inlet position can be used to optimize the stability regarding the thermal-hydraulic instability mode. It has to be mentioned, however, that placing the sparger inlet at a too low position may have negative effects on the reactor safety, since in such a case the risk of a loss of inventory accident due to siphon drainage problems is increased.

4.3.7 Effect of the void reactivity feedback coefficient

The influence of the void reactivity feedback coefficient r_α on the stability of the coupled neutronic-thermal-hydraulic reactor system has been investigated by using both numerical and experimental tools by Zboray and Furuya. Those early works are extended here for the case of a novel natural circulation BWR prototype. Two configurations are studied: The reference case used in sections 4.3.1 to 4.3.5 and the destabilized case from section 4.3.6.

The experiments are obtained by operating the GENESIS facility in the two aforementioned configurations and varying r_α step by step, ranging from 0 (no neutronic feedback effect) to twice the nominal value. The resulting trends in the DR and in the f_{res} are depicted in Figure 4-4.

In the reference case a clear increase in the f_{res} can be observed when increasing r_α . The value of f_{res} is then stabilized for r_α above the nominal value of $r_\alpha = -0.103$. In this case the larger r_α the more unstable the system is. This effect is explained as follows. At $r_\alpha = 0$ the only instability mechanism present

in the system is attributed to density waves traveling through the core plus chimney sections, with an associated low f_{res} . When the neutronic feedback mechanism is included, another instability mechanism appears which is related to the vapor transport through the core section only. This process is faster than the previous one which explains the higher frequency at larger values of r_α . The relative stabilization of the f_{res} value is explained by fact the vapor transport in the core remains unchanged since the working point of the facility is the same for all cases. The trend of the DR is due to the fact the thermal-hydraulic mode is extremely stable for this configuration (see the low DR value corresponding to $r_\alpha=0$) when compared to the reactor-kinetic instability mode. By increasing the value of r_α the reactor-kinetic instability mode becomes more important and thus the DR increases. Interestingly the shift from one instability mechanism to the other one is smooth as it is revealed by the f_{res} and the DR trends.

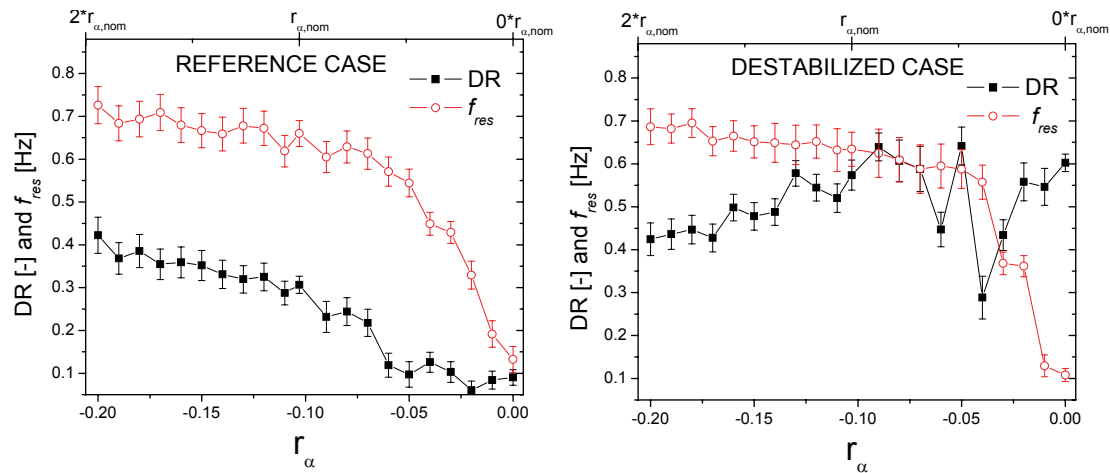


Figure 4-4: Effect of varying the void reactivity coefficient in the system stability.

For simplicity, in the following discussion the value of r_α is considered in an absolute sense, thus, omitting its negative sign.

For the thermal-hydraulic destabilized case it can be seen that, as a result of the variations in the void reactivity coefficient, the system exhibits a complex behavior. In this case, the system is less stable than in the reference case regarding the thermal-hydraulic mode since the DR is larger when $r_\alpha=0$. Increasing r_α clearly affects the stability performance. In particular, a transition region characterized by fluctuations in the obtained value of the DR is found for $-0.06 < r_\alpha < -0.03$. A strong effect can be observed on f_{res} in this region, even for very small values of r_α . When increasing the importance of the neutronic feedback mechanism (i.e. increasing r_α) in the range of $-0.15 < r_\alpha < -0.06$ the system shows a slight increase in the stability performance while the value of f_{res} corresponds to the Type-II neutronic-thermal-hydraulic mode.

In order to understand these findings, numerical results obtained by Zboray with a reduced order model are recalled¹⁶. Figure 4-5 shows the

stability maps obtained when different void reactivity coefficients are used in the numerical simulations. The root-loci diagrams corresponding to the points A and B are also included in the right hand side plots.

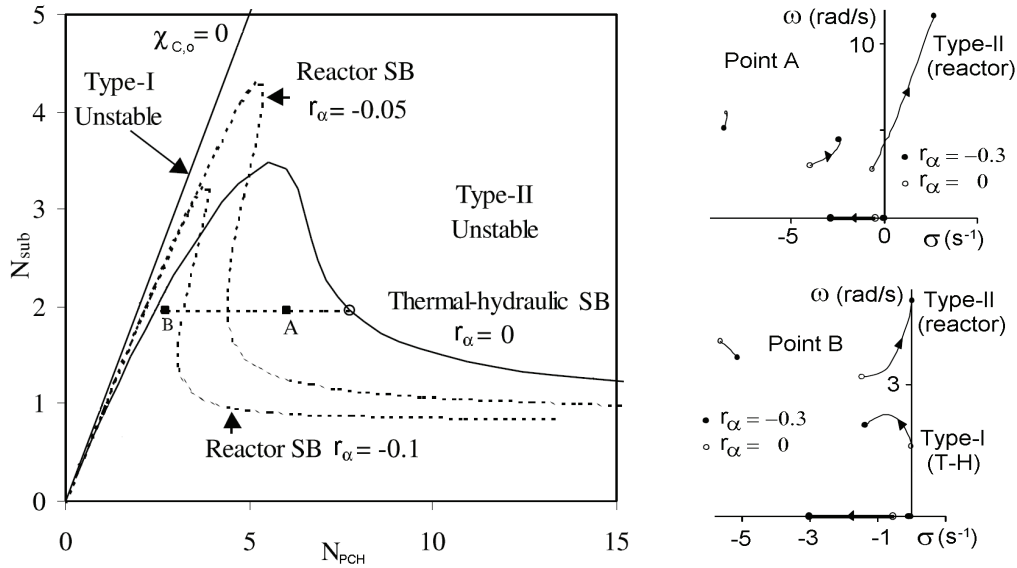


Figure 4-5: Stability map for different values of the void reactivity coefficient obtained by Zboray¹³. The root-loci corresponding to the points A and B are also presented.

The reference case can be related to the point A in the stability map since it corresponds to a relatively stable system from the thermal-hydraulic point of view. From the root-loci diagram, it is seen that for $r_\alpha=0$ the thermal-hydraulic stability mode dominates but as soon as $r_\alpha<0$, the pole associated to the reactor instability mode moves to the right destabilizing the system.

The so-called destabilized case can be compared to the point B in the stability map since it describes a relatively unstable system regarding the thermal-hydraulic instability mode. In this case, the root-loci shows that for $r_\alpha=0$, the pole associated to the reactor-kinetic mode is rather far from the unstable half plane. In contrast, the pole related to the thermal-hydraulic mode is close to the stability boundary and therefore dominates. By increasing the value of r_α the reactor-kinetic pole moves to the right and the thermal-hydraulic pole moves to the left. As a result of this, a range of r_α values with associated low DR values is found. This phenomenon can therefore be associated to the interchange of the importance of the poles corresponding to the two instability modes. As a result of this, a range of r_α 's with low DRs is found.

In the GENESIS experiments two different resonance frequencies exist which can be related to the fluid transit time through the core plus chimney sections and the core section only, corresponding to the thermal-hydraulic oscillatory mode ($f_{res} \approx 0.15$ Hz) and the reactor oscillatory mode ($f_{res} \approx 0.66$ Hz) respectively. In order to further investigate the trend from one mode to the other one, the power spectral decomposition of the detrended flow inlet

signal obtained for the reference case, is analyzed. The PSD calculated for different values of r_α for the reference case is shown in Figure 4.6 a).

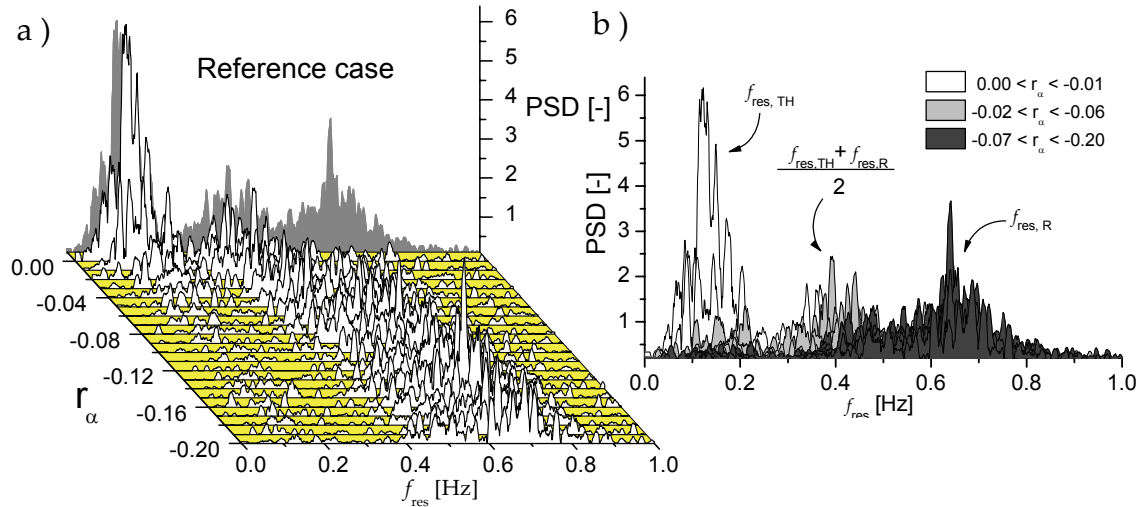


Figure 4-6: a) PSD of the inlet flow signal for different values of r_α . b) The projection of all PSD functions is also presented.

As indicated before, f_{res} varies smoothly from the low frequency value, corresponding to the thermal-hydraulic mode, to higher ones in which the neutronic mode is dominant. As soon as $r_\alpha < 0$, the effects of the T-H mode are strongly diminished since the PSD function at such low frequencies is drastically reduced. This result agrees with the strong stabilization of the T-H mode observed in the destabilized case when the VRF system is included.

On top of the smooth transition between the two resonance frequencies of the system, when projecting all the PSD functions in the PSD - f_{res} plane, it is observed that three clear peaks exist located at three different frequencies. To better characterize this finding, the experiments are divided into three groups according to the shape of the PSD functions. The results are also shown in Figure 4-6 b). It is observed that the first low frequency region, which is associated with the T-H mode, is characterized by only two cases corresponding to zero or very low values of r_α . The region located at intermediate frequencies is defined by the cases with r_α between -0.02 and -0.06. The existence of this peak has not been reported in the past and may be related to a new mechanism for instabilities. Further investigations are needed to elucidate this issue. Its location coincides with an intermediate frequency ($f_{res} \approx 0.4$ Hz). The third region groups the experiments obtained with r_α between -0.07 and -0.20. This peak is associated with the void-neutronic feedback mechanism and its location can be related to the time for the heat transport within the rods plus the boiling process and the transport of such a vapor through the core section.

4.4 Conclusions

As a result of the parametric study which uses a more advanced implementation of the VRF system developed in this chapter, the following conclusions could be drawn:

- When using a first order model for the compensation function of the VRF system, care has to be taken on selecting the appropriate time constant since this parameter influences the resulting stability performance.
- Modeling the reactor fuel rods as a first order system (with the time constant obtained by fitting the time response with a first order solution) leads to a too low estimate of the decay ratio (DR). A higher order model implementation is therefore needed to avoid erroneous results.
- Changing the fuel rods diameter to a half (doubling) decreases (increases) the stability performance of the system while the resonance frequency increases (decreases). This effect is probably be less pronounced than when the fuel rods are modeled as first order systems because in the last case the rods more effectively filters high-frequencies which are of relevance for Type-II instabilities.
- The use of MOX fuels in a BWR is found to slightly decrease the stability performance of the reactor since the smaller effective delayed neutron fraction brings the system closer to prompt-criticality. In addition, the resonance frequency is found to be higher than that for UO_2 fuels.
- The pressure has little influence on the thermal- hydraulic stability of the system when studied in the non-dimensional plane (for $66 \text{ bar} < P < 74 \text{ bar}$).
- Lowering the position of the feedwater sparger position affects the thermal-hydraulic stability of the system. This effect may be used to optimize the stability margin of the reactor regarding that instability mode.
- Small values of the void reactivity feedback coefficient may strongly affect the thermal-hydraulic instability mechanism.
- A strongly destabilized system regarding the thermal-hydraulic mode can destabilize a reactor when considering the neutronic-thermal-hydraulic mode. The last could be particularly important in accidental situations like in the case of a blockage of a channel.
- A clear peak is found in the power spectral decomposition of the flow signal at intermediate frequencies (regarding the resonance frequencies of the thermal-hydraulic and the reactor-kinetic instability modes) when the void reactivity coefficient is varied. Further investigations are therefore needed in order to confirm the origin of this finding.

4.5 References

- ¹ Paladino, D., Auban, O., Huggenberger, M., Candreia, P., Strassberger, H.J., Bandurski, T., Description of PANDA Including Test Matrix, PSI Internal Report TM-42-01-14/ALPHA-01-03-0 (2002).
- ² Ishii, M., Revankai, S.T., Dowlati, R., Bertodano, M.L., Babelli, I., Wang, W., Pokharna, H., Ransom, V.H., Viskanta, R., Wilmarth, T., Han, J.T., Scientific Design of Purdue University Multi-Dimensional Integral Test Assembly (PUMA) for GE SBWR. NUREG:CR-6309, PU-NE 94:1 (1996).
- ³ Zboray R., An experimental and Modeling Study of Natural-Circulation Boiling Water Reactor Dynamics, Delft University of Technology PhD thesis (2002).
- ⁴ Furuya M., Experimental and Analytical Modeling of Natural Circulation and Forced Circulation BWRs. Delft University of Technology PhD thesis (2006).
- ⁵ Degen, C., Dynamics of the GENESIS fuel rods (Bachelor thesis), (2006).
- ⁶ Earni, S., Wang, S., Mohan, R., Shoham, O., Marrelli, J. Slug Detection as a Tool for Predictive Control of GLCC[®] Compact Separators. J. of Energy Resour. Techn., 125, 145-152 (2003).
- ⁷ Van der Hagen, T. H. J. J., Experimental and theoretical evidence for a short effective fuel time constant in a boiling water reactor, *Nucl. Technol.* 83, 171, (1988).
- ⁸ Van Bragt, D.D.B., Rizwan-uddin, and T.H.J.J.van der Hagen. 1998b. Stability of Natural Circulation Boiling Water Reactors: Part II-Parametric Study of Coupled Neutronic-Thermal-hydraulic Stability. *Nucl. Techn.*, Vol. 121, (2006).
- ⁹ Furuya, M. Inada, F. Van der Hagen, T.H.J.J. Characteristics of Type-I Density Wave Oscillations in a Natural Circulation BWR at Relatively High Pressure, *J. Nucl. Sci. Technol.*, Vol.42, No.2, 191-200, (2004).
- ¹⁰ Demazière, C., Reactor physics calculations on MOX fuel in Boiling water reactors (BWRs).
- ¹¹ Bailly H., Mènessier D. and Prunier C., The nuclear fuel of pressurized water reactors and fast reactors, Intercept Ltd., (1999).
- ¹² Leppanen, J., Preliminary calculations on actinide management using advanced PWR MOX technology, Technical report, VTT, (2005).
- ¹³ Van Rooijen, W. Personal communication, (2007)
- ¹⁴ Kloosterman J.L. and Kuijper, J.C., VAREX, a code for variational analysis of reactivity effects: description and examples. PHYSOR 200, Seoul, South Korea, October 7-10 2000. ANS.
- ¹⁵ Van Bragt, Rizwan-uddin, D.D.B. and Van der Hagen, T.H.J.J. Stability of Natural Circulation Boiling Water Reactors: Part I-Description Stability Model and Theoretical Analysis in Terms of Dimensionless Groups. *Nucl. Techn.*, Vol. 121, (1998).
- ¹⁶ Zboray, R., Kruijff W.J.M.de, Van der Hagen, T.H.J.J. and Van Dam H.. Investigating the Stability Characteristics of Natural Circulation Boiling Water Reactors Using Root Loci of a Reduced-order Model. *Nucl. Techn.*, Vol. 136, No. 3, (2001).
- ¹⁷ Podowski, M. Z. and Pinheiro Rosa, M. Modeling and numerical simulation of oscillatory two-phase flows, with application to boiling water reactors. *Nucl. Eng. Des.*, 177, 179-188, (1997).

Chapter 5

Experimental and analytical investigations on flashing-induced instabilities in a single channel

5.1 Introduction

The tall adiabatic chimney placed on top of natural circulation BWR cores makes flashing very likely to occur during the low pressure start-up phase of these reactors. The feedback between vapor generation in the chimney and buoyancy of the natural-circulation loop may, under specific conditions, give rise to flow oscillations. In modern designs such as in the ESBWR, the vapor separation is performed in the steam separators, which are placed on top of the chimney (see Figure 1-1). These devices induce a large pressure drop concentrated mainly at the swirlers¹. To what extent this restriction can influence the stability of the system is unknown and needs to be investigated in order to assure a stable start-up of these reactors. On top of this, the flashing mechanism is not fully understood and also discrepancies exist regarding the results of the numerical simulations (see Manera² for a comprehensive review). In order to thoroughly understand the mechanism of

flashing-induced oscillations and to generate an accurate experimental database, the CIRCUS facility equipped with a single chimney is used. The experiments are presented in a novel manner, allowing observing the dynamic evolution of the temperature, void fraction and pressure axial profiles. As a result, a very good characterization of the instability mechanisms can be done. The experiments are then used to benchmark a numerical code especially developed for simulating flashing-induced instabilities. The model is afterwards used to investigate the effect of having different restrictions placed at the chimney exit.

5.2 The CIRCUS facility in the single chimney configuration

The CIRCUS facility³ is a steam/water facility designed to perform studies on two-phase flow dynamics relevant for the starting-up of natural circulation BWRs. CIRCUS is an axially fully scaled, radially lumped version of the Dodewaard reactor⁴. A simplified scheme of the CIRCUS facility including technical details is given in Figure 5-1.

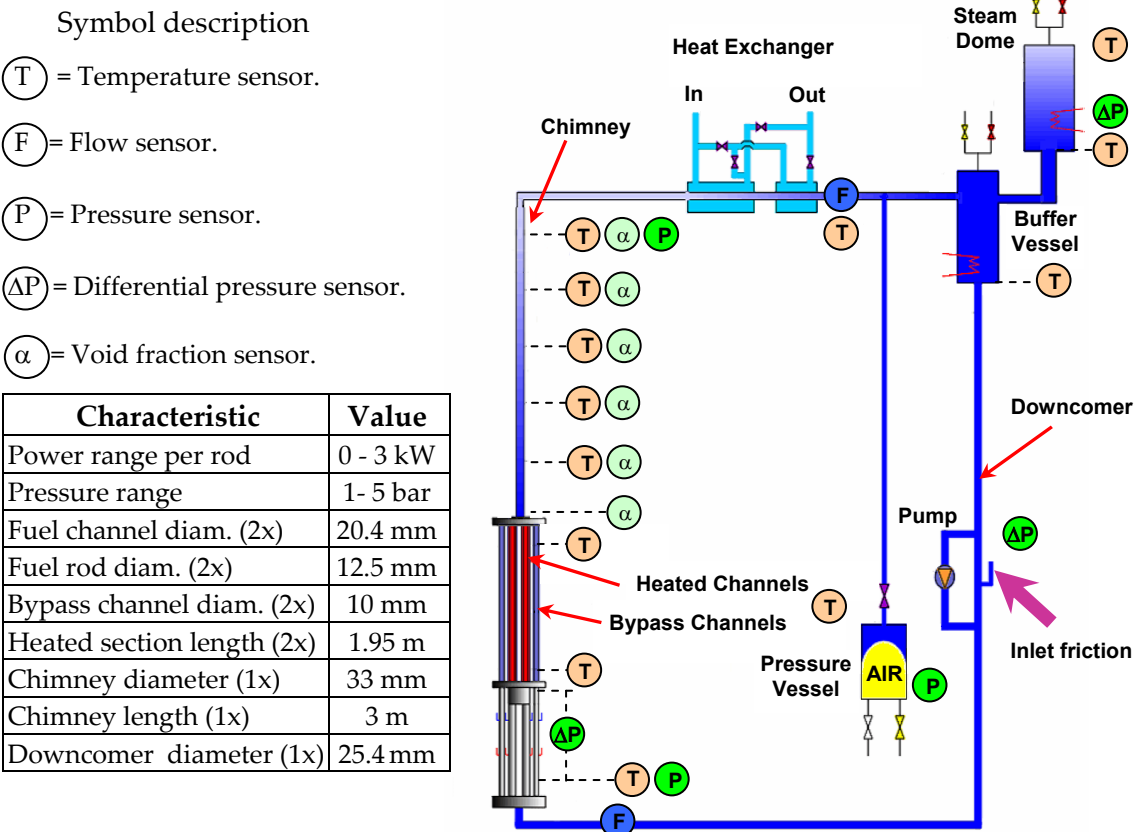


Figure 5-1: Schematic view of the CIRCUS facility and its sensors in the single chimney configuration (not to scale).

CIRCUS can be operated in two different ways: the single chimney configuration and the two parallel chimneys configuration. In the first one, CIRCUS is equipped with a single tall adiabatic section representing the

reactor chimney which is placed on top of the heated section. The heated section simulates the reactor core and consists of two heated channels with two bypasses. For this reason this section is also referred as the 'core' section.

The steam produced in the heated section and in the chimney is condensed in the heat exchangers and to some extent in the steam dome. A buffer vessel is used to damp temperature oscillations at the downcomer inlet, ensuring a constant inlet subcooling. Two magnetic flow-meters (maximum inaccuracy of ± 0.01 l/s) characterize the flow at the heated section inlet and chimney outlet. Several thermocouples (maximum inaccuracy of $\pm 0.5^\circ\text{C}$) are located at the inlet and outlet of each heated channel, along the chimney section, in the heat exchanger and in the steam dome. Two PT100 sensors are located at the inlet of the core section and in the steam dome for more accurate temperature measurements. Absolute pressure sensors are placed at the inlet of the core section, at the chimney outlet and in the steam dome. Differential pressure sensors are mounted across the steam dome, for measuring the water level, and across the core inlet valve. Advanced measuring techniques are used for detailed high sampling rate void-fraction measurements, e.g. conductivity needle probes and capacitance-based sensors. The channels in the facility are made of glass, allowing visual inspection during the operation. To reduce the heat losses to the surroundings, all the sections are covered with removable thermal isolation.

CIRCUS can be operated from 1 to 5 bar, the maximum electrical power per rod is 3 kW. By varying the inlet subcooling and the applied power, several configurations can be studied in the power-subcooling plane. The core inlet valve allows changing the inlet restriction coefficient.

5.3 Experimental results

The following experiments are performed with the steam dome open to the surroundings, thus the pressure at the top of the facility is assumed to be always at 1 bar. Three non-dimensional numbers characterize a thermal-hydraulic two-phase system at low pressure: the phase change number N_{PCH} , which is defined in terms of the power-to-flow ratio, the subcooling number N_{Sub} , and the flashing number N_{Flash} ⁵. Due to the fact that all the experiments are performed at the same pressure (1 bar at the steam dome), the comparison can be assessed in the N_{PCH} - N_{Sub} plane since N_{Flash} remains unchanged.

Each experimental point is obtained by fixing the power applied in the heating rods and varying the inlet temperature by changing the power applied in the buffer vessel. By repeating this process at different powers, the whole operational map can be covered. The operational conditions used for the experimental study are summarized in Table 5-1.

Three different configurations are investigated corresponding to different core inlet restriction values (see Figure 5-1):

- no friction, i.e. the inlet restriction is fully open and thus $K_{in}=0 \pm 1$,
- moderate friction, with an associated friction factor $K_{in}=8.65 \pm 1$,
- large friction, with an inlet friction factor being equal to $K_{in}=340 \pm 10$.

Magnitude	Value
Power per rod	0-3000 W
Inlet Temperature	50-99 °C
Pressure	1 bar
Flow circulation	Natural
Core-bypass channels	Closed
Number of chimneys	1

Table 5-1: Experimental conditions for the measurements presented in this chapter.

The value of the friction coefficients is obtained experimentally by taking the downcomer flow area A_{DC} as a reference and using the following equation

$$K_{in} = \frac{2A_{DC}^2 \rho_{l,in}}{M^2} \Delta P_{in}, \quad (5-1)$$

where the mass flow rate M and the inlet restriction pressure drop ΔP_{in} are measured. The coolant inlet density $\rho_{l,in}$ is found from the inlet temperature. The chimney outlet friction is estimated from the bending of the tubes connecting the chimney with the heat exchanger (see Figure 5-1).

5.3.1 The stability maps

The stability maps for the three cases are shown in Figure 5-2. To enhance clarity, the measured points defining the stability boundaries (SBs) of Figure 5-2a) are not displayed. The inlet subcooling is defined in terms of the saturation temperature at the steam dome (100°C).

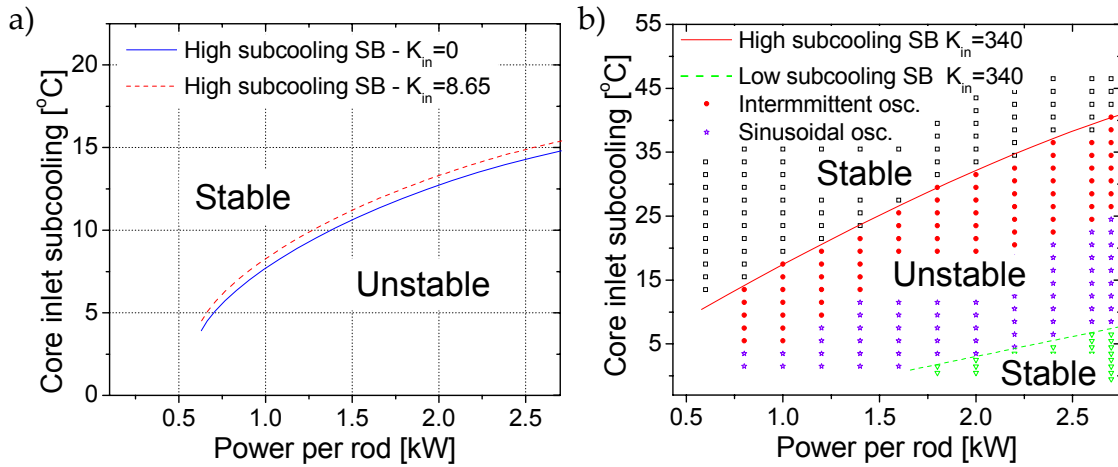


Figure 5-2: Measured SBs for the cases with $K_{in}=0$, $K_{in}=8.65$ and $K_{in}=340$.

From the results it is clear that increasing the core inlet restriction enlarges the subcooling at which the instabilities start i.e. the so-called high

subcooling stability boundary (HS-SB). This effect is mainly related to the resulting flow decrease which increases the coolant core outlet temperature thus promoting the onset of flashing. For $K_{in}=0$ and $K_{in}=8.65$, no stable two-phase regime is found at low subcoolings, while a stable flashing situation is found at high power and low subcooling conditions when $K_{in}=340$ which onset defines the low subcooling stability boundary (LS-SB). A further characterization of the instabilities reveals two different behaviors: intermittent and sinusoidal oscillations which are described in section 5.3.3.

To compare the stability boundaries of the different configurations, the experiments are plot in terms of the intrinsic variables of the system. Such a comparison is given in Figure 5-3.

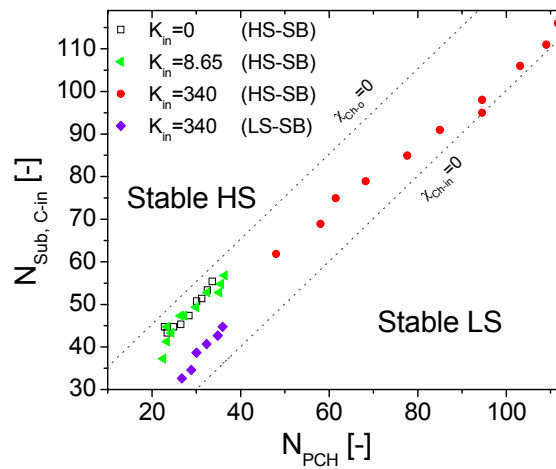


Figure 5-3: High subcooling (HS) and low subcooling (LS) stability boundaries found when $K_{in}=0$, $K_{in}=8.65$ and $K_{in}=340$. The dotted lines show the location where the quality reaches the zero value at the chimney inlet and outlet.

The figure shows that by increasing the inlet restriction, the location of the high subcooling SB significantly deviates from the chimney outlet zero quality line ($\chi_{Ch-o}=0$). The fact that the onset of instabilities does not coincide with such a line agrees with the visual observations of some bubbles present in the chimney prior to the onset of instabilities. For the case with $K_{in}=340$ the points defining the high subcooling SB are found at lower N_{PCH} values which correspond to higher mass flow rates.

5.3.2 Dynamical characterization of the instabilities

In order to clarify the origin of the instabilities the period of experimental oscillations are compared with typical periods of DWO in this section. The fluid transit time in the channel is estimated as

$$\tau_{Channel} = \frac{V_{Ch} + \frac{1}{2}V_{heated}}{Q}, \quad (5-2)$$

where Q is the time averaged coolant volumetric flow rate, V_{Ch} the volume of the chimney section and V_{heated} the total volume of the core section. The factor $\frac{1}{2}$ before V_{heated} appears since a perturbation of the inlet flow rate produces a

perturbation of the enthalpy at the core outlet with an average phase lag corresponding to half of the transit time from the inlet to the outlet of this section². Since the transit time is a time-dependent variable in case of flow oscillations, it is evaluated on the basis of the mean flow rate.

Oscillatory cases obtained by applying 2 kW per rod and $K_{in}=8.65$ have been selected for this investigation. The relation between the oscillation period and the transit time for such experimental cases is shown in Figure 5.4.

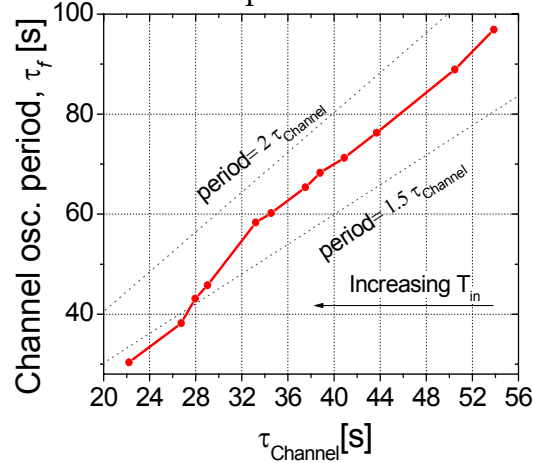


Figure 5-4: Period of the oscillations vs. characteristic channel transit time.

The oscillation period from the experiments agrees well with the estimated one from DWOs (being between one-and-a-half to two times the coolant transit time through the channel) indicating the density wave character of the flashing-induced oscillations. For small oscillation periods, which correspond to low subcooling values, the period slightly deviates from these limits. In order to understand this, a more detailed characterization of the experiments is needed. Such a study is presented in the following section.

5.3.3 From single-phase to stable two-phase flow

It is known that by increasing the inlet temperature (while maintaining the power constant) four different types of behavior are observed^{2,6}: (a) stable flow at high subcooling, (b) unstable *intermittent* two-phase flow, (c) unstable *sinusoidal* two-phase flow and (d) stable flow at low subcooling. To clarify these behaviors, four experiments corresponding to $K_{in}=340$, a power of 2 kW per rod and different inlet subcooling are further investigated.

To characterize the facility at any position and time, the temporal evolution of the axial temperature profile in the channel together with the pressure and void fraction axial profiles in the chimney are included in special plots developed for that purpose. In these plots the color scale represents the value of the corresponding variable while the horizontal and vertical axes refer to the time and the axial position respectively. The temperature profile is obtained from the eight different places where the

temperature is measured (see Figure 5-1). The void fraction evolution is reconstructed from the six void sensors placed in the chimney. The local pressure at locations where flashing occurs is difficult to measure since flashing is a fast process which occurs in an explosive manner. Due to this, this pressure is estimated by using the thermocouples and the void detectors placed at the same axial location. The estimation is as follows. If vapor is not detected, the pressure is found from the weight of the water column above that location. If vapor is identified, the pressure is estimated by assuming a thermal equilibrium between steam and water and by using the saturation line from the water equation of state with the temperature as input. A small scheme of CIRCUS is included to clarify the axial positions in the plots.

Time traces of the core inlet coolant flow are plotted together with the power spectral decomposition (PSD) and the wavelet decomposition⁷ (done with the Coiflet package) which allow displaying different scale-pseudo-frequency components of the signal at any time.

5.3.3.a High subcooling stable flow circulation

Figure 5-5 shows a case with high subcooling stable flow circulation which is found at $T_{in} < 68^\circ\text{C}$. Single phase buoyancy plays a major role here.

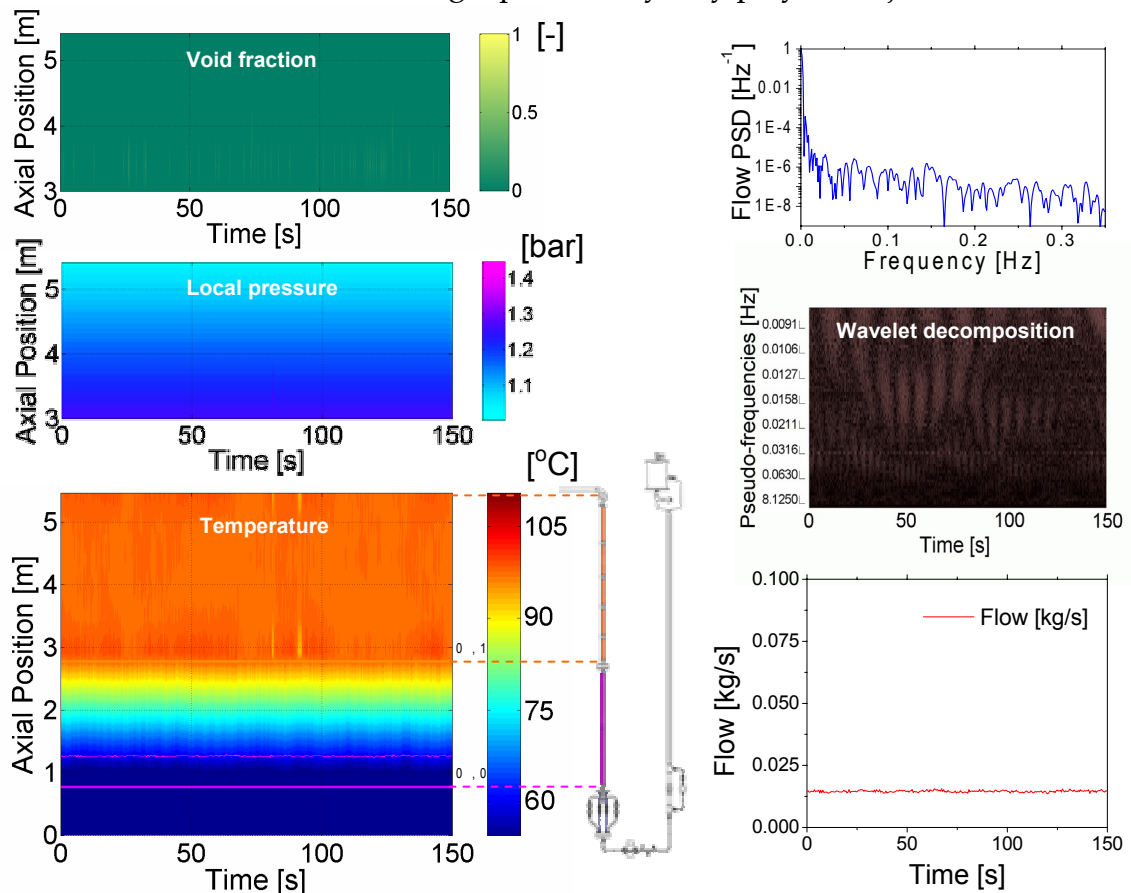


Figure 5-5: Stable high subcooling flow circulation. Very low vapor values and a constant axial temperature profile in the chimney characterize this case. The flow signal is roughly constant only exhibiting some noise.

The figure presents the axial temperature evolution and the void and pressure plots for a case measured with an inlet temperature of 56°C.

Cold water enters the channel and is heated in the core section. The coolant then travels through the chimney section with no significant heat losses. The axial pressure plot shows a linear profile in the chimney given by the linear relation between the hydrostatic pressure and the height of the water column. In some cases located close to the high subcooling SB, vapor bubbles were identified in the chimney. For this reason in this work this case is not denoted as *stable one phase behavior*, as some authors proposed².

The temperature profile and the flow remain unchanged in time, only exhibiting small fluctuations which can be attributed to statistical fluctuations and turbulence. This is in accordance with the PSD plot and the wavelet decomposition of the flow signal, since no natural frequency is seen. In this particular case, no vapor is detected in the chimney (see void fraction plot).

5.3.3.b Intermittent oscillations

By reducing the coolant inlet subcooling the high subcooling stability boundary is crossed. Intermittent oscillations are found for the cases in which $68^{\circ}\text{C} < T_{\text{in}} < 83^{\circ}\text{C}$. Figure 5-6 shows the case with an inlet temperature of 77°C.

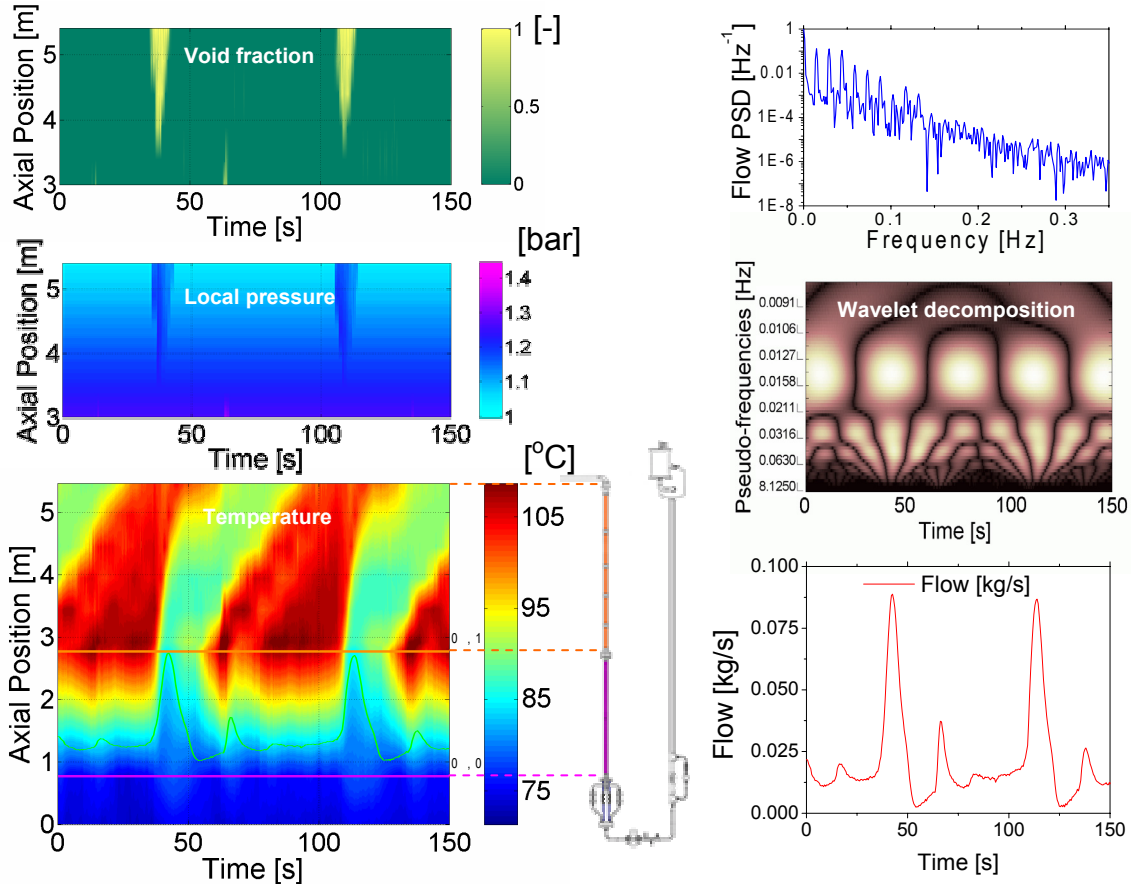


Figure 5-6: Unstable *intermittent* oscillations. This case is characterized by periodical oscillations occurring after a certain incubation time. The PSD and the wavelet decomposition plots show clear frequencies.

In order to clarify the details of the dynamic process shown in the plots, let us focus on what happens at ~ 30 s. The coolant is heated in the core, driving the flow upwards due to single phase natural circulation (no vapor is identified in the chimney). At a certain point flashing occurs in the chimney since the saturation temperature is reached by the hot coolant. As vapor is created rapidly, the local pressure inside the steam bubbles initially increases. This effect causes a thermal non-equilibrium between liquid and vapor phase which can be very pronounced when flashing is not yet developed. The same effect is reported in a previous work performed by Manera². Such a thermal non-equilibrium in the flashing bulk is reflected in the pressure plots as high pressure spots located at the onset of the flashing events. The magnitude of the temperature difference between liquid and vapor decreases during the development of steam production until thermal-equilibrium is reached. The high pressure spots decrease accordingly.

The vapor created by flashing enhances the flow circulation, allowing the vapor to expand and the effect of vapor compression is thus diminished. Due to the flow increase, the coolant passes the heated section faster and therefore is heated less. This liquid bulk is not hot enough to vaporize in the chimney and flashing thus stops. As result of this, the driving mechanism is again single-phase buoyancy and the flow circulation decreases. This flow decrease causes the coolant to stay longer in the heated section and consequently the temperature at the chimney inlet starts to increase. Some vapor is consequently created by boiling at regions close to the core exit, causing a small second flow increase which disappears soon after entering the chimney. The hot front originated in the heated section travels upwards and, when the superheated coolant reaches the chimney outlet, the cycle starts again. Since from one flashing event to the next one a certain time is needed (the so-called incubation time) this behavior is denoted intermittent flashing.

The PSD and the wavelet decomposition plots show numerous frequencies after the main frequency indicating the presence of higher modes.

5.3.3.c Sinusoidal oscillations

The unstable case with sinusoidal oscillations is found for $83^{\circ}\text{C} < T_{\text{in}} < 97^{\circ}\text{C}$. The results of the measurements performed with an inlet temperature of 87°C are depicted in Figure 5-7.

In contrast to the intermittent oscillations case, in the sinusoidal oscillation case, during the flashing event vapor appears in the core section first. The coolant flow shows a regular behavior with a nonexistent incubation time (see the PSD and the wavelet decomposition of the flow signal).

The pressure plot shows that at the onset of a flashing event, an increase in the local pressure exists. This means the (saturated) temperature of the

flashing bulk corresponds to pressures higher than the hydrostatic pressure prior the onset of flashing. In contrast, for the tail of the flashing bulk, the local pressure is close to the single-phase hydrostatic pressure since the water-vapor mixture reaches thermal equilibrium.

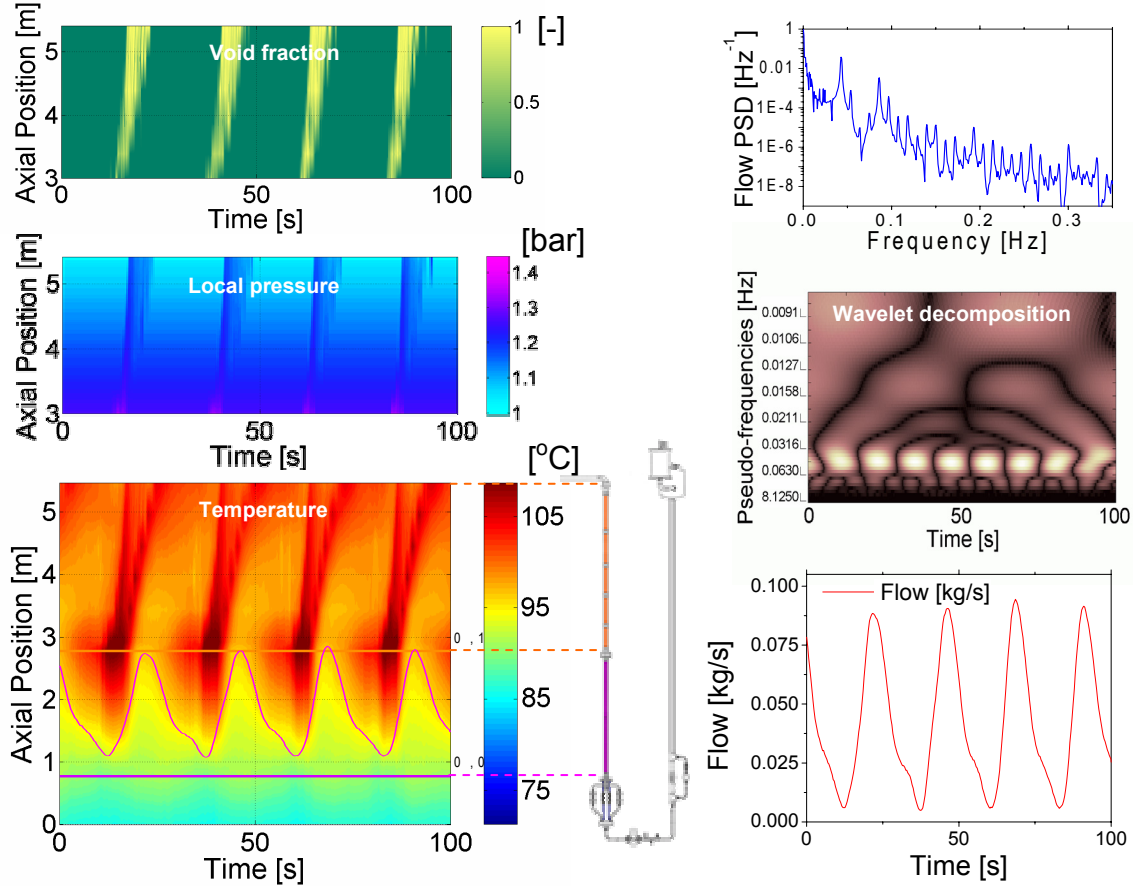


Figure 5-7: Sinusoidal oscillations case. This behavior is characterized by regular oscillations with a practically non-existent incubation time. The flashing/boiling front starts inside the heated section.

Unlike in the intermittent oscillations case, the combination of small inlet subcooling and power allows creating superheated coolant in the heated (section since the buoyancy mechanism is not efficient enough to transport the hot coolant through the chimney). Consequently it is seen that just before the steam is produced in the core, the temperature profile shows a clear hot spot. It is expected that the existing negative temperature gradient may diminish the vapor creation. An extreme example of this effect is the geysering phenomenon which can lead to sustainable oscillations. Since the geysering mechanism[†] is characterized by a much shorter oscillation period than that of DWOs, having such temperature profile prior to the flashing event would tend to reduce the oscillation period. This agrees with the shorter oscillation periods found for the cases with low subcooling values shown in Figure 5-4.

[†] Originally defined for stagnant flow, i.e. with zero flow circulation.

5.3.3.d Low subcooling stable flow circulation

By increasing the coolant temperature at the core inlet even further, the low subcooling stable case is found when $97^{\circ}\text{C} < T_{\text{in}}$. Figure 5-8 shows the case corresponding to a coolant inlet temperature of 98.5°C .

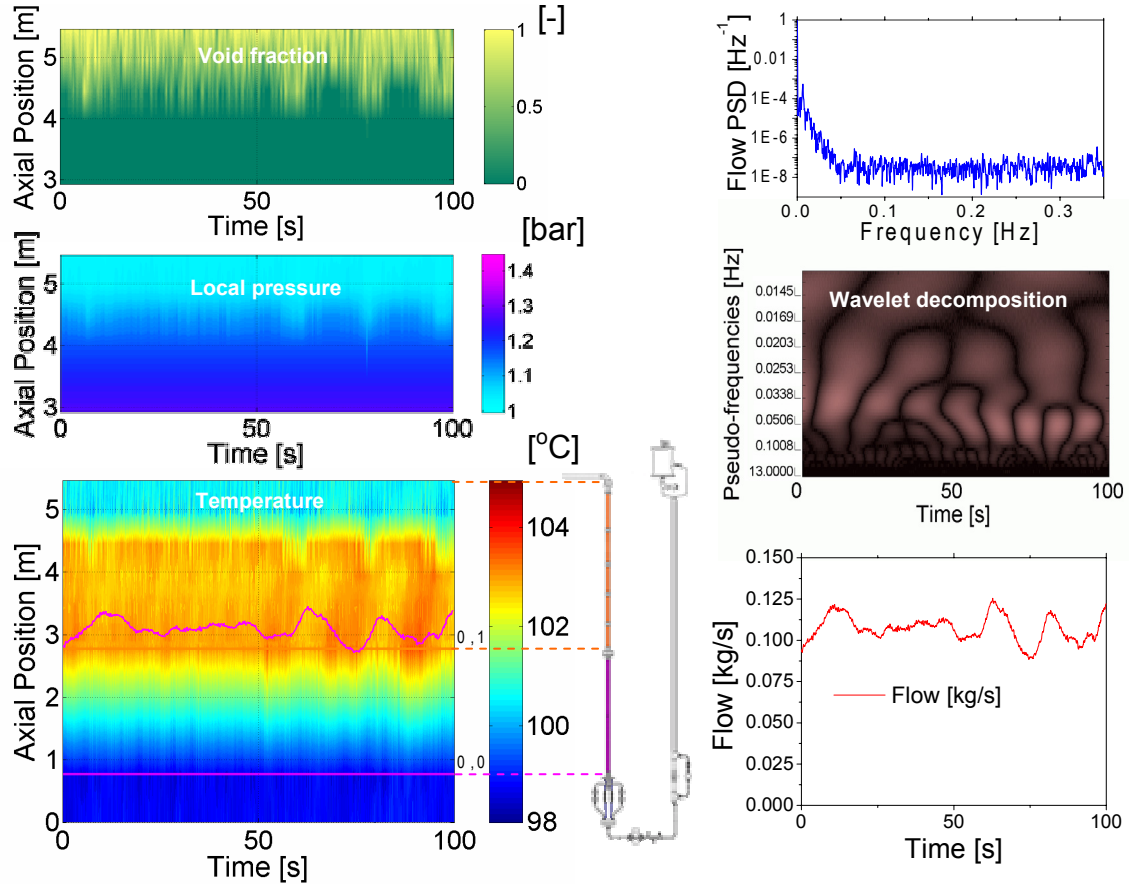


Figure 5-8: Stable two-phase case. This behavior is characterized by stable two-phase buoyancy driven flow. The flashing zone is characterized by a decrease in both hydrostatic pressure and temperature.

In this case, coolant in a two-phase state is permanently present in the chimney. The temperature profile is characterized by a sudden temperature decrease in the flashing region (see the temperature plot). This decrease is due to the strong decrease in the hydrostatic pressure induced by the smaller two-phase mixture density compared to that from the liquid. Unlike the unstable cases, in this case no dynamics effects are introduced by the vapor production and, therefore, the flow inertia does not play any role. Consequently, the pressure profile in the flashing zone can be well estimated by the hydrostatic pressure profile. Note that the pressure at the chimney bottom is also slightly smaller than that from the previous cases.

The PSD and the wavelet plots show no natural frequency in this case.

5.3.4 Analysis of the dynamics of the flashing front

In this section, the dynamics of the flashing front for the two oscillatory cases is further investigated. The signals from the non-intrusive, high frequency, capacitance-based void detectors are used for this purpose.

The cases used in this section correspond to the experiments reported in Figure 5-6 and Figure 5-7. The time traces of the signals from the void fraction sensors placed in the chimney are shown in Figure 5-9. To facilitate the comprehension, the sensor positions are numbered from bottom to top, being the lowest one number “1” and the top one number “6”.

Figure 5-9a) shows that in the case of intermittent oscillations the flashing front starts at the top of the chimney, at positions 6 and 5. The flashing front then reaches the lower regions in the chimney, at positions 4 and 3. This evolution is explained by the fact the liquid is hotter downstream (see the temperature profile prior to the onset of flashing from Figure 5-6) and therefore flashing is likely to occur at higher positions where the hydrostatic pressure is lower. The flashing front then travels upwards leaving the chimney.

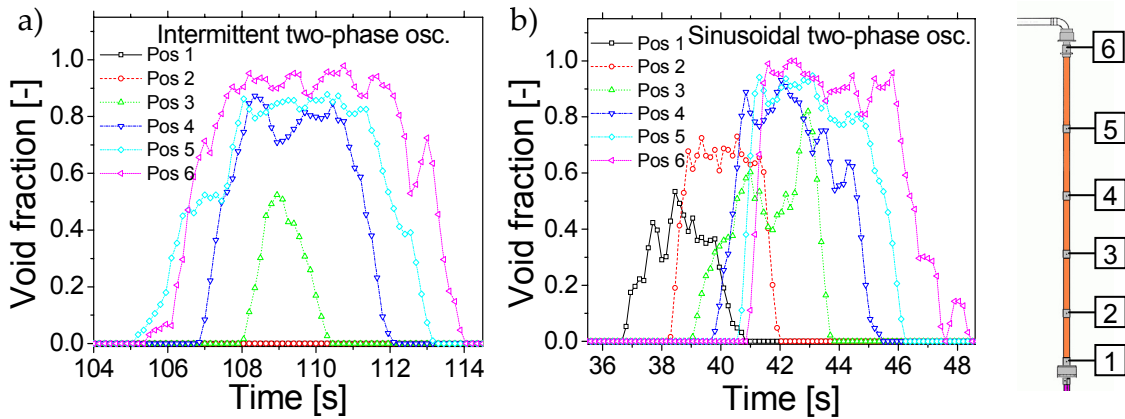


Figure 5-9: a) Time evolution of the flashing front for the intermittent oscillations and b) Flashing front time evolution for the sinusoidal oscillatory case.

The flashing front evolution for the sinusoidal two-phase oscillatory case is presented in Figure 5-9b). As can be observed, in this case vapor appears at the lowest void sensor location first and then travels upwards along the chimney. It is to be expected that the area below the different vapor curves increases when moving to higher positions in the chimney. Sensors 2 and 3, however, have similar areas, indicating that the amount of vapor detected by these sensors was the same. This result confirms the existence of condensation effects induced by the negative axial temperature gradient which tends to inhibit the creation of vapor by means of flashing.

5.3.5 Analysis of the inertia of the loop

During the oscillations the buoyancy in the system is mainly due to the two-phase driving force which, per unit of area, is defined as follows

$$F_{driv}^* = (\rho_l - \rho_v) \alpha L g, \quad (5-3)$$

where α is the mean void fraction (obtained by integrating in space the temporal evolution of the axial void fraction in the channel) and L the channel length. The use of fast response void fraction and pressure drop sensors assure that no dynamic effects are introduced by the measurement system (besides some delay which may be introduced by the void transport).

The system response due to a change in the driving force can be accounted by the kinetic energy per unit of volume, which is defined as expressed by Equation (5-4).

$$E_{kin}^* = \rho_l v_{in}^2 / 2. \quad (5-4)$$

where v_{in} is the coolant velocity at the core inlet.

Figure 5-10 illustrates the response of the kinetic energy to changes in the two-phase driving force, for intermittent oscillations measured with $K_{in}=8.65$ an inlet temperature of 88°C and a power input of 2 kW per rod.

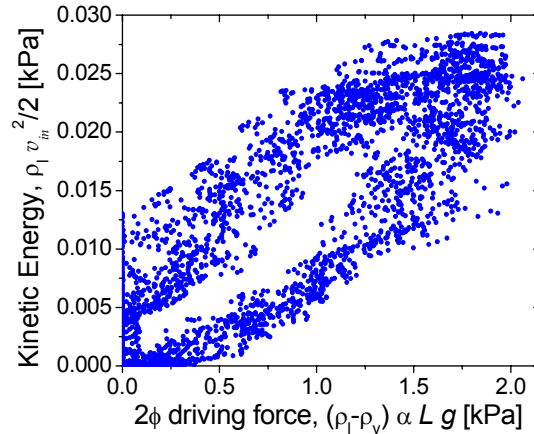


Figure 5-10: Relation between the driving force and the kinetic energy.

The figure clearly shows that no linear relation exists between the two plotted quantities. To clarify this issue, the cross correlation of the mean void fraction and the coolant velocity is calculated and plotted in Figure 5-11.

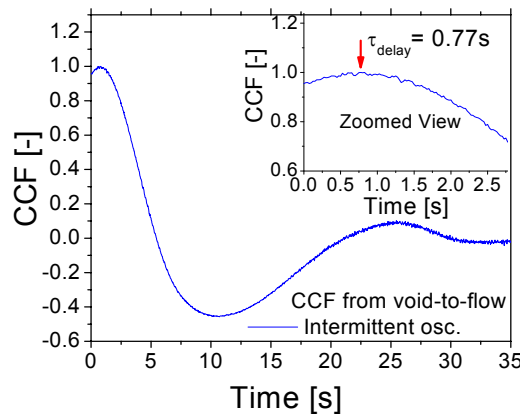


Figure 5-11: Cross correlation between the void fraction and resulting flow response.

A clear time delay of ~0.77 s exists between these two signals, which also has been mentioned by Manera².

The time constant of the transfer function from void-fraction fluctuations to flow rate can be estimated from a first-order transfer function derived from a model based on the linearized version of the momentum balance (see e.g. section 2.2.3) in which two driving mechanisms are considered: the single-phase and the two-phase natural circulation.

$$\tau = \frac{M_0 \sum_i \frac{l_i}{A_i}}{2L g \left[< \alpha >_{Ch} (\rho_{l,Ch} - \rho_v) + (\rho_{l,DC} - \rho_{l,Ch}) \right]}. \quad (5-5)$$

A time constant of $\tau_{\text{model}}=0.91$ s is found from the model, which is in the same range as the time delay from the cross correlation ($\tau_{\text{delay}}=0.77$ s). The inertia term $\Sigma l_i/A_i$ is particularly important in natural circulation systems and therefore has to be taken into account. In other words, the flow cannot be considered to instantaneously adjust itself to changes in driving force and friction.

It can be concluded that the delay between the two-phase driving force and the kinetic energy is caused by a combination of two effects: the inertial effects of the fluid plus some delay which may be introduced by the void determination system.

5.4 A lumped parameter model

A numerical model is developed to investigate the influence of the friction distribution on the mechanism of flashing-induced instabilities. The model describes the heated section and the chimney with three regions: one representing the whole heated section and the other two the single-phase and the two-phase part of the flashing chimney (see Figure 5-12).

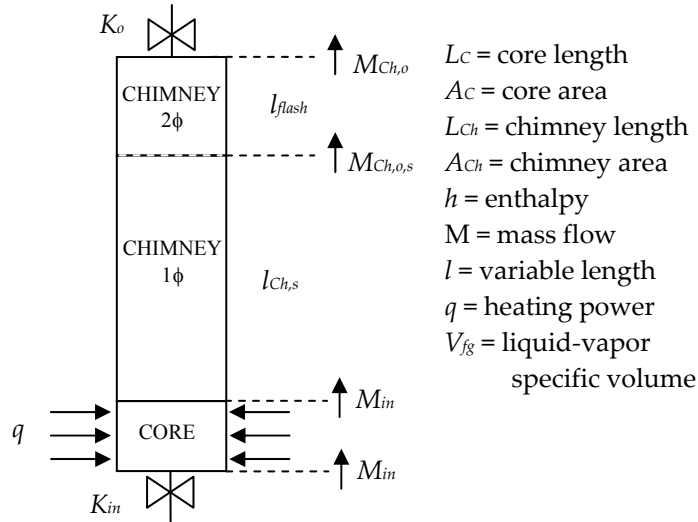


Figure 5.12: Schema of the modeled flashing channel which consists of 3 regions: the core, the single phase part of the chimney and the two-phase part of the chimney.

Two local restrictions are considered: one at the core inlet and another at the chimney outlet. The following is considered in the model:

- The homogeneous equilibrium model is assumed.
- Natural circulation drives the flow.
- Subcooled boiling is neglected.
- The heat flux is constant and axially uniform.
- The inlet subcooling is constant.
- The friction losses are concentrated at the channel inlet and outlet.
- The Boussinesq approximation is valid.

The following balance equations are used to describe each of the regions.

Core region

$$A_c \rho_l L_c \frac{d(h_c)}{dt} = M_{in} (h_{c,in} - h_{c,o}) + q \quad (5-6)$$

Chimney single-phase region

$$A_{ch} \rho_l \frac{d(l_{ch,1\phi})}{dt} = M_{c,in} - M_{ch,1\phi,o} \quad (5-7)$$

$$A_{ch} \rho_l \frac{d(l_{ch,1\phi} h_{ch,1\phi})}{dt} = M_{in} h_{c,o} - M_{ch,1\phi,o} h_{ch,1\phi} \quad (5-8)$$

Chimney flashing region

$$A_{ch} \frac{d(\rho_{2\phi} l_{2\phi})}{dt} = M_{ch,1\phi,o} - M_{ch,2\phi,o} \quad (5-9)$$

$$A_{ch} \frac{d(\rho_{2\phi} l_{2\phi} h_{2\phi})}{dt} = M_{ch,1\phi,o} h_{ch,1\phi} - M_{ch,2\phi,o} h_{2\phi} \quad (5-10)$$

The inertia terms in the momentum equation are neglected. A quasi-static balance of forces in the momentum equation is used thus the gravitational pressure head is balanced by the drag forces,

$$(K_{in} - 1) \frac{M_{in}^2}{\rho_l} + (1 + K_o) \frac{M_{ch,2\phi,o}^2}{\rho_{2\phi}} = A_c^2 g [\rho_l (L_c + L_{ch}) - L_c \rho_{l,1\phi} - l_{ch,1\phi} \rho_{l,1\phi} - l_{ch,2\phi} \rho_{2\phi}] \quad (5-11)$$

where the friction coefficients are defined as $K = \rho A c^2 \Delta P / M^2$. Note that the core area is used for both friction coefficients.

The following constitutive relation is used to close the model

$$\rho_{2\phi} = \left[\frac{1}{\rho_l} + \frac{V}{h_{fg}} (h - h_{sat}) \right]^{-1} \quad (5-12)$$

The resulting equations are non-dimensionalized and linearized around the steady state point. The solutions are represented by the next general form,

$$X = X_0 e^{(\lambda t)} \quad (5-13)$$

After some algebraic manipulation a third order eigenvalue problem is obtained, which can be represented as

$$(\lambda I - D)X = 0, \quad (5-14)$$

where I is the identity matrix and the chosen state variables are the non-dimensional variation of the core exit enthalpy, $\delta \hat{h}_o$; the non-dimensional variation of the enthalpy in the chimney being at single phase, $\delta \hat{h}_{Ch,s}$; and the non-dimensional length of the chimney being at single phase, $\delta \hat{l}_{Ch,s}$

$$X = \begin{pmatrix} \delta \hat{h}_o \\ \delta \hat{h}_{Ch,s} \\ \delta \hat{l}_{Ch,s} \end{pmatrix}. \quad (5-15)$$

The matrix D and details of the model can be found in APPENDIX E.

The stability is investigated by studying the roots of the characteristic polynomial. The model and the stability conditions are implemented in the Matlab environment. Special attention has been paid to implement an accurate estimation of the thermo-physical properties of water and steam. For that reason the XSteam computer program⁸ is used in the model.

From the non-dimensionalization of the balance Equations (5-6) to (5-10), it is found that the friction effects are approximately controlled by a single factor⁹, the so-called non-dimensional friction factor, which is defined as

$$\Upsilon = \frac{K_{in}^* + K_o^*}{1 + K_o^*}, \quad (5-16)$$

where K_{in}^* and K_o^* are the local friction factors defined in terms of the cross sectional area of the core. This result implies that two systems with the same value of the non-dimensional friction factor would have the same stability boundary in the non-dimensional plane.

5.5 Experimental results vs. numerical results

In the following section, simulations performed with the numerical model are compared with the experiments shown in section 5.3. Such a comparison for the cases with $K_{in}=0$ and $K_{in}=8.65$ is shown in Figure 5-13.

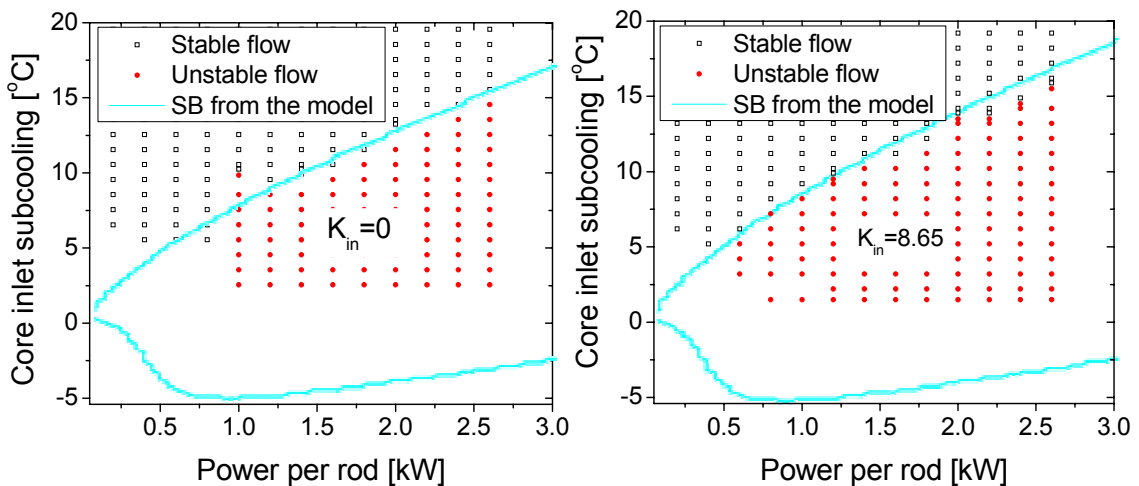


Figure 5-13: Experimentally and numerically obtained stability maps for the configurations with $K_{in}=0$ and $K_{in}=8.65$.

As can be seen, a very good agreement is found between the experiments and the numerical simulations for the location of the high subcooling SB. This result is surprisingly good considering the simplicity of the model. Regarding the low subcooling SB, no comparison can be made, since as predicted by the model, this boundary is located at negative subcooling values, which is far from the CIRCUS operational range.

The model is also applied to the case with $K_{in}=340$. From the resulting comparison shown in Figure 5-14, it is clear that the model can predict both the high subcooling and the low subcooling SBs well.

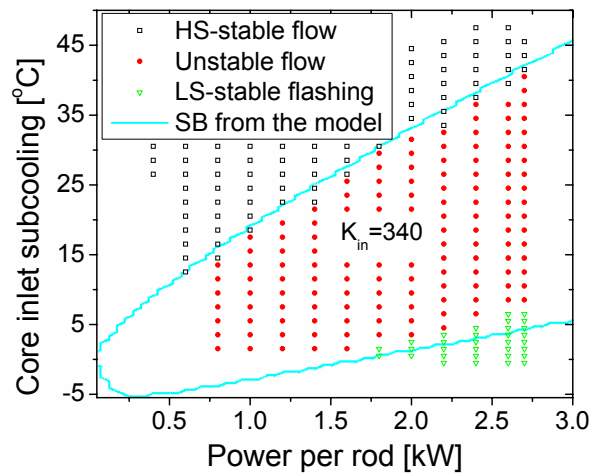


Figure 5-14: Experimental and numerical results when $K_{in}=340$.

The good prediction capabilities of the model indicate that the phenomena which are not modeled (e.g. subcooled boiling, condensation effects, etc.) play a secondary role in determining the stability of the system.

5.6 A numerical parametric study

Since the model demonstrated to be capable of predicting the stability regarding flashing-induced instabilities, it can also be used to perform a parametric study. In the following, the effect of the friction distribution on the flashing-induced instabilities is numerically investigated. For a given configuration, numerous cases are simulated with which the roots of the characteristic polynomial determining the stability of the system are calculated. The unstable cases are shown in the non-dimensional plane. Hence, the area above these points indicate stable flow, whereas the area below represents stable flashing, i.e. the high subcooling SB and the low subcooling SB. All the friction factors are defined in terms of the core area. The CIRCUS configuration is used in this investigation.

The result of varying the inlet friction factor K_{in} is shown in Figure 5-15. As observed in the experiments, also in the simulations the high subcooling SB does not coincide with the chimney outlet zero quality line, χ_{Ch-o} . This

result may have important implications. Since vapor can be created when the reactor is still in a stable condition, pressure can be built up in the reactor without encountering instabilities. By increasing the system pressure, the flashing number reduces and therefore flashing-induced oscillations are less likely to occur.

By increasing the inlet friction coefficient the system becomes more unstable since the unstable area considerably enlarges. For the case with $K_{in}^*=805$ and low subcooling number values, the low subcooling SB crosses the zero quality line regarding the chimney inlet, χ_{Ch-in} . The points located below this line, represent cases in which the core was also in a two-phase situation which is beyond the model assumptions.

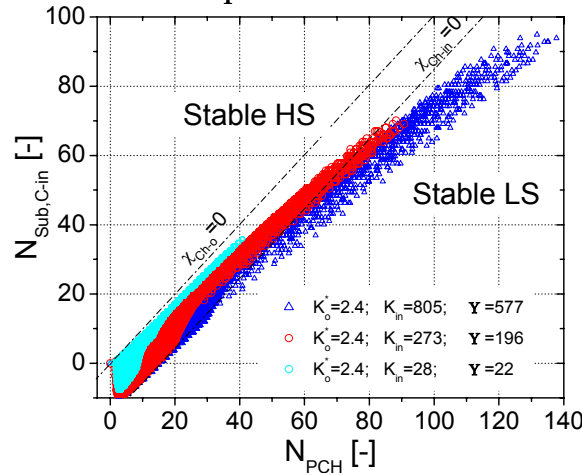


Figure 5-15: Comparison of the resulting unstable cases in the non-dimensional N_{PCH} - N_{Sub} plane, numerically obtained for different inlet friction coefficients.

The effect of having a different friction distribution while maintaining the same total friction is also studied. The results are shown in Figure 5-16 a).

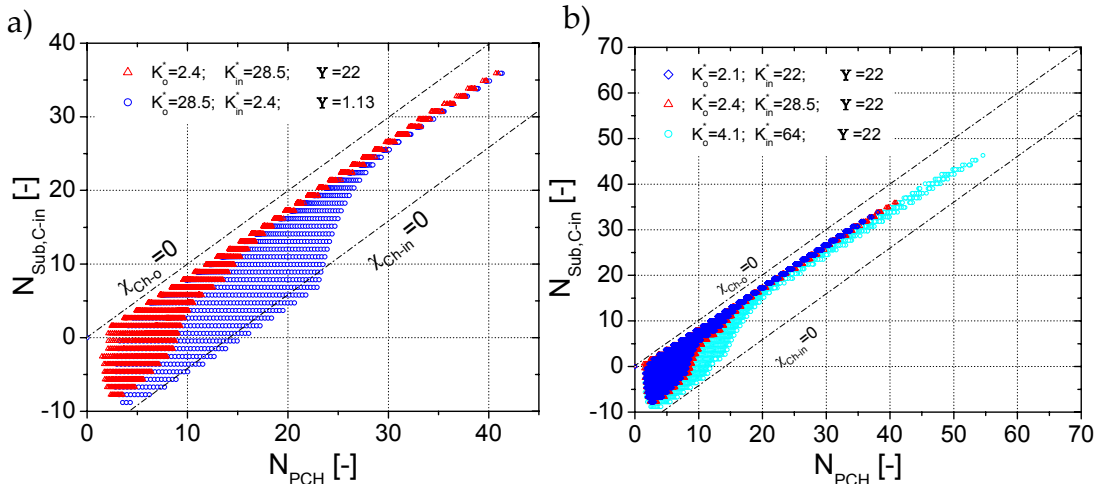


Figure 5-16: a) Effect of the friction distribution in the resulting stability and b) Unstable cases obtained for different friction coefficients representing the same non-dimensional friction factor.

From the figure it is clear that when the friction is concentrated at the chimney outlet, the unstable region enlarges. The results indicate that while

the high subcooling SB remains practically unchanged, the position of the low subcooling SB is largely affected. This finding means that the large chimney outlet restriction practically does not affect the ESBWR¹⁰ stability at high subcooling values. On the other hand, the simulations indicate that the large friction coefficient associated to the swirlers in the ESBWR may degrade the stability of the reactor regarding flashing-induced instabilities at low subcooling values.

Different combinations of inlet and exit restriction values, corresponding to the same value of the non-dimensional friction factor Υ , are also simulated with the model. The results are presented in Figure 5-16 b).

In this case, the points defining the three unstable regions are roughly grouped in the same area. This finding agrees well with the expected behavior since the same value for Υ was used in all the experiments which (as a first approximation) determines the stability of the system.

5.7 Conclusions

The effect on the stability performance of natural circulation BWRs regarding flashing-induced instabilities, when placing a large restriction at the chimney outlet, has motivated this investigation. In order to validate a numerical model specially developed for such a study, detailed experiments have been performed with the help of the CIRCUS facility in the single channel configuration. A novel representation of the results allowed a thorough understanding of the flashing mechanism. As result of this investigation, the following is concluded.

The four different behaviors reported by previous authors are seen in the experiments: stable flow at high subcooling; intermittent flow oscillations; sinusoidal flow oscillations and stable flow at low subcooling.

A thermal unbalance has been detected in the flashing bulk in the onset of the flashing event occurring during the instabilities.

The flashing front develops from the chimney top to bottom during intermittent oscillations and from bottom to top in the sinusoidal oscillations.

Despite the simplifications done in the modeling, a good agreement is found between the experiments and the numerical simulations.

Both the experiments and the numerical results show that a two-phase stable region exists at high subcooling values prior to the instabilities. This region may help to build up the pressure in the reactor vessel which in turn would reduce the effects of flashing as a mechanism for instabilities. The drawback of a possible start-up procedure based on this effect is the long time needed to build up the aforementioned pressure since, for reactor conditions,

this two-phase stable region is very narrow and the vapor production may be small.

When increasing the inlet friction, the numerical model predicts a more stable system at high subcooling values while it predicts a reduction of the stability performance at low subcooling values.

The model predicts a destabilizing effect in the system at low subcooling values when concentrating the channel friction at the chimney outlet. No changes are observed in the stability at high subcooling values for such a configuration.

As a first approximation, the stability effect of the friction distribution seems to be controlled by the non-dimensional friction factor defined by Equation (5-16).

5.8 References

- ¹ Shiralkar, B.S., Personal communication, (2005).
- ² Manera, A; Rohde, U; Prasser H.-M. and T.H.J.J. van der Hagen; Modeling of flashing-induced instabilities in the start-up phase of natural-circulation BWRs using the two-phase flow code FLOCAL. *Nuclear Eng. and Des.* 235 (14): 1517-1535 (2005).
- ³ De Kruijf, W., Manera, A., de Haas, D.W., Schut, J.G.F., Van der Hagen, T.H.J.J., Mudde, R.F. and Prasser, H-M, Description of CIRCUS Including Test Matrix, EC, 5th Euratom Framework Program 1998-2002, EVOL-NACUSP-D8a, (2001).
- ⁴ Van der Hagen, T.H.J.J., Van Bragt, D.D.B., Van der Kaa, F.J., Karuza, J., Killian, D. Nissen, W.H.M., Stekelenburg, A.J.C. and Wouters, J.A.A. *Ann. Nucl. Energy*, Vol. 24, No. 8, 659-69, (1997).
- ⁵ Van Bragt D.D.B., Van der Hagen, T.H.J.J. Stability of Natural Circulation Boiling Water Reactors: Part I- Description Stability Model and Theoretical Analysis in Terms of Dimensional Groups. *Nuc. Tech.* 121:40-51 (1998)
- ⁶ Furuya, M., Inada, F. and Van der Hagen, T.H.J.J. Flashing Induced Density Wave Oscillations in a Natural Circulation Loop with a Chimney – Mechanism of Instability and Stability Map. *Nuclear Eng. Des.* 235(15): 1557-1569 (2004).
- ⁷ Daubechies, I., Ten Lectures on Wavelets, Soc. for Ind. and App. Math, (1992).
- ⁸ Holmgren, M; www.x-eng.com, XSTEAM for Matlab (2006)
- ⁹ Guido, G., Converti, J. and Clausse, A., Density-wave oscillations in parallel channels - an analytical approach, *Nuclear Engineering and Design*, 125, 121-136, (1991).
- ¹⁰ Cheng, H.S., Khan, H.J. and Rohatgi, U.S., Simulation of SBWR Startup Transient and Stability, BNL-65535, (1998).

Chapter 6

Flashing-induced oscillations in parallel channels

6.1 Introduction

In natural circulation BWRs the chimney section is usually divided into subchannels to avoid cross flow and to better divide the coolant flowing through the core. Flashing-induced instabilities occurring in parallel channels may occur during the start-up phase of a natural circulation BWR equipped with such adiabatic sections. Such instabilities may be different than the more common flashing-induced oscillations occurring when only one chimney is present, i.e. as those discussed in Chapter 5. Experimental investigations on this field are still very limited. Aritomi *et al.* studied the low pressure stability of parallel channels with a chimney^{1,2} but in their experiments, the chimneys were too short compared to those from modern natural circulation BWRs, and therefore flashing played a secondary role. For this reason, experimental investigations are needed in order to clarify this issue which is important to assure a safe start-up process of novel natural circulation BWRs.

In this chapter, flashing-induced instabilities in parallel channels relevant for the start-up of natural circulation BWRs are experimentally investigated in the CIRCUS facility. The physical mechanisms behind flashing-induced instabilities are discussed in depth, thereby focusing on the coupling between the channels. The large number of experiments performed in this work allowed constructing stability maps. Characteristics such as the temperature profile in the chimneys during the oscillations, the partial flow for each channel and the axial void fraction profile are discussed in detail thanks to the novel way of displaying the results introduced in Chapter 5. These experimental investigations demonstrated the existence of operating conditions of the test facility with parallel channels, where the prediction of the dynamics of the system seemed to be difficult. More precisely, it is observed that the oscillations behaved a-periodical³.

It is well known that the dynamics of two-phase flows is governed by several nonlinear phenomena^{4,5,6}. A good characterization of the physics behind the experiments is important since this usually determines the degree of sophistication needed in the modeling and also the numerical algorithms to be used. Selected experimental cases are measured for this purpose, resulting in long experimental data series allowing studying the possible presence of non-linear effects. Focus is placed on the cases exhibiting a-periodical behavior in order to determine whether they are chaotic and if they exhibit a fractal structure. For such an investigation a multi-fractal formalism is applied to the experiments. As a result of that study it is found that the a-periodical oscillations have a multi-fractal structure in the dynamics which revealed the presence of deterministic chaos in the experiments.

6.2 Description of the CIRCUS facility with two chimneys

The single chimney CIRCUS facility⁷ used for the measurements described in Chapter 5 is modified in order to place two chimneys on top of the core section. Figure 6-1 shows a schematic view of the CIRCUS facility with a two-parallel channels configuration.

Two parallel chimneys are installed above the four electrically heated channels representing the core, from which two of these are connected to each chimney. *Channel 1* represents the set of heated channels number 1 and 2 together with Chimney 1; *Channel 2* represents the set of heated channels 3 and 4 together with Chimney 2. In this configuration, the CIRCUS facility is equipped with 16 void sensors for measuring the axial void-fraction profile in the chimneys. Moreover, 30 thermocouples allow measuring the temperature in the loop. Reverse flow (counter-current flow) may occur in the channels during very strong oscillations. Special high sensitive dp-sensors capable of

measuring both negative and positive pressure drops are therefore installed at the inlet of each heated channel and core bypass channels where the coolant is always in liquid phase for all conditions.

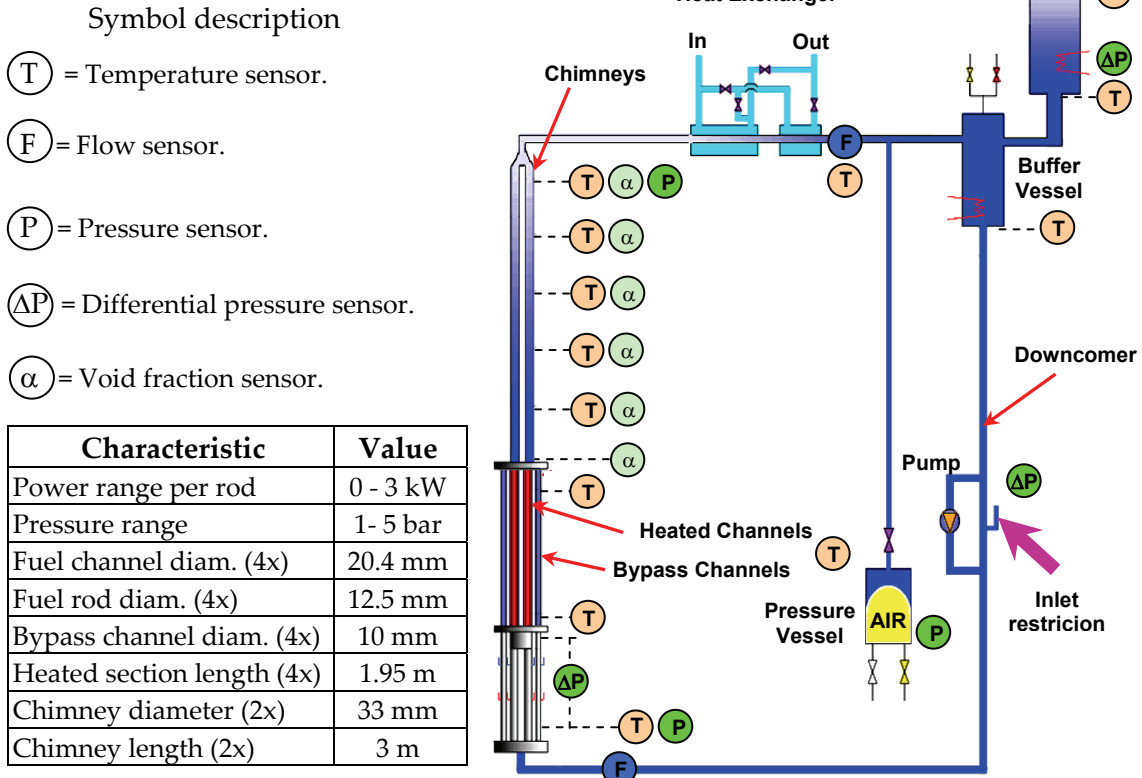


Figure 6-1: Schema of the CIRCUS facility with two parallel channels (not to scale).

6.3 Experimental results

During the experiments the power applied in the heating rods is fixed and the inlet temperature is varied by changing the electrical power applied in the buffer vessel (see Figure 6-1). By repeating this procedure with different powers, the full operational map can be covered. In addition, all the experiments are carried out without external pressurization to avoid any influence of the pressure-drop oscillation mechanism⁸ in the system. Therefore, the steam dome is open to the surroundings. The operational conditions used in this study are summarized in Table 6-1.

Magnitude	Value
Power per rod	0-3 kW
Inlet Temperature	70-99 °C
Pressure	1 bar
Flow circulation	Natural
Core-bypass channels	Closed
Number of chimneys	2

Table 6-1: Experimental conditions corresponding to the measurements performed in the CIRCUS facility with parallel channels presented in this chapter.

The pump is not used in the experiments, thus the only driving force is buoyancy. Moreover, the core-bypass channels are kept closed and the same power is applied to each heating rod. In addition, the same inlet restriction is used in all experiments. The friction coefficient is found as indicated in Chapter 5. The inlet temperature is varied from low values (which lead to single phase natural circulation) to higher values where a two-phase flow is found, limited only by the maximum temperature achievable at the channel inlet. The inlet subcooling is measured in terms of the saturation temperature at 1 bar, i.e. 100°C.

6.3.1 The stability behavior

In the out-of-phase oscillation mode, the primary flow remains constant, i.e. the total pressure drop in the parallel channels remains the same. Such oscillatory behavior, however, is never observed in our experiments. As soon as the system loses stability, the primary flow exhibited oscillations.

Figure 6-2 shows the stability map found when $K_{in}=8.65$ is set. The stability map is divided into four regions, each one characterizing a different behavior for which typical time traces of the primary flow are also included in the figure.

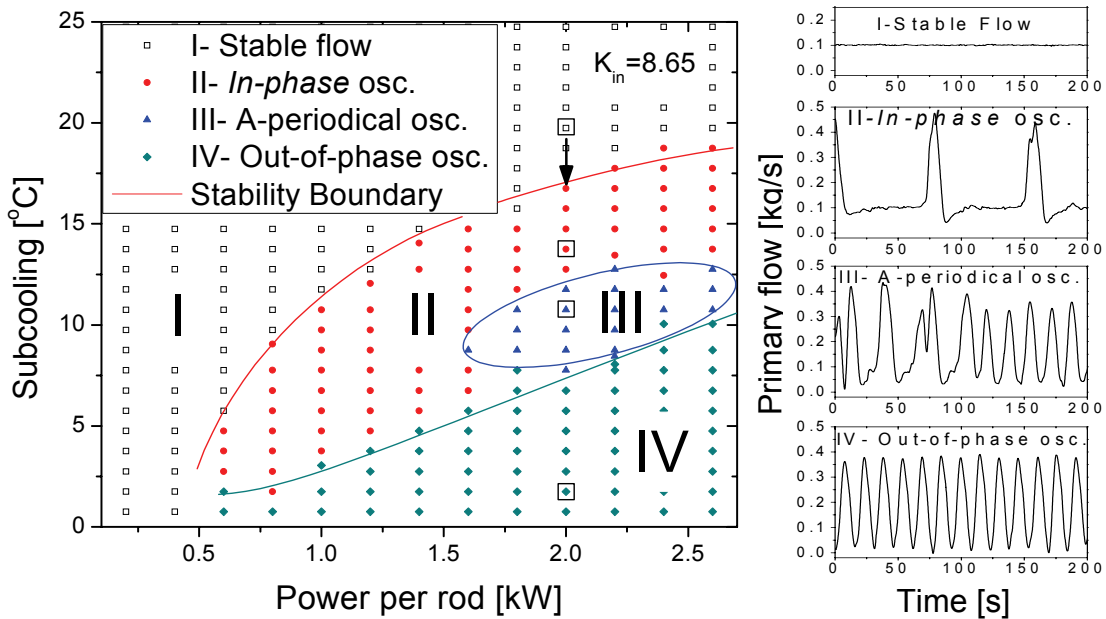


Figure 6-2: Stability map and typical time traces of the flow found when the inlet friction is set to a value equal to $K_{in}=8.65$. The experiments marked with a '□' are analyzed in detail in section 6.3.2. The arrow indicates the points used in the investigations presented in sections 6.3.3 and 6.3.5.

The first region I is mainly characterized by stable single-phase flow. In the proximity of the stability boundary small bubbles were observed at the chimney exit corresponding to low vapor quality values.

The so-called *in-phase* oscillations are observed in region II. This region exhibits regular oscillations in which the period and time of occurrence of the cycles is the same for both the channel partial flows and the primary flow.

In region III, so called a-periodical oscillations take place in the system.

In the last region IV regular oscillations, which are out-of-phase regarding the partial flow in the channels, are found.

A more detailed description of the four behaviors is provided in the next section. It has to be remarked that no stable flashing region is observed in this set of measurements.

6.3.2 Phenomenological description - From region I to IV

To clarify the four behaviors introduced earlier, selected experiments performed with a power input of 2 kW per rod are presented in detail in this section. These cases are marked with '□' in Figure 6-2.

The dynamics of the axial temperature profile and the void fraction profile in the two channels is displayed by using the same technique used in Chapter 5. These profiles are obtained from the sixteen different positions where the temperature and the void fraction is measured (see Figure 6-1). A small scheme of the facility is included to see the axial positions in the plots. Finally, to easily correlate the dynamics of the flow changes with the void and the temperature fluctuations in the channels, the partial flows are also superimposed on the axial temperature plots.

The partial flows time traces are plotted to show the differences between the cases. The primary flow signal power spectral decomposition (PSD) and wavelet decomposition⁹ (done by using the Coiflet package) are also shown.

6.3.2.a Region I – High subcooling stable flow circulation

A measurement performed with an inlet temperature of 80°C is selected as example of the stable behavior of region I. Figure 6-3 shows this case where stable single-phase natural circulation occurs in the facility.

The temperature profile is similar in both channels. The partial flows only exhibit small fluctuations which can be attributed to statistical fluctuations and turbulence. In this case no natural frequency is observed in the PSD and the wavelet decomposition plots of the primary flow signal.

From the figure it is observed how cold water entering into the channels is heated in the core section. The coolant then travels through the chimney section with no significant heat losses. The main flow circulation driving mechanism is single-phase buoyancy since no significant void is detected.

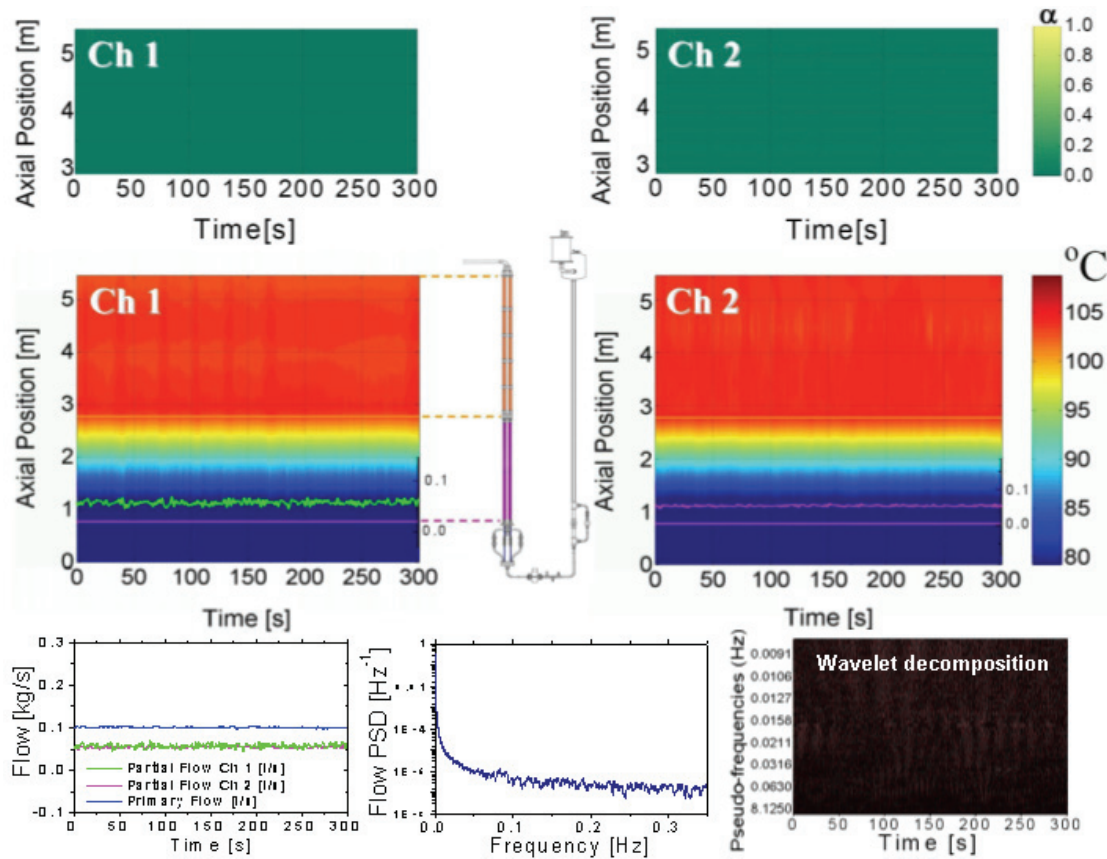


Figure 6-3: Region I is characterized by identical axial temperature profiles in the channels and stable flows, similarly to the high subcooling stable cases from Chapter 5

This behavior is similar to the high subcooling stable flow circulation behavior reported in Chapter 5 obtained when having a single chimney.

6.3.2.b Region II – Unstable *in-phase* flow circulation

Figure 6-4 shows the typical behavior from region II. This particular case is obtained by operating the facility with an inlet temperature of 87°C .

Here, flashing occurs almost simultaneously in both chimneys (see the large peaks in the partial flow signals) since the conditions for flashing in both channels are fulfilled practically at the same time. In this region the period and time of occurrence of the oscillations is the same for both partial flows and primary flow. The coupling between the channels cause that during the flashing events the partial flows behave out-of-phase.

In order to clarify the process, let us focus on what happens at ~ 100 s. As can be seen in Figure 6-4, (see plots with vapor), large amounts of vapor are present in Channel 2 while Channel 1 still contains liquid water. Consequently, a strong increase in flow appears in Channel 2 due to buoyancy. As a result, reversed flow occurs in Channel 1 due to the large inertia of the coolant in the downcomer. This reversed flow forces hot coolant to re-enter the core section and triggers the creation of large amounts of vapor in Channel 1. As a consequence, the partial flow in Channel 1 strongly increases, thereby now reversing the flow in Channel 2. Hence,

the water present in the core of Channel 2 is also heated twice (similar to Channel 1). The temperatures in the lower part of the chimney in Channel 2 are too low to create vapor now. Some flashing, however, occurs due to the presence of hot coolant at the middle of the chimney in Channel 2. The partial flow in Channel 2 increases for a second time which causes (again) reversed flow in Channel 1. The coolant in Channel 1, however, is now too cold to flash again.

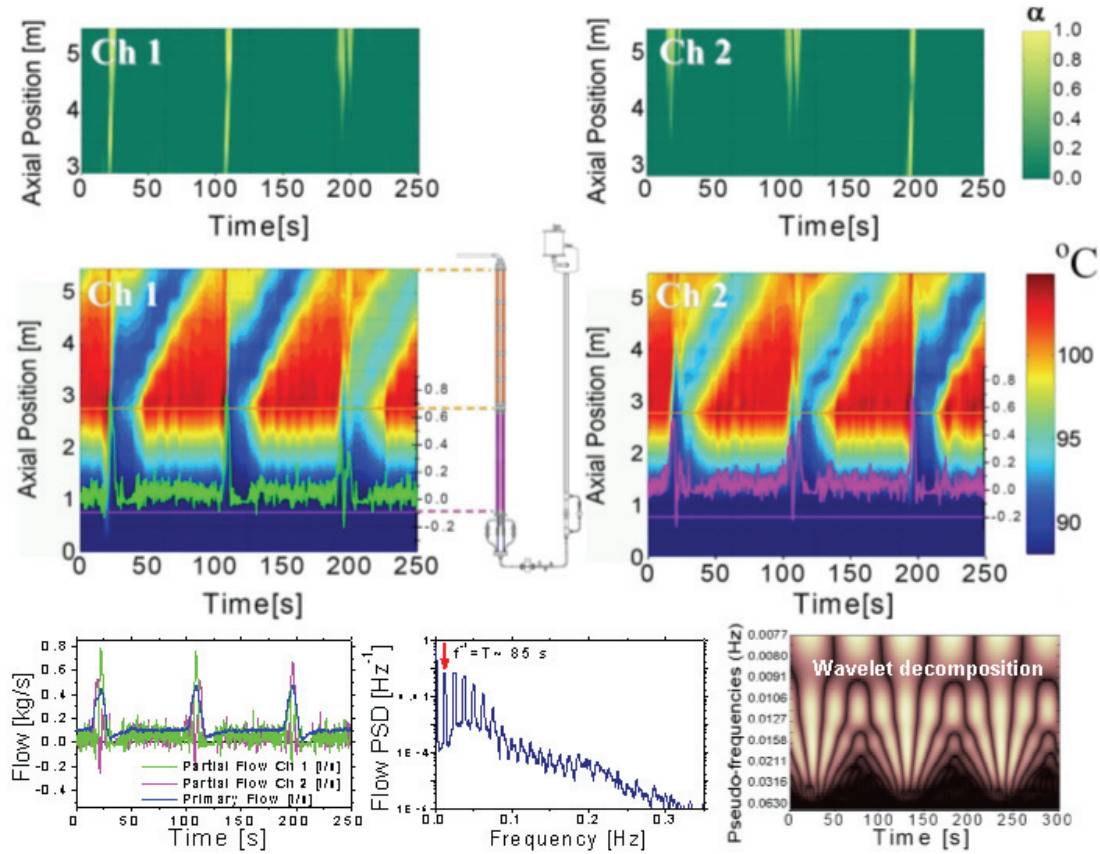


Figure 6-4: Region II. The *in-phase* oscillations are characterized by showing similar temperature axial profiles in both channels at any time. Large amplitude oscillations take place followed by a relative long incubation time.

To summarize, the parallel channels show reversed flow and flashing in an alternating, but not sustainable way due to the relatively low power and low inlet temperature. Since the channels behave more or less independently (whereas the mutual coupling only triggers the flashing events synchronizing the channels) this behavior can be compared with the intermittent oscillations reported in Chapter 5 occurring in a system with a single chimney.

From the analysis of the primary flow signal, two different time scales can be identified: the fast changes in flow (~ 3 s), caused by the very strong coupling between the channels during flashing, and the long incubation time (~ 85 s) needed to build up the conditions that will lead to the next flashing cycle in the channels. Numerous frequencies appear in the PSD and also the wavelet decomposition shows a rather complex but ordered structure.

6.3.2.c Region III – Unstable a-periodical oscillations

A further increase in the inlet temperature leads to the a-periodical oscillations of region III. A typical case of this behavior is shown in Figure 6-5, obtained with the inlet temperature set equal to 88.5°C.

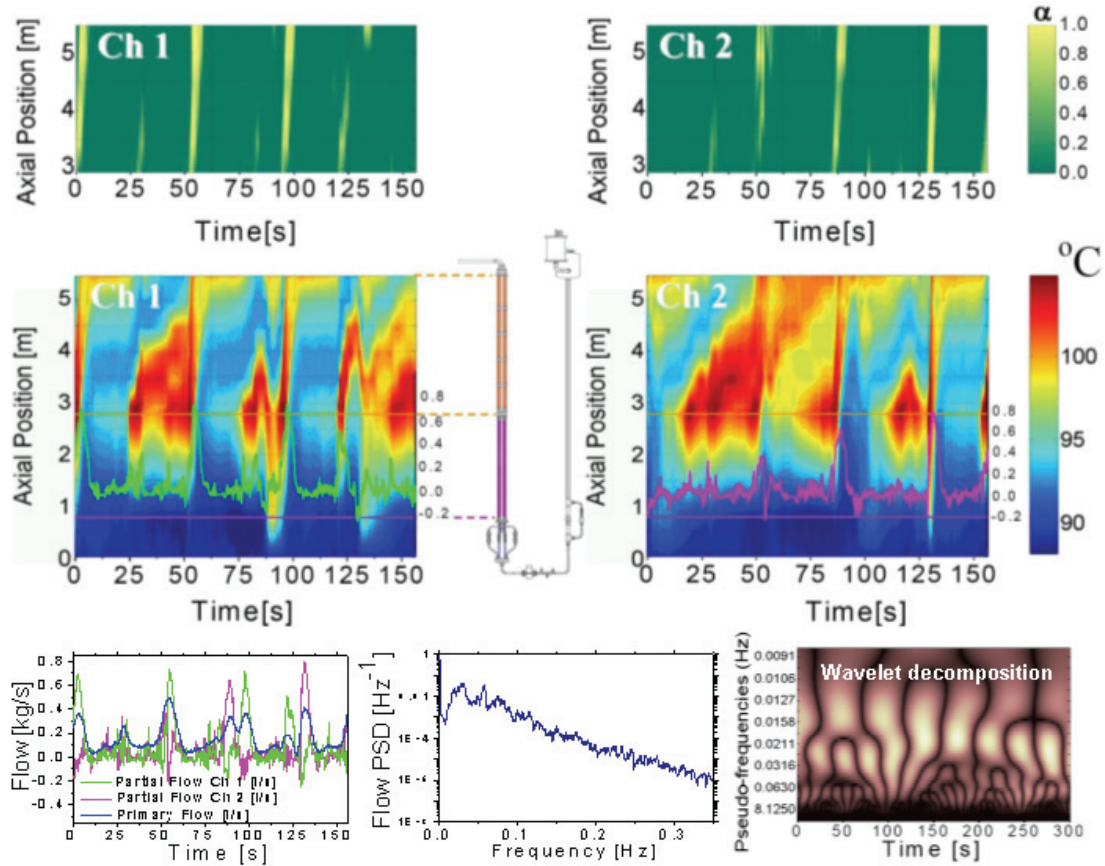


Figure 6-5: Region III. The a-periodical oscillations exhibit a very complex temperature and void fraction axial profile in the channels.

In this case, the combination of power and inlet temperature leads to very complex dynamics resulting in a-periodical oscillations which are clearly visible in the axial void fraction and temperature plots. This behavior is hard to predict, contrasting with the regular oscillations from region II and IV.

In this region, since the periodicity is lost, a broad range of amplitudes and frequencies is found in the PSD of the primary flow signal which is characterized by the absence of clear peaks. The wavelet decomposition shows a pattern which exhibits interesting self-similarities, suggesting the presence of some fractal properties.

Despite the complex axial temperature profiles existing in the channels, the correspondence between the presence of void and the increase in flow can still be seen. This a-periodical region is studied in depth in section 6.3.3.

6.3.2.d Region IV – Unstable out-of-phase oscillations

Increasing the inlet temperature even more leads to region IV, where so-called out-of-phase regular oscillations are found. The experiment depicted in Figure 6-6 is obtained by setting the inlet temperature equal to 98.0°C.

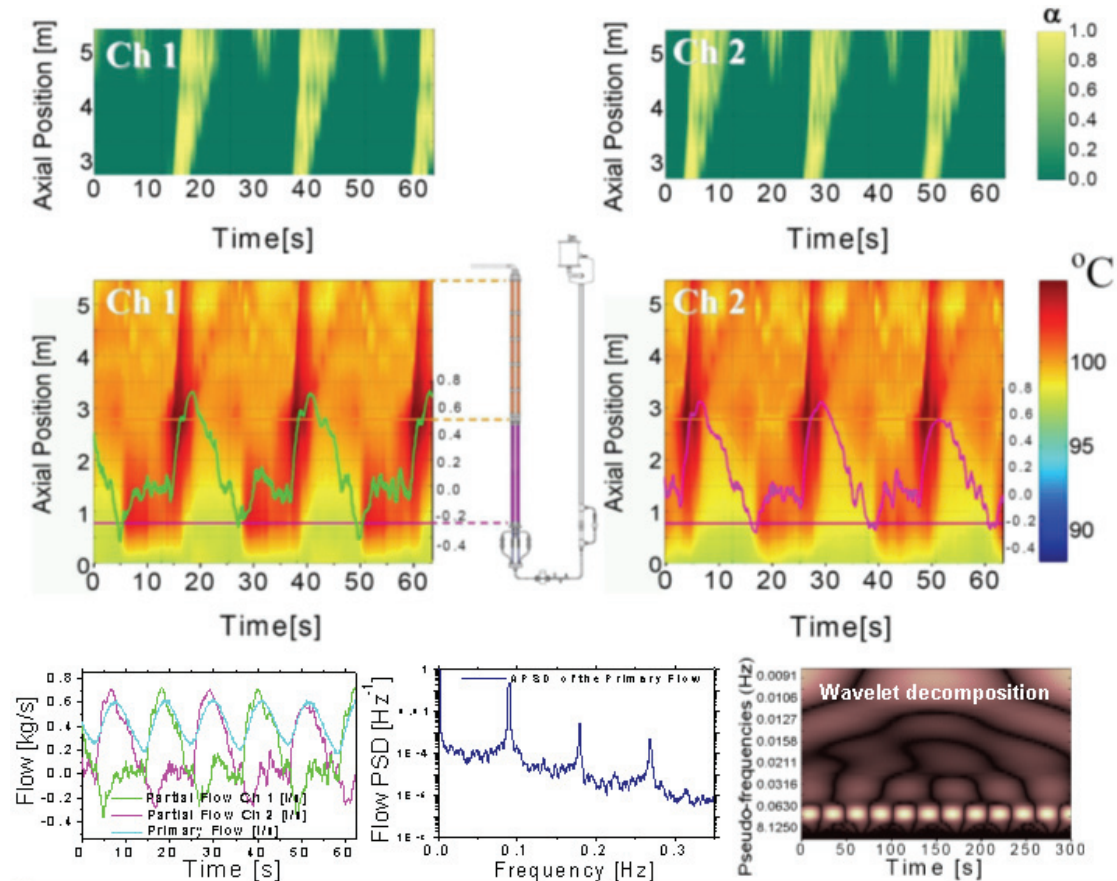


Figure 6-6: Region IV. The out-of-phase oscillations are extremely regular, where reverse flow plays an important role creating ‘hot spots’ which will flash afterwards.

To better explain the process taking place in this region, we will focus on what happens at ~39 s. The high core inlet temperature causes very hot coolant being present at the exit of the heated section of Channel 1 resulting in large amounts of vapor in the chimney (see void plot in Channel 1), while Channel 2 still contains liquid water. As a result of the vapor appearance in Channel 1, buoyancy abruptly increases the partial flow in this channel. The large increase in the Channel 1 flow causes reversed flow to occur in Channel 2, due to the large inertia of the coolant present in the downcomer. This reversed flow forces hot coolant to re-enter the heated section of Channel 2, where it is heated for the second time.

The combination of high power and inlet temperature causes the alternation of flashing events in both channels to be sustained, in contrast to the cases from region II. Due to the small inlet subcooling, the coolant that is heated twice starts to boil inside the heated sections. The noticeable gradient

in the chimney axial temperature profile prior flashing causes condensation that suppresses the vapor creation during the resulting oscillations (see the vapor decrease in the middle part of the flashing chimney). This behavior reminds to the sinusoidal oscillations of Chapter 5 in which the geysering mechanism played a role in the instability mechanism.

The time evolution of the void fraction profile shows a clear correlation in time between the vapor creation and the flow increase in the corresponding channel. A more detailed study will show, however, that a small time delay exists between those two. It is also found that some vapor produced in one channel enters the other channel due to reversed flow.

The PSD of the primary flow signal exhibits a clear peak at the oscillation frequency and also higher harmonics. The wavelet decomposition is characterized by high powers at scales associated to the corresponding normal oscillation frequency.

6.3.3 Analysis of the instability mechanism

Since two possible instability mechanisms are identified, flashing and geysering, the periods of the unstable cases obtained when applying a power input of 2 kW per rod (indicated in Figure 6-2 with an arrow) are compared with two characteristic parameters of density wave oscillations^{10,11} (DWO) and geysering oscillations¹: the traveling time through the channel τ_f and the boiling delay time plus the bubble transit time $\tau_{bd} + \tau_{b,tt}$.

Figure 6-7a) shows the relation between the oscillation period and the flow where the inlet temperature is included in the upper axis.

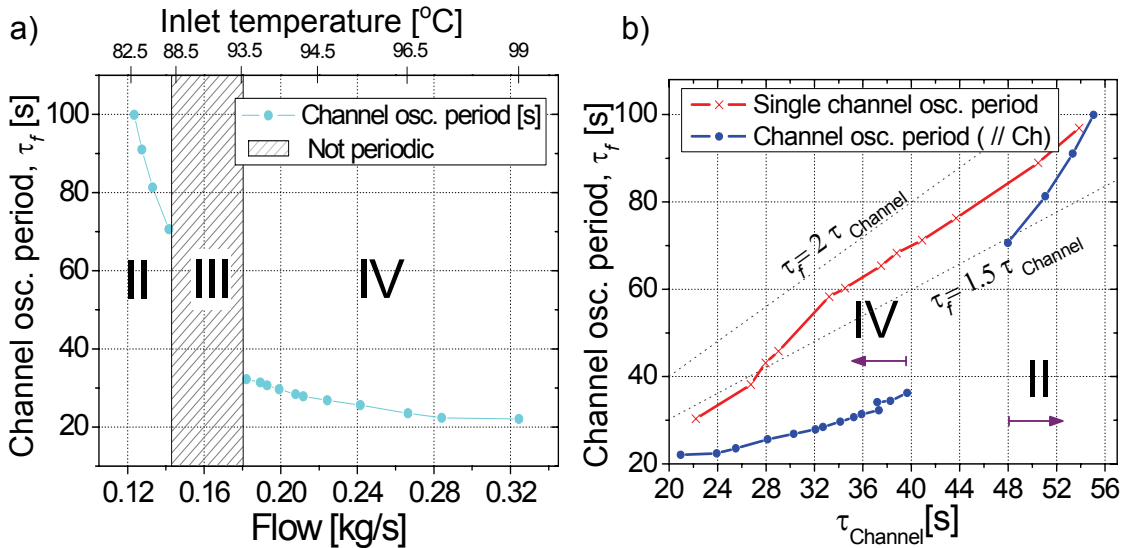


Figure 6-7: a) Period of the oscillations vs. partial flow. The a-periodical region is marked with a shaded rectangle. b) Channel oscillation period vs. characteristic transit time in the channels for both, the single and parallel channels configuration.

It is found that the oscillation period monotonically decreases with the inlet temperature, which was also found for the single chimney configuration (see e.g. Chapter 5). The figure also reveals the long incubation time from region II relative to the small oscillation period in region IV.

Figure 6-7 b) shows the relation between the channel oscillation period and the transit time of the flow which is estimated for one channel as

$$\tau_{Channel} = \frac{V_{Ch} + \frac{1}{2}V_{heated}}{q_{Channel}}, \quad (6-1)$$

where $q_{Channel}$ represents the time averaged volumetric partial flow rate, V_{Ch} the volume of one chimney section and V_{heated} the volume of one heated section.

The results for the single chimney configuration at equivalent conditions (in terms of the power per channel, inlet subcooling and common inlet restriction) already discussed in Chapter 5 are also included in the figure.

Figure 6-7 b) clearly shows that the two regions with periodical oscillations, i.e. regions II and IV, exhibit different slopes, suggesting the instability mechanism to be different. The smaller slope of the (roughly) straight line associated with region IV is due to the strong effect of the reversed flow in the mechanism which promotes the appearance of vapor since a certain amount of hot coolant passes the heated section twice. The figure also shows that for all experiments, the parallel channels have a shorter oscillation period than that from the single chimney configuration. This difference, however, is reduced for large values of transit times, which confirms that for high subcooling/low power conditions the channels behave more independently, i.e. like in the single channel case from Chapter 5.

The existence of the geysering mechanism¹², which may complement flashing, is also investigated. In experiments performed with a chimney it is reported that the period of geysering-induced oscillations τ_f , is nearly equal to the boiling delay time τ_{bd} plus the bubble transit time $\tau_{b,tt}$ ¹. Details regarding the definition of these two quantities are provided in APPENDIX E. The periods of the oscillations τ_f are therefore plotted in Figure 6-8 versus $\tau_{bd} + \tau_{b,tt}$.

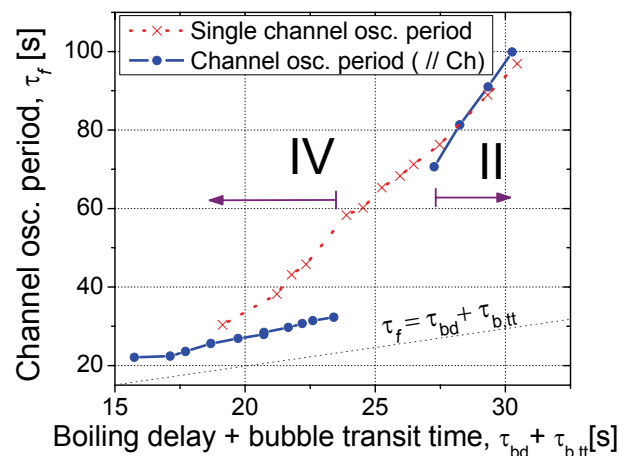


Figure 6-8: Channel oscillation period vs. boiling delay time plus bubble transit time.

The regular oscillations from regions II and IV exhibit linear relations with different slopes. In region II the slope is roughly similar to that in the case of single channel oscillations. Since the oscillation period is several times the boiling delay time, it can be concluded that geysering plays a secondary role in this case. In contrast, the slope of the linear profile of region IV is similar to that from geysering instabilities. The magnitude of the periods, however, is systematically underpredicted, suggesting that the instability mechanism cannot be attributed to geysering only. This difference can be explained as follows. The boiling delay time assumes the flow is zero during the heating up process. The coolant flow, however, is not zero and therefore some enthalpy is transported by the coolant, which is not used in the vaporization. As a result the system needs more time to complete a cycle than that predicted by the geysering mechanism. For this reason, the period of the oscillations in region IV is overestimated by DWO based estimations and underestimated by predictions based on geysering oscillations.

6.3.4 Single channel behavior vs. two-parallel channels behavior

In the ESBWR the chimney is divided into more than two channels. Whether increasing the number of interacting channels can influence the stability of the system during start-up is therefore of importance. Such a question cannot be fully answered with the help of the experimental results obtained from the single channel configuration (Chapter 5) and the two-parallel channels configuration (this Chapter). A comparison between those experiments, however, may help understanding the physical mechanisms present in a multi-channel situation.

Table 6-2 shows the main features of the behaviors found for the two aforementioned configurations while the inlet temperature is increased.

Single Channel	Parallel Channels
a - <i>Stable flow</i> mainly driven by single phase natural circulation.	I - <i>Stable flow</i> mainly driven by single phase natural circulation.
b - <i>Intermittent flow oscillations</i> driven by flashing. Flat chimney axial temperature profile prior to the flashing occurrence.	II - <i>In-phase flow oscillations</i> driven by flashing and to some extent to boiling. Almost flat axial temperature profile in the chimneys prior to the flashing occurrence.
c - <i>Sinusoidal flow oscillations</i> driven by boiling plus flashing. Non-flat chimney axial temperature profile prior to the flashing occurrence.	III - <i>A-periodical flow oscillations</i> caused by flashing, boiling and geysering. Non-flat axial temperature profile in the chimneys. Reverse flow of great importance for the phenomenon.
d - <i>Stable flow circulation</i> induced by flashing.	IV - <i>Out-of-phase flow oscillations</i> driven by boiling, flashing and geysering. Non-flat chimney axial temperature profile prior to the flashing occurrence. Reverse flow of great importance for the phenomenon.
Note: The cases are ordered according to their respective inlet temperature, with cases with lower values first.	

Table 6-2: Summary of the different behaviors found in the experiments obtained with the single channel and the parallel channel configuration.

First, it should be noted that the physical phenomena causing the dynamical behavior could be different for the single channel and the parallel channels configurations. A direct comparison between the behaviors a and I, b and II etc. as stated in Table 6-2 is therefore not always meaningful. Second, it has to be stressed that the configurations used in both sets of experiments make use of the same loop and therefore, although the number of channels is doubled, the rest of the sections remains the same (this is different from a situation where a chimney is divided into smaller sections).

From the experiments it is observed that the stable flow circulation behavior corresponding to very low quality values in the chimney (a and I) are similar for the two configurations. This similarity can be observed in the channel axial temperature profiles, the chimney pressure profiles and the stable mass flow rate (see Figure 5-5 and Figure 6-3). The very high subcooling natural circulation mechanism is efficient enough to cool the heated section. Apparently the cooling mechanism is able to suppress any perturbation which would lead to instabilities in the channel(s).

The intermittent oscillations occurring in the single channel configuration (b) show analogies to the in-phase oscillations observed in the parallel channels configuration (II). This is related to the fact that flashing is the only instability-generating mechanism present here. As can be seen from Figure 5-6 and Figure 6-4, the axial temperature profiles are similar, except for the short time in which reverse flow occurs for the case with parallel channels. The low-quality natural circulation mechanism is not efficient enough to sufficiently cool the heating rods and reach a steady-state situation. In this case, flashing induced instabilities and low-quality natural circulation are alternating phenomena.

The a-periodical flow oscillations (III) involving flashing, boiling and geysering effects show a high degree of complexity and are not found in the single channel configuration. The strong coupling between the channels together with the aforementioned effects creates very complex, time-dependent, axial temperature profiles.

Some similarities exist between the sinusoidal oscillations observed in the single channel configuration (c) and the out-of-phase oscillations in the parallel channel case (IV), such as the axial temperature profile exhibiting the same trend (see Figure 5-6 and Figure 6-4). The reverse flow from the latter case, however, is not present in the single channel configuration. Reverse flow shortens the flashing cycle since part of the fluid is heated twice, as can be clearly seen in Figure 6-7b). The frequencies of the partial flow in the parallel channel configuration are therefore found to be higher than for the single channel configuration (see Figure 6-7b).

The stable flow circulation induced by flashing observed in the single channel configuration (d) has not been found in the parallel channels case.

The stability characteristics obtained for the single channel and the parallel channels configuration are compared for the case in which the inlet coefficient is $K_{in}=8.65$. The stability boundaries resulting from these experiments plotted in the dimensionless plane are presented in Figure 6-9.

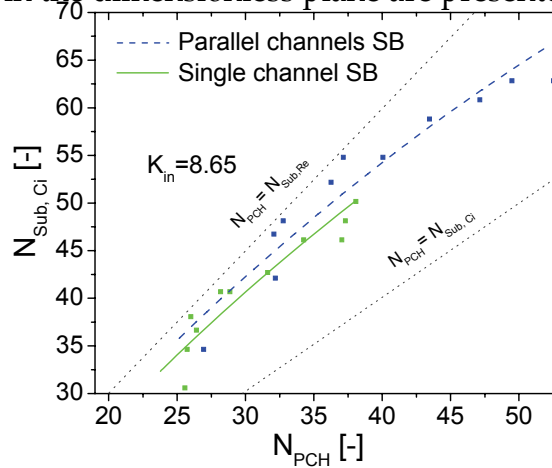


Figure 6-9: Stability boundaries (SBs) obtained with the single channel and the parallel-channels configuration expressed in the dimensionless plane (lines represent a fitted second-order polynomial).

It is clear that the high subcooling stability boundaries obtained from the experiments with one channel and two parallel-channels configurations are close to each other. The dispersion of the experimental points, however, is too large to draw more general conclusions regarding a multi-channel configuration. From the figure it can be observed that both stability boundaries are located below the saturation line corresponding to zero quality at the chimney exit ($N_{PCH}=N_{Sub,Ci}$). This result is in agreement with both our visual observations of small steam bubbles in the chimney section and with the numerical results of Cheung *et al.*¹³ (2005). The important implication of this finding is that the ESBWR can thus be started-up safely if it is operated in the high subcooling stable region (the region between the high subcooling stability line and the chimney exit zero-quality line): pressure can be built-up by the vapor generated without encountering instabilities.

If we consider the ESBWR with many parallel channels, the pressure driving the counter current flow is most probably reduced by the channels surrounding the flashing channel. It is therefore to be expected that the counter current flow would be less likely to occur in the ESBWR. Such reasoning is in agreement with the numerical results obtained for different start-up procedures reported by Cheung *et al.*¹³ (2005). In the work of Cheung *et al.*, reverse flow is not observed, except for peripheral fuel bundles in a particular start-up case in which relative high power was used (2.77% of rated

power). Experimental evidence, however, is desirable in order to confirm the findings of Cheung *et al.*

6.3.5 Non-linear analysis of the oscillations

This section presents an investigation on the nonlinear dynamics of the behaviors presented previously. A bifurcation analysis, together with an attempt of determining the nature of the a-periodical oscillations is performed. The largest Lyapunov exponent¹⁴ and the Kolmogorov entropy^{15,16} are estimated in APPENDIX F.

In this section, experiments obtained at an input power equal to 2 kW per rod and with an inlet friction coefficient $K_{in}=8.65$ are used. The inlet temperature is varied in small steps of 0.5 °C. Each experiment is preceded by waiting one hour before measuring, to reduce as much as possible any long term drift in the inlet subcooling. Then, each point is measured for one hour in order to get enough statistics for this analysis.

6.3.5.a Experimental evidence of bifurcations

Figure 6-10 a) is a contour plot that shows the PSD of the primary flow signal for all the measured cases. A Henning window is used. The color represents the logarithmic value of the power level for the corresponding frequency component. Figure 6-10 b) presents the PSD for three cases.

In the out-of-phase region IV, the spectrum shows the trend of the main frequency together with higher harmonics. By decreasing the inlet temperature, a period-doubling occurs at around 96°C. The amplitude of the successive bifurcations becomes hard to be identifiable in practice after the first period-doubling due to measurement noise.

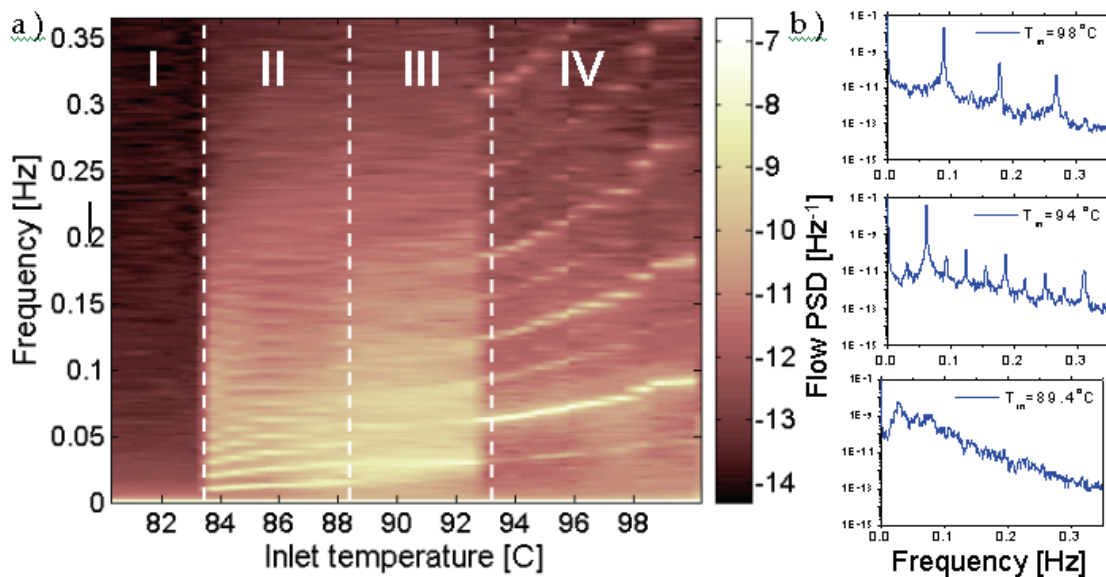


Figure 6-10: a) Contour plot of the primary flow PSD. b) PSD for three particular cases. A bifurcation occurred from the first to the second plot.

An abrupt change in the frequency pattern is seen when reaching the a-periodical region III. Here, a broad band of frequencies emerges around the main frequency. As predicted by the Feigenbaum scenario¹⁷, this may be due to a cascade of period-doubling bifurcations which creates many possible oscillation modes which are impossible to discriminate from each other.

In region II, the PSD clearly shows higher harmonics. A further decrease in the inlet temperature leads to the stable region I characterized by no peaks.

6.3.5.b Investigations on the nature of the a-periodical oscillations

Here a further characterization of the a-periodical cases from region III is done. In particular, the dimension of the oscillations from the case with $T_{in}=89.7^{\circ}\text{C}$ is calculated. In order to perform such a task, two traditional algorithms are used first: the Higuchi's and the Detrended Fluctuation Analysis (DFA) methods^{18,19}. Then, a novel wavelet-based approach²⁰ is also developed and used in this analysis.

The Higuchi's method and the Detrended Fluctuation Analysis (DFA) method

Higuchi's method is based on the calculation of the length of a curve associated to the measured time series. A new time series $Z_p(k)$ is then constructed from the original one by making use of time delays k . The length of the curve $L_p(k)$ corresponding to $Z_p(k)$ is then calculated with Higuchi's formula. The average value of $L_p(k)$ over $p=1, \dots, k$ sets of $Z_p(k)$, denoted as $\langle L_p(k) \rangle$, should exhibit a scaling law according to the relationship given by:

$$\langle L_p(k) \rangle \propto k^{-g(k)} \quad (6-2)$$

If the function g depends on k , the object has a multi-fractal structure. Otherwise, the object is mono-fractal. A plot of $\log \langle L_p(k) \rangle$ versus $\log k$ therefore shows whether the object has a mono- or a multi-fractal structure.

The DFA algorithm starts with the construction of a new time series from the measured one, where each term in the new time series is defined as:

$$z_k = \sum_{i=1}^k (x_i - \bar{x}) \quad (6-3)$$

where $k=1, \dots, N$ and \bar{x} represents the mean value of the time series. The integrated time series is then divided into boxes of equal length n , and a least-squares line fit to the data in each box of length n is performed. The coordinate of the straight line in each box of length n is denoted by $z_{n,k}$ and thus represents the trend in each box. The following quantity is then calculated:

$$F(n) = \sqrt{\frac{1}{N} \sum_{k=1}^N (z_k - z_{n,k})^2} \text{ for } n = 2, \dots, N \quad (6-4)$$

$F(n)$ should exhibit a scaling law according to the following relationship:

$$\langle F(n) \rangle \propto n^{-g(n)} \quad (6-5)$$

If the function g depends on n , the object has a multi-fractal structure. Otherwise, the object is mono-fractal. A plot of $\log \langle F(n) \rangle$ versus $\log n$ therefore shows whether the object has a mono- or a multi-fractal structure.

Results from the Higuchi's and DFA methods

The plot of $\log L(k)$ vs. $\log k$ obtained with the Higuchi's method and the plot of $\log \langle F(n) \rangle$ vs. $\log n$ from the DFA method are given in Figure 6-11.

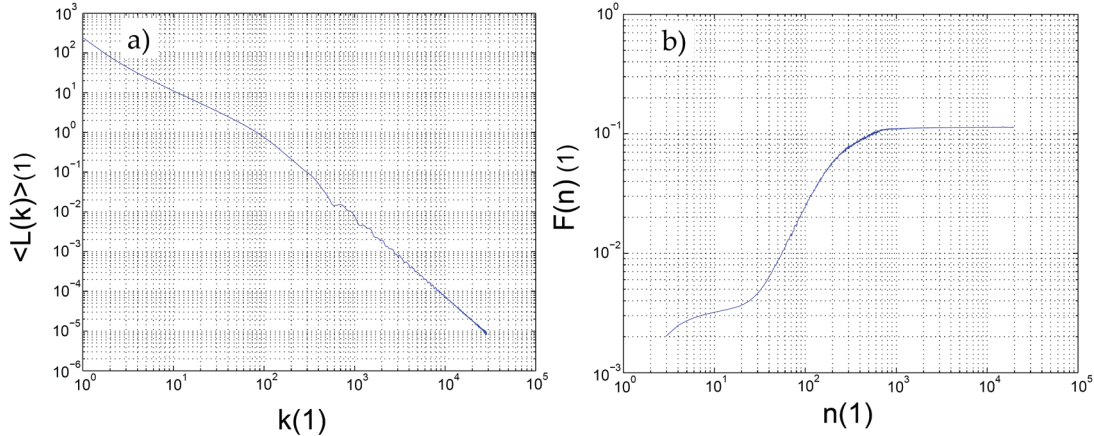


Figure 6-11: a) $\text{Log}(\langle L_p(k) \rangle)$ vs. $\log k$ calculated by using the Higuchi's method.

b) $\text{Log} \langle F(n) \rangle$ vs. $\log n$ obtained by using the DFA method.

The calculated relations sensibly deviate from linearity in both figures, indicating a multi-fractal character of the time series from region III.

Wavelet-based multifractal approach

The main advantage of wavelets compared to the traditional Fourier analysis method is their ability to deal with non-stationary signals and thus to analyze local behaviour of functions. Any scaling behaviour present in fractal objects (i.e. self-similarity) is revealed by a wavelet transform²¹.

The so-called Continuous Wavelet-Transform (CWT) can be used to approximate the measured time-series $f(t)$ as

$$T_\psi[f](t, a) = \frac{1}{a} \int_{-\infty}^{+\infty} \psi\left(\frac{x-t'}{a}\right) f(t') dx \quad (6-6)$$

where $a > 0$ represents the scale parameter and ψ the wavelet function.

If $f(t')$ has a singularity at time t_0 , the strength of such singularity can be represented by a local scaling or Hölder exponent²² $h(t_0)$. These singularities determine the Hausdorff dimension of the set of points where those singularities exist. It can be proved that the following scaling law holds

$$T_\psi[f](t_0, a) \propto |a|^{h(t_0)}, \quad \text{if } h(t_0) < n_\psi, \quad (6-7)$$

with n_ψ the n^{th} order derivative of the analyzing wavelet in the singular point.

As can be seen from Equation (6-7) any scaling law characteristic of fractal signals can be detected by a CWT by means of the power of the corresponding scale parameter a . By using wavelets for analyzing fractals is allows exhibiting any self-similarity in the time- and frequency-domains.

Figure 6-12 a) and b) show the spectrum of amplitudes of the CWT of the primary flow respectively, in the time- and frequency-domains.

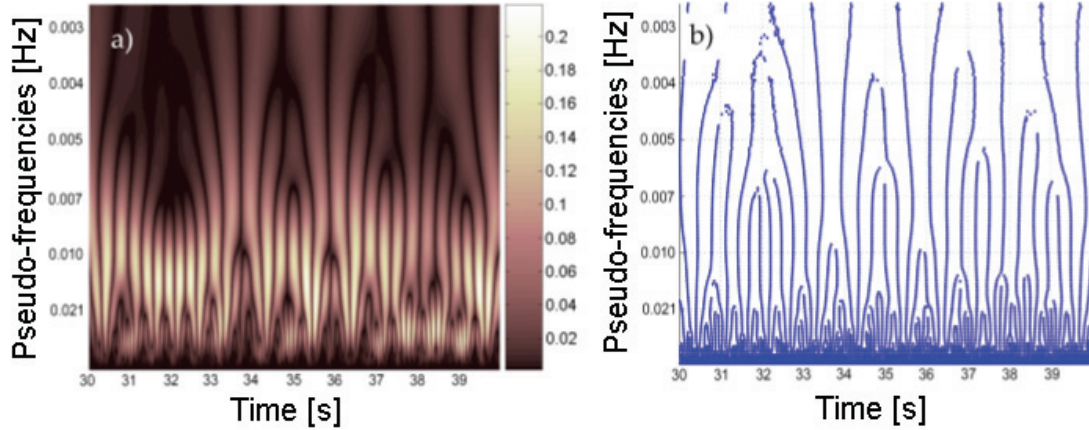


Figure 6-12: a) Amplitude and b) skeleton of the CWT for the measured data (the 5th-order derivative of the Gaussian function was used as wavelet).

The Hausdorff dimension $D(h)$ for the set where the Hölder exponent is equal to h can be defined as

$$D(h) = \dim_H \{t | h(t) = h\}. \quad (6-8)$$

In order to avoid using redundant information existing in the CWT, the Wavelet-Transform Modulus-Maxima (WTMM) formalism is implemented. In the WTMM implementation, a partition function $Z(q, a)$ (being q^{th} moment of the measure). In the limit $a \rightarrow 0$, the partition function $Z(q, a)$ is expected to scale as

$$Z(q, a) \propto a^{\tau(q)} \quad (6-9)$$

and thus

$$\tau(q) = \lim_{a \rightarrow 0} \frac{1}{\log a} \log Z(q, a). \quad (6-10)$$

If the slope of $\log Z(q, a)$ vs. $\log a$ deviates from linearity, i.e. if the scaling exponent $\tau(q)$ has multiple values, the system is multi-fractal.

To compute the singularity spectrum $D(h)$, two methods are used: a direct Legendre transform and a computation of the so-called Boltzmann weights from the WTMM¹⁸ with which the first one is avoided.

From the multi-fractal formalism, the generalized or Rényi dimensions are found to be given as

$$D_q = \frac{1}{q-1} \tau(q). \quad (6-11)$$

Further details on the wavelet-based multifractal approach used in this work are given by Demazière *et al.*²⁰.

The partition function $Z(q,a)$ computed along the chain maxima lines is given in Figure 6-13 a). Deviations from a straight line in the double logarithmic scale are clear.

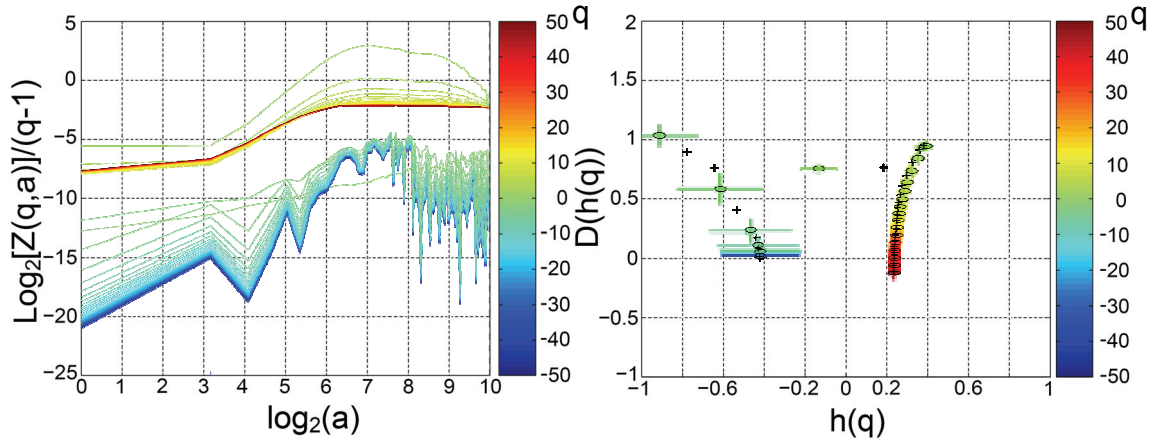


Figure 6-13: a) Partition function $Z(q,a)$ for the a-periodical oscillations. b) Fractal spectrum found by using the Legendre transform, marked with '+'; and by using the Boltzman weights from the WTMM, marked with ellipses.

The fractal spectrum, computed from the two methods based on the WTMM, is presented in Figure 6-13 b). Both methods of computing the fractal spectrum give the same results. It is clear that the fractal spectrum does not reduce to a single point, thus indicating a multi-fractal character of the system. Furthermore, the spectrum is roughly divided into two branches: a branch with positive Hölder exponents, and a branch with negative Hölder exponents. The scaling exponent $\tau(q)$ as a function of q is given in Figure 6-14.

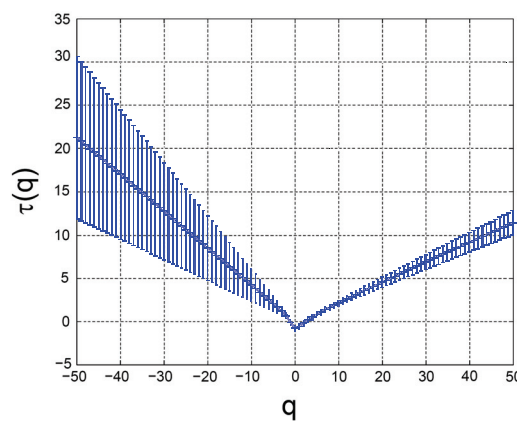


Figure 6-14: Scaling exponent τ with the associated uncertainty for the measured data.

Again, the corresponding curve significantly deviates from a straight line. Based on Equation 6-17, it is found that the Rényi dimensions all differ from each other, thus characterizing a multi-fractal object²⁰. The box-counting dimension gives a dimension equal to 0.77 ± 0.02 .

All methods clearly demonstrated a multi-fractal structure in the dynamics of the measured signal, thus revealing that the nature of the a-periodical oscillations (region III) is deterministic chaos. The physical mechanism driving these flow oscillations is mainly flashing combined with some geysering. Although the chaos is proven to be deterministic, such a chaotic behaviour of the flow oscillations is difficult to be modelled, since there is sensitive dependence on initial conditions. Therefore, when trying to model the behaviour of the facility for the transition region via a time-domain code, any inaccuracy in the determination of the initial conditions would lead to radically different responses of the facility. Any attempt to model such behaviours is further complicated by the strong asymmetrical response of each pair of heated channels/chimney. The present investigation shows that on top of the difficulties reported to model flashing-induced instabilities, in a multiple chimney configuration, natural circulation BWRs might encounter a chaotic region where most of the time-modelling techniques will fail, due to the sensitive dependence on initial conditions. From a safety point-of-view, such a region has to be avoided in real plants. This can be done by building up pressure by means of vapour production which will reduce the importance of the water saturation temperature difference for different locations.

6.4 Conclusions

In this chapter, the instability mechanisms existing when having parallel channels, have been thoroughly investigated (at conditions relevant for the start-up phase of natural circulation BWRs) by using the CIRCUS test facility.

As a result of this study it is concluded that four different behaviors can be expected in a system of two identical heated channels equipped with parallel chimneys. These are:

1. stable flow circulation (corresponding to very low vapor quality values);
2. periodic oscillations in which the primary flow is roughly in-phase with the partial flow in both channels and the main instability mechanism is due to flashing. The two channels behave more or less independently except for the clear synchronization of the flashing events which can be attributed to the coupling between the channels;
3. a-periodical oscillations which are attributed to multifractal deterministic chaos. The wavelet decomposition of the primary flow signal exhibited self-similarity properties; Bifurcations have been observed in the experiments which suggest that period-doubling is the route to chaos followed by the system. This result has never been reported before;
4. out-of-phase periodical oscillations in which the primary flow exhibits a period which is half of the period of the partial flows in the channels. Two main instability mechanisms seem to coexist in this case being flashing and geysering. The channel coupling creates reversed flow which causes hot spots in the channels. This effect creates large gradients in the axial temperature profile that favors the occurrence of condensation effects.

As a result of this investigation it is concluded that, in a multiple chimney configuration, natural circulation BWRs might encounter a chaotic region during the start-up phase. Such a dynamical behaviour may be difficult to predict by most of the time-modelling techniques, due to the sensitive dependence on initial conditions.

No clear differences can be observed between the location of the stability boundaries obtained in the experiments with the single channel and the two parallel channels configuration.

In order to avoid any instability during the start-up phase of natural circulation BWRs, pressure has to be built up. Since it is found that vapor produced by means of flashing is already present in the stable region I, the reactor can be operated in such a state until the dependence of the local pressure in the saturation temperature can be neglected (~ 15 bar). Such a start-up procedure can also be followed in the case the reactor chimney is split up into many channels, as Cheung *et al.*¹³ (2005) have proposed.

6.5 References

- ¹ Aritomi, M. and Chiang, J. H., Fundamental studies on safety-related thermohydraulics of nat. circ. boiling parallel channel flow systems under start-up conditions (mechanism of geysering in parallel channels), *Accident Analysis, Nuclear Safety*, 33(2):170–182, (1992).
- ² Subki, M., Aritomi, M., Transport Mechanism of Thermohydraulic Instability in Natural Circulation BWRs during Startup, *J. Nuc. Sci. Tech*, 40 (11), 918-931, (2003).
- ³ Marcel, C. P., M. Rohde, T. H. J. J. van der Hagen, “Out-of-phase flashing induced instabilities in the CIRCUS facility,” *Proc. of the 11th Int. Topical Meeting on Nuclear Reactor Thermal-Hydraulics (NURETH-11)*, France, October 2-6, 2005 (2005).
- ⁴ Clausse, A. and Lahey, R.T., The Analysis of Periodic and Strange Attractors During Density-Wave Oscillation in Boiling Flows, *Chaos, Solitons and Fractals*, 1:167, (1991).
- ⁵ Der Lee, J., Pan, P., Non-linear Analysis for a Double-channel Two-phase Natural Circ. Loop Under Low-pressure conditions, *Ann. of Nuc. Energy*, 32, 299-329, (2005).
- ⁶ March – Leuba, J., D. Cacuci and Perez, R. B., Non-linear Dynamis and Stability of Boiling Water Reactors: Part I – Qualitative Analysis, *Nucl. Sci. Eng.*, 93, 111, (1986).
- ⁷ De Kruijf, W., Manera, A., Haas, D.W. de, Schut, J.G.F., Van der Hagen, T.H.J.J., Mudde, R.F. and Prasser, H.-M., Description of CIRCUS Including Test Matrix, European Commission, 5th Euratom Framework Program 1998-2002, EVOL-NACUSP-D8a, (2001).
- ⁸ Yin, Jie, R., Lahey, T, Podowski, M and Jensen, M. K., An Analysis of interacting instability modes (2004) conference
- ⁹ Daubechies, I., Ten Lectures on Wavelets, *Soc. for Ind. and App, Math*, (1992).
- ¹⁰ Bouré, J. A., Bergles, A. E. and Tong, L., Review of Two-phase Flow Instability, *Nuc. Eng. Des.*, 25, 165-192, (1973).
- ¹¹ Yadigaroglu, G., Two-phase flow instabilities and propagation phenomena, chapter 17, 353-403, *Hemisphere Publishing Corporation*, (1981).
- ¹² Nakanishi, S., “Recent Japanese research on two-phase flow instabilities”, In *Proc. of Japan-US Seminar on Two-phase Flow Dynamics. Hemisphere Publishing Corporation*, (1979).
- ¹³ Cheung Y.K; Shiralkar B.S; Marquino, W. Analysis of ESBWR Startup in Natural Circulation, *Proceedings of ICAPP '05 Seoul, KOREA*, paper 5484 (2005).
- ¹⁴ Rosenstein, M.T., Collins, J.J and De Luca, C.J., A practical method for calculating largest Lyapunov exponents from small data sets, *Physica D* 65:117-134, *MTRChaos*, (1993).
- ¹⁵ Grassberger, P. and Procaccia, I., Characterization of strange attractors, *Phys. Rev., Lett.* 50, 346, (1983).
- ¹⁶ Grassberger, P. and Procaccia, I., Measuring the strangeness of strange attractors, *Physica D*, 9, 189, (1983).
- ¹⁷ Feigenbaum, M. J., The transition to aperiodic behavior in turbulent systems, *Commun, Math. Phys.*, 77, 65-86, (1980).
- ¹⁸ Higuchi, T., Approach to an irregular time series on the basis of the fractal theory, *Physica D*, 31 (2), 277-283, (1988).
- ¹⁹ Higuchi, T., Relationship between the fractal dimension and the power law index for a time series: a numerical investigation, *Physica D* 46 (2), 254-264, (1990).
- ²⁰ Demazière, C., Marcel, C., Rohde, M. and Van der Hagen, TH.J.J., Multi-fractal analysis of chaotic flashing-induced instabilities. To be submitted
- ²¹ Addison, P. S., *The Illustrated Wavelet Transform Handbook – Introductory Theory and Applications in Science, Engineering, Medicine and Finance*, Institute of Physics Publishing, Bristol and Philadelphia, (2002).
- ²² Muzy, J. F., Bacry, E. and Arneodo, A., Multifractal formalism for fractal signals: The structure-function approach versus the wavelet-transform modulus-maxima method, *Physical Review E* 47 (2), 875-884, (1993).

Chapter 7

Conclusions and recommendations

New boiling water reactor (BWRs) designs use buoyancy to make the coolant/moderator to flow through the reactor core. Buoyancy, however, creates new feedback mechanisms which can affect the stability of those reactors. Such phenomena are difficult to assess and therefore need to be investigated by using dedicated experimental facilities and numerical models. Many aspects of stability analysis were considered in this thesis including, coupled neutronics-thermal-hydraulics and low pressure stability in single and parallel channels configurations. The Economical Simplified Boiling Water Reactor (ESBWR) design from the General Electric Company (GE) was thereby taken as a reference.

High pressure/high power conditions

In order to investigate the ESBWR stability performance at rated conditions (high-pressure and high-power conditions) as accurately as

possible, a downscaled research facility, the so-called GENESIS facility, was designed and constructed by using fluid-to-fluid scaling modeling. Such an approach allows considerable reduction of the power, pressure, temperature and dimensions to be used. A complete fluid-to-fluid downscaling procedure, especially developed for performing stability investigations, was therefore derived. It was found that for stability investigations of boiling systems, the same geometrical scaling factor has to be applied for calculating the radial and axial dimensions in the downscaled loop. In addition, it was found that an explicit rule applies for the time ratio which is dependent on the geometrical scaling. As a result it was found that the power per rod is reduced to 2% of the power in a typical reactor fuel rod; the pressure is decreased from 75 bar to 11.4 bar and all dimensions are reduced by a factor two.

For the thermal-hydraulic system, it was found that the characteristic resonance frequency is much lower (~ 0.11 Hz) than in forced-circulation BWRs (~ 1 Hz), indicating a static head dominated phenomenon (since it corresponds well with typical frequencies of density wave oscillations traveling through the core-plus-chimney sections).

In order to investigate the reactor, the void reactivity feedback was included in the experiments via a so-called void reactivity feedback system (VRF); this system includes a number of refinements compared to earlier developed VRF systems, such as a second order modeling of the reactor fuel rods and a detailed determination of the boiling boundary. The GENESIS facility (with VRF) was operated in a wide range of conditions, so that stability maps for the ESBWR prototype could be constructed. Among other things, it was experimentally found that the GENESIS facility, representing the ESBWR, is stable with a large margin to instability ($T_{\text{Sub}} > 30$ K) for a large range of conditions in terms of power (and thus flow).

In addition, a benchmark study with numerical calculations obtained with the TRACG system code and the ATHLET system code was performed. As a result, an excellent agreement between the GENESIS and the TRACG results was found for the reference reactor at rated conditions. In particular, the agreement in the resonance frequency confirmed the appropriate downscaling design regarding the time scaling. Regarding the decay ratio, the agreement is most probably a result of the compensation of a number of conservative and non-conservative assumptions used in the downscaling process. In contrast to the agreement between the TRACG results and the GENESIS results, large differences in the estimated decay ratio were observed between the ATHLET results and the TRACG/GENESIS results. The fact that the uncertainties from the ATHLET calculations are not known, however, makes drawing conclusions a difficult task. Nevertheless, the findings clearly show that predicting the BWR stability is still a challenging task. Therefore,

considerations based on merely numerical results (even for best-estimate thermal-hydraulic codes) have to be taken with care. This point emphasizes the importance of acquiring accurate experimental data regarding BWRs stability in order to validate numerical codes.

Taking advantage of the flexibility of the GENESIS test facility, a detailed parametric study was also performed. As a result of such an investigation, the following was found:

- when simulating heat transfer situations both the GENESIS heating rods and the reactor fuel rods have to be represented by (at least) second order systems in order to avoid important sources of uncertainty;
- the use of MOX fuels in a BWR slightly decreases the stability performance of the reactor since the smaller effective delayed neutron fraction brings the system closer to prompt-criticality. From the experiments it was also found that the resonance frequency is significantly higher than that for UO₂ fuels;
- the pressure has little influence on the thermal-hydraulic stability of the system (when the operational point is expressed in the dimensionless plane) for a wide range of pressures ($66 \text{ bar} < P < 74 \text{ bar}$). This result may allow controlling the reactor power by slightly adjusting the operational pressure, an issue that is being investigated by researchers from General Electric;
- it was experimentally found that (as predicted numerically by Zboray¹), changing the position of the feedwater sparger affects the loop stability regarding the thermal-hydraulic mode. This effect may be used to enlarge the reactor stability margin regarding such an instability mode;
- when the void reactivity coefficient is varied, a clear peak appeared in the power spectral decomposition of the flow signal at intermediate frequencies regarding the natural frequencies of the thermal-hydraulic and the reactor-kinetic instability modes. This finding may indicate the presence of a new instability mechanism existing in natural circulation BWRs which, for certain conditions, may be dominant. Further investigations are needed in order to explore the origin of this finding.

Low pressure/low power (start-up) conditions

Two important issues which are of relevance for the starting up of novel natural circulation BWR designs were investigated: first, the effect of a large restriction on top of the chimney (induced by the so-called steam separators in the ESBWR design) on the flashing instability mechanism; second, the possible effect of dividing the chimney section into separate channels (another

specific feature of the ESBWR design) which may cause parallel channels instabilities.

The effect of placing a large restriction at the chimney exit was studied by using a numerical model and very detailed measurements with the help of the water based CIRCUS facility. From those experiments it was observed that depending on the coolant inlet temperature, four different behaviors can be expected in a *single channel* in which flashing is likely to occur. These are:

- stable flow at high subcooling (corresponding to very low qualities);
- unstable intermittent flow oscillations characterized by the existence of a flat temperature profile in the chimney prior to the flashing event. In this region the flashing front develops from the chimney top to bottom;
- unstable sinusoidal flow oscillations in which the temperature profile exhibits a clear hot spot at the chimney inlet prior the flashing event;
- stable flow at low subcooling in which vapor produced by flashing is continuously present in the chimney.

In addition, a very good agreement was found between the location of the stability boundary observed in the experiments and the stability boundary as predicted by the numerical simulations. Both the experiments and the numerical results show that a two-phase stable region exists at high subcooling values prior to the instabilities. This region can help to build up the pressure in the reactor vessel during the start-up phase, which in turn would reduce the effects of flashing as a mechanism for instabilities.

Regarding the friction distribution, increasing the core inlet restriction stabilizes the system at high subcooling values according to the numerical model and destabilizes the system at low subcooling values. In addition, the model predicts a destabilizing effect of the chimney exit restriction coefficient at low subcooling values while no changes are observed in the stability at high subcooling.

From the study on flashing-induced instabilities in *parallel channels*, performed with the help of the CIRCUS facility equipped with two parallel channels, four different behaviors were observed, viz.

- stable flow circulation (corresponding to very low vapor qualities);
- periodic oscillations in which flow in the two channels behave very similarly to the oscillations found in the single channel configuration;
- a-periodical oscillations which are attributed to multi-fractal deterministic chaos. Supercritical bifurcations were observed in the experiments, suggesting that period-doubling is the route towards chaos;

- out-of-phase periodical oscillations in which the primary flow exhibits a period which is half of the period of the partial flows in the channels. Two instability mechanisms seem to be present in this case, being flashing and geysering-like phenomena.

From the CIRCUS results obtained in this work (experiments obtained with the single channel configuration, the parallel channels configuration and also by the numerical experiments performed by using the lumped parameter model) it was found that vapor can be created by means of flashing in the high subcooling stable region. This finding confirms the numerical results obtained by Cheung *et al.*² who have found start-up trajectories in which the ESBWR remains stable. It is therefore concluded that the ESBWR can be started-up safely if it is operated in the high subcooling stable region until enough pressure is built-up by the flashing generated vapor.

Concluding remarks and recommendations

New reactor designs always need to be investigated beforehand by using both numerical and experimental tools. In this frame benchmark studies are of great importance in order to identify the instability mechanisms and assure enough margins to instabilities. In such studies test facilities as those used in this thesis, which are simple to model, should occupy an important place.

To quantify the simulation capabilities of the numerical codes and also the downscaling rules, it is recommended to numerically simulate (preferably by using a validated code with a known uncertainty such as the TRACG code) a water-based up-scaled version of the GENESIS facility and to benchmark the results. In this way sources of uncertainties related to geometrical discrepancies between experiments and simulations can be eliminated allowing a direct comparison of the benchmark results.

In order to enhance the similarities between the heated section of the facility and the reactor core, heating rods with a more realistic power shape than the axially uniform one used in the GENESIS facility should be used. In such a case, a more sophisticated neutronic model has to be implemented in which flux weighting factors for the void reactivity feedback need to be incorporated. This refinement would need a more advanced methodology for estimating the core axial void profile for which a number of pressure drop sensors located across the core spacers can be used. A disadvantage of using such a method could be the so-called pressure recovery length behind the spacer which may degrade the accuracy of the void reconstruction method.

To increase the operating range of the GENESIS facility, heat exchangers placed in the lower part of the downcomer section can be used. Such a modification would allow reaching a larger range of subcooling numbers, which can help determining the ESBWR margin to instability more accurately.

At start-up conditions, the effect of dividing the reactor chimney into many sub-channels (as in the ESBWR case) on the stability is not fully understood and should be experimentally studied in the future. An extended version of the CIRCUS facility, equipped with more than two parallel channels, can be used for such an investigation.

From the numerical results obtained with the help of the nodal model at start-up conditions it was found that the channel friction distribution affects the stability performance. In order to confirm such a result, the CIRCUS facility can be used. A number of variable flow restrictions (i.e. valves) should therefore be installed, allowing investigating different configurations regarding the friction distribution.

References

- ¹ Zboray R., An experimental and Modeling Study of Natural-Circulation Boiling Water Reactor Dynamics, Delft University of Technology PhD thesis (2002).
- ² Cheung Y.K; Shiralkar B.S; Marquino, W. Analysis of ESBWR Startup in Natural Circulation, Proceedings of ICAPP '05 Seoul, KOREA, paper 5484 (2005).

APPENDICES

APPENDIX A

The GENESIS facility technical details

The following table presents the technical details for the ESBWR and the GENESIS facility.

Parameter	Symbol, (unit)	ESBWR	Facility	Ratio
Power per rod	P_{rod} , (kW)	43	1.05	0.22
Pressure	P , (bars)	71	11.4	0.16
Temperature	T_{sat} , (K)	560	317	-
Number of fuel bundles	NB , (-)	1132	1	-
Fuel pins per fuel bundle	NP , (-)	92	25	~0.25
Heating rods diameter	D_{rod} , (m)	0.01026	0.006	0.58
Water rods per fuel bundle	NW , (-)	2	0	-
Water rods diameter	D_{Wrod} , (m)	0.02489	-	-
Pitch	p , (m)	0.01295	0.006	0.47
Chimney cell hydraulic diam.	D_{ch} , (m)	0.6	0.04	0.07
Nº of fuel bundles per chimney cell	$N_{fb/ch}$, (-)	16	1	-
Subcooling temperature	T_{sub} , (K)	12		
Fuel bundle area	A_{fb} , (m ²)	0.008895	0.002	0.22
Bypass area	A_b , (m ²)	0.0008895	-	-
Core mass flux (no bypass)	$G_{m,0}$, (kg/m ² s)	994	1001	1.007
Core hydraulic diameter	D_h , (m)	0.009	0.00351	0.39
Heated length	$L_C \equiv L_{heated}$, (m)	3.0	1.41	0.47
Chimney Length	L_R , (m)	6.61±2.0	4.05	0.47
Steam separator length (effective)	L_{ss} , (m)	4.2	1.97	0.47
Downcomer length	L_{DC} , (m)	16.4	7.71	0.47
Core exit quality	χ_{out}	0.169	0.169	1

Table A-I: Technical details for the ESBWR¹ and the GENESIS facility².

The GENESIS core

The GENESIS core bundle consists of 25 heating rods arranged in a 5x5 square configuration. Its most important details are given in the following figure. Since the long heated elements would tend to bend, six spacers are included which simulate the six ESBWR spacers. The figure also includes a plot of a typical spacer. The spacers are constructed from a single piece of aluminum covering 33% of the free flow area.

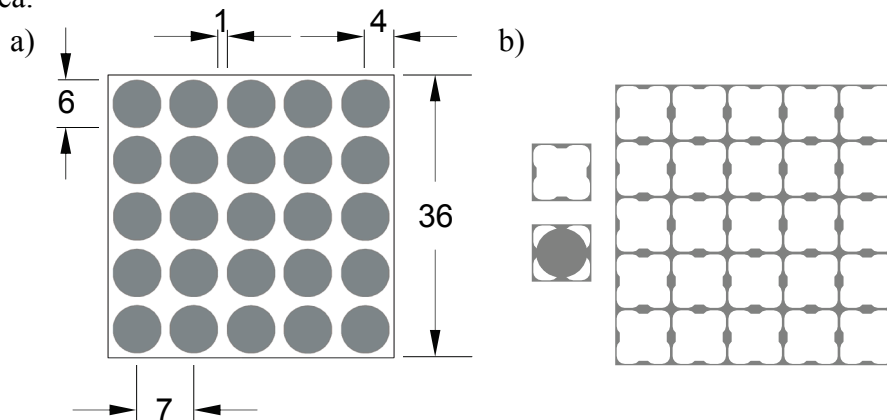


Figure A-1: Details of the GENESIS bundle: a) Configuration and dimensions (in mm). b) Core spacer geometry.

A typical GENESIS heating rod consists of an electrically heating wire embedded in a magnesium oxide matrix. A stainless steel cladding provides the necessary mechanical stability to the compound. An x-ray picture of a GENESIS rod is shown in Figure A-2.



Figure A-2: X-ray picture of a GENESIS heating rod. The helicoidal heating wire is clearly visible³.

References

- ¹ Shiralkar, B.S., Personal communication, (2004).
- ⁸ Marcel C. P., Development of the scaling laws for a natural circulation loop, GE Proprietary Report, (2004).
- ³ Degen, C. Dynamics of the GENESIS heating rods. Bachelor thesis, (2006).

APPENDIX B

Noise analysis basic principles and DR estimation

Noise analysis is based on the fact that a noisy signal usually contains useful information about the system from which it is originated. For instance, consider a simple linear single-input/single-output system. In the frequency domain we can write:

$$Y_{(\omega)} = G_{(\omega)} X_{(\omega)} \quad (\text{B-1})$$

where $Y_{(\omega)}$ and $X_{(\omega)}$ are the Fourier transforms of the output and input signals respectively. $G_{(\omega)}$ is the transfer function of the system. Essential for this method is that the input signal has a noise component at all the frequencies where we wish to determine the transfer function. Often the input signals have sufficient intrinsic noise; otherwise noise must be added to the system in some way. The auto power spectral density function (APSD) of the input signal is defined as¹:

$$APSD = X_{(\omega)}^* X_{(\omega)} = |X_{(\omega)}|^2 \quad (\text{B-2})$$

where * is the complex conjugate operator.

The cross power spectral density function (CPSD) between the input and the output signal is defined as:

$$CPSD_{(\omega)} = X_{(\omega)}^* Y_{(\omega)} \quad (\text{B-3})$$

The APSD and CPSD are related by the transfer function of the system¹:

$$G_{(\omega)} = \frac{X_{(\omega)}^* Y_{(\omega)}}{|X_{(\omega)}|^2} \quad (\text{B-4})$$

From this equation it follows that the transfer function can be determined from the signals X and Y , but only at those frequencies that are contained in the input signal X (otherwise $|X_{(\omega)}|^2 = 0$).

The inverse Fourier transforms of the auto- and cross-power spectral density functions are the auto- and cross-correlation functions (ACF and CCF). These functions represent the data in the time domain rather than in the frequency domain and are often useful for understanding the physical processes taking place in a system. The ACF can also be derived from the time signals¹:

$$ACF_{x(t)}(\tau) \equiv \lim_{T \rightarrow \infty} \frac{\frac{1}{T} \int_0^T x(t)x(t+\tau)dt}{\frac{1}{T} \int_0^T x(t)^2 dt} \quad (\text{B-5})$$

The ACF always lies between zero and one. The CCF can be derived in a similar manner. One of the most used applications of the CCF is for transit time estimations. If a signal disturbance (like a bubble) travels from one sensor to another, the CCF of the two signals will exhibit a peak at the average transit time of this disturbance¹.

The ACF can show the existence of 'memory' in the system. If the ACF is not equal to zero at some time delay t_{delay} it means that there is some physical mechanism present which causes a fluctuation of the variable to have an effect on the same variable a time t_{delay} later. This physical mechanism can of course be a complex combination of mechanisms and it may not be possible to separate these. Since white noise has no 'memory' (the value at each time instant does not depend on the values at other times) the ACF of white noise is zero for every time shift t_{shift} except for $t_{\text{shift}}=0$.

The decay-ratio is commonly used to characterize the stability of BWRs¹. For a second-order system the DR is defined as the ratio of two consecutive maxima of the impulse response function which can also be obtained from the ACF². In higher order systems one parameter cannot fully describe the stability of the system and the ratio between two consecutive maxima of ACF will depend on exactly which maxima are chosen². Therefore, the DR is uniquely defined only for a second-order system. It is possible to derive the ACF for higher-order systems and to obtain the DR from that. In this thesis we use a third-order model to fit the measured ACF to estimate the DR. Such a fitting is performed by ignoring the first peak since the contribution of the least stable pole pair, which determines the stability, dominates in the impulse response and the contributions of other poles die out soon.

To determine the stability, noise measurements are performed on the system. The inlet flow signal is used for that purpose which is measured for a relatively long record length (6000s-24000s) compared to the time constant of the dominant processes (1-2 s), which reduces the windowing effects derived from the limited length of the data. For the noise analysis technique to work, one needs (real) fluctuations in the physical processes, parasitic (e.g. electronic) noise is not useful. Boiling in a two-phase flow system is a stochastic process, but in a relatively stable operating condition these fluctuations are too small to be practical. In this case the system has to be disturbed by external noise. For this reason, a wide-band random noise signal is added to the driving signal of the electrically heated rods to enable noise measurement.

To study the stability of the GENESIS facility, the signal to be analyzed is first de-trended by its mean and normalized before a fit to a third order model is carried out. The third order model used to fit the time responses has the form:

$$y = b_1 e^{b_4 t} \cos(b_5 t) + b_2 e^{b_4 t} \sin(b_5 t) + b_3 e^{b_6 t} \quad (\text{B-6})$$

where t is time. For such a model the DR is given by

$$DR = e^{2\pi b_4 / \text{abs}(b_5)} \quad (\text{B-7})$$

and the corresponding frequency f is given by

$$f = 2\pi / \text{abs}(b_5) \quad (\text{B-8})$$

As an example the following figure is presented. The cross correlation exhibits decreasing oscillations indicating a stable behavior. For this particular case, the resulting decay ratio was found to be $DR \approx 0.85$.

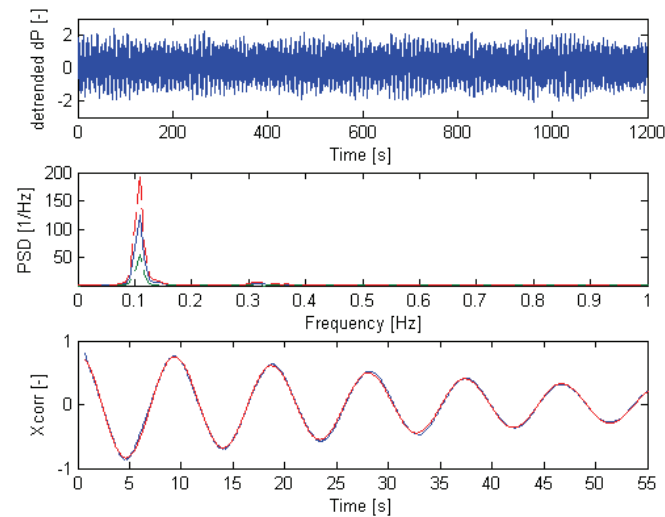


Figure B-1: Procedure followed to calculate the DR by using noise analysis techniques.

References

- ¹Priestley, M.B. *Spectral Analysis and Time Series*, Academic Press Inc. London (1981)
- ²Van der Hagen, T.H.J.J, Pázsit, I., *et al.* Methods for the determination of the in-phase and out-of-phase stability characteristics of a BWR. *NuclearTechnology*, 107, 193–214 (1994).

APPENDIX C

MOX fuel reference Neutronic data

The neutronic data used for the investigations in which the MOX fuel rods are simulated are presented in Table C-1 and Table C-2. For completeness, the data for typical UO₂ fuel rods are also included.

MOX fuel with 5% Pu loading	
U-234	0.002 %
U-235	0.250 %
U-238	99.748 %
Pu-238	4.000 %
Pu-239	50.000 %
Pu-240	23.000 %
Pu-241	13.000 %
Pu-242	10.000 %

Table C- 1: Composition of the MOX fuel implemented in the GENESIS VRF system.

	Delay neutrons decay constant (s ⁻¹)	Delayed neutrons fraction	Neutron generation time (μs)
ESBWR UOX fuel (MOC)	$\lambda_1=0.0125$ $\lambda_2=0.0306$ $\lambda_3=0.1150$ $\lambda_4=0.3110$ $\lambda_5=1.2100$ $\lambda_6=3.2000$ $\lambda_{\text{effective}}=0.09$	$\beta_1=0.03$ $\beta_2=0.21$ $\beta_3=0.19$ $\beta_4=0.39$ $\beta_5=0.13$ $\beta_6=0.05$ $\beta_{\text{Total}}=0.00562$	$\Lambda=50$
EPR MOX fuel (BOC)	$\lambda_1=0.01318$ $\lambda_2=0.03054$ $\lambda_3=0.1234$ $\lambda_4=0.3329$ $\lambda_5=1.282$ $\lambda_6=3.479$ $\lambda_{\text{effective}}=0.08$	$\beta_1=0.02$ $\beta_2=0.21$ $\beta_3=0.18$ $\beta_4=0.37$ $\beta_5=0.17$ $\beta_6=0.05$ $\beta_{\text{Total}}=0.004079$	$\Lambda=5.95$

Table C- 2: Neutronic for the ESBWR UOX fuel (Reference case) provided by GE¹, and for the EPR (MOX fuel²), obtained by Van Rooijen³ by using the VAREX code⁴

References

- ¹ Shiralkar, B.S., Personal communication, (2005).
- ² Leppanen, J., Preliminary calculations on actinide management using advanced PWR MOX technology, Technical report, VTT, (2005).
- ³ Van Rooijen, W. Personal communication, (2007)
- ⁴ Kloosterman J.L. and Kuijper, J.C., VAREX, a code for variational analysis of reactivity effects: description and examples. PHYSOR 200, Seoul, S.Korea, October 7-10 2000. ANS.

APPENDIX D

Analysis of the fluctuations of the primary flow signal

In order to clarify the physical mechanism behind the fluctuations of the primary flow signal, the cross correlation performed between the (detrended) signal of the inlet temperature and the (detrended) signals of the main flow, the feedwater flow and the feedwater temperature are examined. The corresponding results obtained by noise analysis techniques are depicted in Figure D-1.

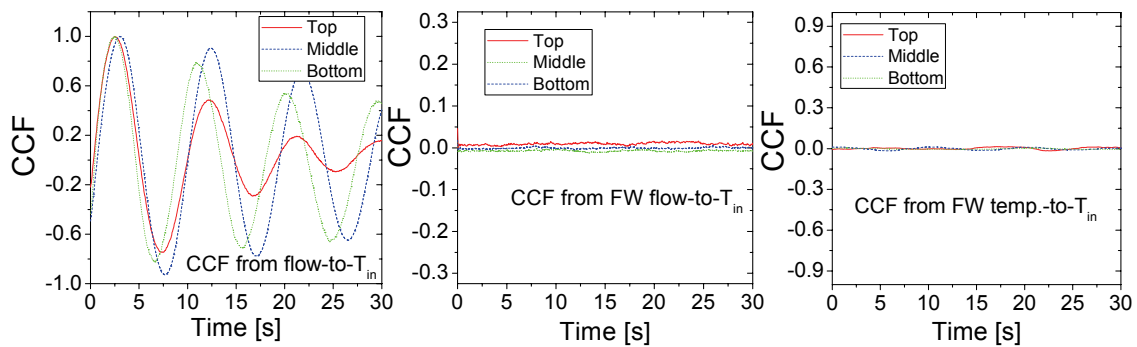


Figure D-1: Cross correlation function obtained by using the inlet temperature signal and the main flow, the feedwater flow and the feedwater temperature signals.

As can be seen from the cross correlation between the signals from the inlet temperature and the primary flow, the location of the sparger inlet influences the stability of the system regarding the thermal-hydraulic mode. To further investigate the origin of such a relation, two more cross correlations are calculated: the cross correlation between the core inlet temperature signal with those from the feedwater flow and temperature. No dependency is seen in these cases, which indicates that the core inlet temperature fluctuations are induced by changes in the primary flow rather than by the feedwater flow dynamics.

APPENDIX E

The nodal model

The matrix form of the linearized balance equations in dimensionless form of the model presented in Section 5.4 is shown below.

$$\dot{X} = A.X;$$

where

$$\dot{X} = \begin{pmatrix} d\hat{h}_o / d\hat{t} \\ d\hat{h}_{Ch,s,j} / d\hat{t} \\ d\hat{l}_{Ch,s,j} / d\hat{t} \end{pmatrix}; \quad X = \begin{pmatrix} \delta\hat{h}_o \\ \delta\hat{h}_{Ch,s,j} \\ \delta\hat{l}_{Ch,s,j} \end{pmatrix};$$

$$A = \begin{pmatrix} -1 & \frac{(1-\hat{h}_{t0})}{\hat{\rho}_{f,0j}\hat{l}_{f,0j}} \frac{2}{\hat{K}_s} \left(\frac{2}{2+(\tau-1)\hat{\rho}_{f,0j}} \right) \left(\frac{1}{2+(\tau-1)\hat{\rho}_{f,0j}} \right) \left[(\tau-1)\hat{\rho}_{f,0j}N_g \left(\hat{l}_{R,f,0j}\hat{\rho}_{f,0}^2 \frac{\hat{V}_{RG0}}{\hat{h}_{RG0}} \hat{K}_s - 1 + \hat{\rho}_{f,0j} + \hat{l}_{R,f,0j}\hat{K}_4 \right) - \left(2 \frac{(1-\hat{h}_{t0})}{\hat{\rho}_{f,0j}\hat{l}_{f,0j}} + \hat{K}_4 + \hat{\rho}_{f,0} (1-\hat{h}_{t0}) \frac{\hat{V}_{RG0}}{\hat{h}_{RG0}} \hat{K}_s \right) \right] \\ \frac{1}{\hat{A}_{R,f,R,s,0j}} & \frac{1}{\hat{A}_{R,f,R,s,0j}} & 0 \\ 0 & \frac{1}{\hat{K}_s \hat{A}_{R,f,R,s,0j} \hat{\rho}_{f,0j} \hat{l}_{f,0j}} & \frac{1}{\hat{A}_{R,f,R,s,0j} \hat{\rho}_{f,0j} \hat{l}_{f,0j}} \end{pmatrix}$$

By calculating the characteristic polynomial associated to matrix A, the stability of a certain configuration can be investigated by analyzing the sign of the roots. Thus,

$$\det(A - \lambda I) = \begin{vmatrix} a - \lambda & b & c \\ d & e - \lambda & 0 \\ 0 & f & g - \lambda \end{vmatrix} = (a - \lambda)(e - \lambda)(g - \lambda) + d.f.c - b.d.(g - \lambda) =$$

$$\det(A - \lambda I) = a.e.g - \lambda(a.e + a.g + e.g) + \lambda^2(a + e + g) - \lambda^3 + d.f.c - b.d.g + b.d.\lambda =$$

$$= -\lambda^3 + \lambda^2(a + e + g) - \lambda(a.e + a.g + e.g - b.d) + a.e.g + d.f.c - b.d.g$$

The Descartes rule of signs is used to derive the stability criteria which are used to characterize the numerical results. Thus,

Stability conditions

$$\begin{aligned} a + e + g &< 0 \\ -(a.e + a.g + e.g - b.d) &< 0 \\ d.f.c - b.d.g &< 0 \end{aligned}$$

APPENDIX F

The Geysering phenomenon

Geysering has been observed in a variety of closed end (or forced flow at small flow rate) vertical columns of liquid which are heated at the base. This process breaks down into three phenomena¹, viz. boiling delay, condensation (or expulsion of vapor), and liquid returning. In experiments performed without a chimney it is reported that the period of flow oscillations τ_f , is nearly equal to the boiling delay time τ_{bd} , because in most cases the boiling delay time is much longer than that of the other two processes. In the case of parallel channels however, as indicated by Aritomi², flow reversal plays a significant role for the occurrence of geysering. Since flow reversal makes the fluid temperature at the channel inlet higher than that of circulation fluid, the definition of τ_{bd} is modified by evaluating the fluid properties at the channel inlet instead of the circulation temperature. Thus, τ_{bd} is defined as the time required for the fluid with subcooling $\Delta T_{sub,in}$, to be heated up to the saturation temperature based on the pressure at the channel inlet and is expressed by

$$\tau_{bd} = \frac{\rho_{l,in} C_{p,l,in} \Delta T_{sub,in} A_C L_C}{q}, \quad (E-1)$$

where the liquid density $\rho_{l,in}$, and the specific heat capacity at constant pressure $C_{p,l,in}$, are computed at the temperature at the channel inlet; A_C and L_C are the flow area and length of the heated section, respectively.

The non-heated chimney influences the geysering period since the effect of the transport of bubbles cannot be ignored². It is found an acceptable correlation for the measured data when the boiling delay time is added to the transit time of the large bubbles passing through the chimney, which can be calculated by the drift velocity v_{gj} , for slug flow in the following manner:

$$\tau_{LB} = \frac{L_{Ch}}{v_{gj} + u_{in}} \quad (E-2)$$

$$\text{with } v_{gj} = 0.35 \left(\frac{g \Delta \rho D_{Chim}}{\rho} \right)^{1/2}, \quad (E-3)$$

g being the acceleration due to gravity, $\Delta \rho$ the density difference between the liquid and vapor phases, and u_{in} the mean inlet velocity.

References

- ¹ Nakanishi, S., "Recent Japanese research on two-phase flow instabilities", In Proc. of Japan-US Seminar on Two-phase Flow Dynamics. Hemisphere Publishing Corporation, (1979).
- ² Aritomi, M. and Chiang, J. H., Fundamental studies on safety-related thermohydraulics of nat. circ. boiling parallel channel flow systems under start-up conditions (mechanism of geysering in parallel channels), Accident Analysis, Nuclear Safety, 33(2):170–182, (1992).

APPENDIX G

The Lyapunov exponents and the Kolmogorov entropy

The largest Lyapunov exponent (LLE)

Systems exhibiting a strong dependence on the initial conditions are described in the phase plane by attractors with a complicated geometrical structure. The Lyapunov exponents are used to identify such a strong dependence on the initial conditions: if the system has a chaotic evolution there is at least one positive exponent. If the system has not such an evolution all the Lyapunov exponents are negative (the so-called point attractors). For regular trajectories it is zero. The LLE is a measure of the rate of divergence if the trajectories within such an attractor separate exponentially in time. Another way to look at the Lyapunov exponents is the loss of predictive ability as we look forward into time. In order to identify chaotic behavior it is sufficient to determine the LLE. The LLEs, estimated with an algorithm based on the tracking of divergence patterns of nearest neighbors^{1,2} implemented in the MTRCHAOS software package³, are presented in Figure G-1.

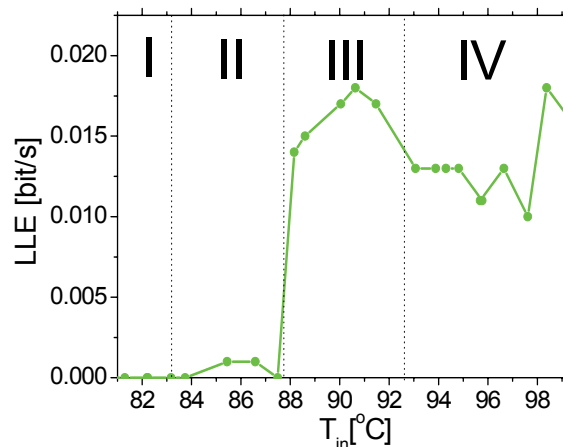


Figure G-1: The LLEs for the four different regions obtained from the primary flow signal.

Clearly, the stable region (I) and the *in-phase* region (II) show very low values of LLEs which agrees with the fact that these cases are very predictable. Thus, the divergence of trajectories is very small. A significant increase in the LLEs can be noticed in region (III), where a-periodical, oscillations are observed. Thus, the trajectories for the corresponding attractors should preserve this degree of divergence. The experimental results of region IV are more difficult to interpret. The experiments show that these cases are very regular. It is to be expected that the attractor keeps this regularity and thus the LLE should be small. The calculation of the LLEs predicted a high degree of divergency of nearby trajectories. A possible cause for this may be the large dispersion of these estimations.

The Kolmogorov entropy (KML)

The Kolmogorov entropy KML is a measure of the rate of information loss (or gain) along the attractor of a certain data set. It is usually expressed in bits/seconds. A positive, finite KML means the time series and the underlying system being chaotic. KML equal to zero represents a regular, cyclic or constant motion. An infinite KML refers to a stochastic, random signal.

In this study the program RRCHAOS⁴, which uses the maximum-likelihood estimation of KML proposed by Schouten⁵, is used for estimating the KML of the experiments. Figure G-2 presents the Kolmogorov entropy KML , as estimated by using the RRCHAOS software.

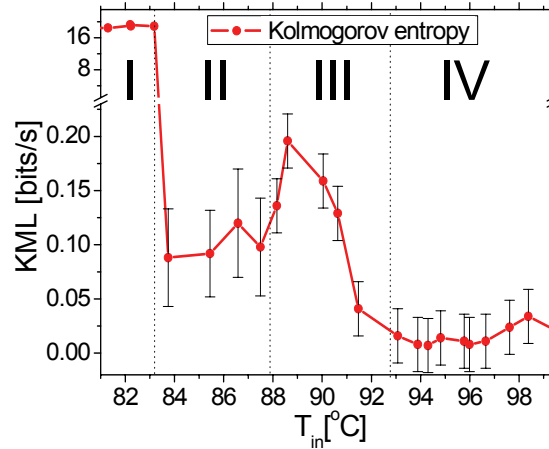


Figure G-2: KML for the four different regions obtained from the primary flow signal.

Cases from region (I) exhibit a large degree of information creation due to the relatively important contributions of the noise. The fact that in region (II) KML is larger than zero may suggest a lack of sufficient statistical accuracy in the data because of the long periods of the oscillations. The large uncertainties found in this case seem to confirm this idea. When entering region (III) the values of the KML increase, indicating a higher sensitivity to external conditions and perturbations. The out-of-phase cases from region (IV) show low KML values characteristic for regular oscillations.

As a result of the LLEs and the KML values, it is concluded that the a-periodical oscillations characterizing region III can be attributed to chaos.

References

- ¹ Grassberger P, Procaccia, I. Charact. of strange attractors, Phys. Rev. Lett. 50 (1983) 346.
- ² Grassberger P. *et al.* Measuring the strangeness of strange attractors, Physica D9 (1983) 189.
- ³ Rosenstein, M.T. *et al.* A practical method for calculating LLEs small data sets. Physica D 65:117-134, 1993.
- ⁴ Schouten, J.C; Takens, F; Van den Bleek, C.M. Maximum-likelihood estimation of the entropy of an attractor, Physical Review E, Volume 49, Number 1 (Jan 1994), pp. 126-129.
- ⁵ Schouten, J.C; Takens, F; Van den Bleek, C.M. Estimation of the dimension of a noisy attractor, Physical Review E, Volume 50, Number 3 (Sep 1994), pp. 1851-1861.

Nomenclature

Normal alphabet

A	cross sectional area (m^2)
c	delayed neutron density (m^{-3})
C_o	distribution parameter (-)
C_p	constant pressure heat capacity ($\text{J kg}^{-1} \text{s}^{-1}$)
D	diameter (m)
E_{kin}^*	kinetic energy per unit of volume (J m^{-3})
F_{driv}^*	two-phase driving force per unit of area (N m^{-2})
f	frictional factor (-)
f_{res}	resonance frequency (Hz)
f_{TP}	two phase frictional factor (-)
g	gravitational acceleration (m s^{-2})
G	transfer function
G_{Conv}	void fraction determination transfer function
G_F	fuel rod transfer function
G_{tt}	traveling time associated transfer function
G_{vp}	vapor production transfer function
h	enthalpy (J kg^{-1})
k	heat conductivity coefficient ($\text{W m}^{-1} \text{°K}^{-1}$)
K	local pressure drop coefficient (-)
l	variable length (m)
L	length (m)
m''	mass flux density ($\text{kg m}^{-2} \text{s}^{-1}$)
M	mass flow rate (kg s^{-1})
n	neutron density (m^{-3})
N_{rod}	number of heating rods
P	pressure ($\text{kg m}^{-1} \text{s}^{-2}$)
q	power (J s^{-1})
q'	linear power transferred from fuel to coolant ($\text{J s}^{-1} \text{m}^{-1}$)
q''	heat flux ($\text{J s}^{-1} \text{m}^{-2}$)
r	reactivity coefficient
s	Laplace variable (s^{-1})
t	time (s)
T	temperature (°K)
v	velocity (m s^{-1})
\bar{u}_{gi}	mean drift velocity (m s^{-1})
v_0	velocity of the coolant at the core inlet (m s^{-1})
V	volume (m^3)
V_{fg}	volumetric density ($\text{m}^3 \text{kg}^{-1}$)
z	axial position (m)

Greek

α	void fraction (-)
β	delayed neutron fraction (-)
χ	quality (-)
δ	small perturbation
γ	scaling dimensionless friction factor
Φ	Romy's multiplier (-)

λ	delayed neutron decay constant (s^{-1})
Λ	neutron generation time (s)
θ	angle with respect to gravity direction (rad)
ρ	density ($kg\ m^{-3}$)
σ	surface tension ($N\ m^{-1}$)
τ_w	wall stress
τ	time constant (s)
Υ	dimensionless friction factor

Subscripts and superscripts

*	dimensionless
<i>0</i>	characteristic
α	void fraction (-)
b	bubble
bb	boiling boundary
bd	boiling delay
cr	critical
C	core
<i>Calc</i>	calculated
Ch	chimney
Channel	chimney plus core section
<i>d</i>	departure of bubbles
<i>driv</i>	driving force
D	Doppler
DC	downcomer
est	estimated
<i>f</i>	relative to the oscillations in the channel
<i>fg</i>	difference between (saturated) vapor and liquid properties
F	fuel
ϕ	phase
g	gravitational acceleration ($m\ s^{-2}$)
G	relative to GENESIS
h	hydraulic
<i>heated</i>	regarding heating rods
in	inlet
<i>l</i>	liquid
<i>loss</i>	referring to losses
LO	liquid only
m	mixture
<i>Meas</i>	measured
o	outlet
r	radial
rod	regarding fuel pin rod
R	reactor
R-134a	Freon R-134a
s	single phase
sp	spacer
SS	steam separation
SV	separator vessel
sat	saturation
t	transit

Nomenclature

tot	total
TH	thermal-hydraulics
TP	two phases
v	vapor

Operators

Δ	difference
\diamond	time average
*	complex conjugate

Abbreviations

BOC	beginning of cycle
BWR	Boiling Water Reactor
CCF	cross correlation function
CHF	critical heat flux
CIRCUS	circulation during startup (experimental facility)
DC	digital controller
DFA	detrended fluctuation analysis
DR	decay-ratio
DWO	density wave oscillations
EOC	ending of cycle
EPR	European Pressurized Reactor
ESBWR	Economical Simplified Boiling Water Reactor
FW	feed water
GE	General Electric Co.
GENESIS	GE natural-circulation experimental scaled facility for investigations on stability
HEM	homogeneous equilibrium model
HS	high subcooling
LME	linearized momentum equation
LS	low subcooling
MOC	middle of cycle
MOX	mixture oxide fuel
NACUSP	natural circulation and stability performance of BWRs
PC	computer
PCH	phase change
PSD	power spectral decomposition
PWR	Pressurized Water Reactor
SB	stability boundary
SIRIUS	simulated reactivity feedback implemented into thermal-hydraulic stability facility
TH	thermal-hydraulic
TF	transfer function
UP	upper plenum
VRF	void reactivity feedback
ZOH	zero - order hold

Dimensionless scaling factors

$X_{a,g}$	axial geometry scaling factor
$X_{Core,a,g}$	core axial scaling factor
$X_{Core,r,g}$	core radial scaling factor i
X_d	dynamic time ratio
X_g	geometrical scaling factor
X_m	mass flux scaling factor
X_P	power scaling factor
X_{Press}	pressure scaling factor
X_t	time ratio
$X_{t,d}$	dynamic time ratio
$X_{t,ss}$	steady state time ratio

Dimensionless numbers

N_{PCH}	Phase change number	$N_{PCH} \equiv \frac{L \cdot q'}{A_C m''_{m,o} h_{fg,o}} \frac{\rho_{l,o} - \rho_{v,o}}{\rho_{v,o}}$
N_{Fr}	Froude number	$N_{Fr} \equiv \frac{m''_{m,o}{}^2}{\rho_{v,o}{}^2 g L_C}$
N_{We}	Weber number	$N_{We} \equiv \frac{(m''_{m,o})^2 L_C}{\rho_l \sigma}$
$N_{Eö}$	Eötvös number	$N_{Eö} \equiv \frac{N_{We}}{N_{Fr}} = \frac{L_C^2 \cdot \rho_v^2 \cdot g}{\rho_l \sigma}$
N_ρ	Density ratio number	$N_\rho \equiv \frac{\rho_{v,o}}{\rho_{l,o}}$
N_{sub}	Subcooling number	$N_{sub} \equiv \frac{h_{l,o,sat} - h_{l,o}}{h_{fg,o}} \frac{\rho_{l,o} - \rho_{v,o}}{\rho_{v,o}}$
$N_{Pé}$	Péclet number	$N_{Pé} \equiv \frac{m''_{m,o} c_{p,l} D_h}{\lambda_l}$
N_g	Geometry number	$N_g \equiv \frac{D_h}{L_C}$
N_f	Friction number	$N_f \equiv f \frac{D_h}{L_0}$
$N_{Fr,Dh}$	Froude number based on D_h	$N_{Fr} \equiv \frac{m''_{m,o}{}^2}{\rho_{v,o}{}^2 g D_h}$
N_{Flash}	Flashing parameter	$N_{Flashing} \equiv \frac{h_{l,C,in} - h_{l,Ch,o}}{h_{fg}} \left(\frac{\rho_{l,Ch,o}}{\rho_{g,Ch,o}} - 1 \right)$
N_{Fo}	Fourier number	$N_{Fo} \equiv t \frac{4k}{\rho C_p D^2}$
N_{Bi}	Biot number	$N_{Bi} \equiv \frac{hD}{k}$

CURRICULUM VITAE



Christian P. Marcel was born in Buenos Aires, Argentina in July 24th in 1975. He attended to the ENET N°1 “Jorge Newbery”, a High School in which he received a strong formation in physics. In 1994 he graduated receiving a fellowship to complete his education in the Argentinean aviation company AUSTRAL S. A. At the same time he decided to continue studying Physics at the Buenos Aires University. After 3 years of hard study, he started to prepare the admission exam for the Balseiro Institute, an excellence academic center located in Bariloche, at the feet of the Patagonian Andes. He passed the examination process together with other 27 students from different points of Argentina and Latin America. After the selection, he moved to Bariloche where he lived for 4 years. In those years he married with Flavia Santamaria. He got the title of “Ingeniero Nuclear” in 2002, being the first of his promotion.

In October 2002 Christian met Tim Van der Hagen at the Bariloche Atomic Center. After that meeting Tim offered him a position to continue his studies as a PhD in the actual Department of Physics of Nuclear Reactors of the Delft University of Technology. The goal of the research was to investigate the stability performance of natural circulation Boiling Water Reactors. As a result of such an investigation he wrote this Doctoral thesis.

In December 2006 he became the father of his first son Kolya.

In January 2007 he continued working in the Department of Physics of Nuclear Reactors as a post-doc investigating the stability of the Supercritical Water Reactor, position that he occupies until now.

September 2007

ACKNOWLEDGMENTS

I would like to express my gratitude to Prof. Tim Van der Hagen for giving me the opportunity to pursue this research in his group Physics of Nuclear Reactors and assisting me during this process. His guidance, interest, motivation and support in all different situations that arose during these years are greatly appreciated.

Special thanks to Dr. Martin Rohde who was supporting me not only from the technical point of view but also from the human side. Martin, thanks a lot for all these years of continuous support and for sharing your nice office with me!

I would like to address a special thank to Dick de Haas and August Winkelman, for helping me in the design, construction and operation of the GENESIS facility. It would have been impossible to successfully finish the GE project (and more important, this thesis!) without your high efficiency and precision. The support that you guys always gave me also at the CIRCUS facility was invaluable and greatly appreciated. You always came with a fast solution every time I had a technical problem. It was a pleasure to work with you two! I am also thankful to Camiel Kaaijk and to Jelle Schut who were part of the world famous Fab Four Technical group. It was a pity that we could only work few months together.

I am greatly indebted to Ine Olsthooorn for helping with all the daily big and small problems, simplifying my life a lot.

I wish to thank all the people from the group of Physics of Nuclear Reactors for the nice research environment you create every day.

A very special acknowledgment to my 'European' friends who have help to enjoy all these long years being far from home. From them I have learnt the importance of sharing thoughts, having political discussions and planning the life. Vicente, Rosa Ana and Paula, Carlos (C), Stavros and Vicky, Andrea and Alessandra, Paulo and Heloisa, Carlos (G) and Diana, Irene and Marteen, Antonio and Cristina, Paulo, Gianluca and Diana you have demonstrated to have an infinite patience, generosity and being great human beings. Thanks for being my friends! In particular I will never forget the incredible trips to Spain and Greece in which we received unconditional love and affect from our foster homes. Thanks for the warm hospitality and I hope we can offer you the same when you came to visit Argentina.

I am thankful to my family and friends from Argentina who always believed in me and helped me and my family to forget there was an ocean between us.

Last but not least I like to thank to my beloved wife, Flavia and our little son Kolya, to whom this thesis is dedicated. Fla, muchas gracias por ser mi compa era y por estar siempre a mi lado m s all  de los contratiempos. Si esta aventura ha tenido un final feliz es sencillamente por tu apoyo continuo y por tu inconmensurable amor.

